NOTICE

AVIS

The quality of this microform is heavily dependent upon the quality of the original thesis submitted for microfilming. Every effort has been made to ensure the highest quality of reproduction possible.

If pages are missing, contact the university which granted the degree.

Some pages may have indistinct print especially if the original pages were typed with a poor typewriter ribbon or if the university sent us an inferior photocopy.

Reproduction in full or in part of this microform is governed by the Canadian Copyright Act, R.S.C. 1970, c. C-30, and subsequent amendments.

La qualité de cette microforme dépend grandement de la qualité de la thèse soumise au microfilmage. Nous avons tout fait pour assurer une qualité supérieure de reproduction.

S'il manque des pages, veuillez communiquer avec l'université qui a conféré le grade.

La qualité d'impression de certaines pages peut laisser à désirer, surtout si les pages originales ont été dactylographiées à l'aide d'un ruban usé ou si l'université nous a fait parvenir une photocopie de qualité inférieure.

La reproduction, même partielle, de cette microforme est soumise à la Loi canadienne sur le droit d'auteur, SRC 1970, c. C-30, et ses amendements subséquents.

Canada

UNIVERSITY OF ALBERTA

Performance Prediction for Steamflooding Marginal Heavy Oil Reservoirs
Using Horizontal Wells

by

Luong T. Doan   Ⓒ

A THESIS
SUBMITTED TO THE FACULTY OF GRADUATE STUDIES AND RESEARCH
IN PARTIAL FULFILMENT OF THE REQUIREMENTS FOR THE DEGREE OF

Master of Science

IN

Petroleum Engineering

Department of Mining, Metallurgical and Petroleum Engineering

Edmonton, Alberta
Spring 1996

UNIVERSITY OF ALBERTA

LIBRARY RELEASE FORM

NAME OF AUTHOR   Luong T. Doan

TITLE OF THESIS   Performance Prediction for Steamflooding Marginal
Heavy Oil Reservoir Using Horizontal Wells.

DEGREE FOR WHICH THESIS WAS PRESENTED   Master of Science

YEAR THIS DEGREE GRANTED   1996

Permission is hereby granted to THE UNIVERSITY OF ALBERTA LIBRARY to reproduce single copies of this thesis and to lend or sell such copies for private, scholarly or scientific research purposes only.

The author reserves other publication rights, and neither the thesis nor extensive extracts from it may be printed or otherwise reproduced without the author's written permission.

(SIGNED) _Doantthtuong_

PERMANENT ADDRESS:
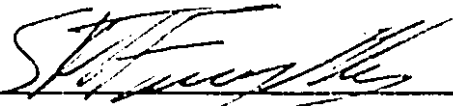
    2933 - 111 B ST

    EDMONTON . AB

    T6J - 4R5

DATED _APRIL 17/96_

UNIVERSITY OF ALBERTA

FACULTY OF GRADUATE STUDIES AND RESEARCH
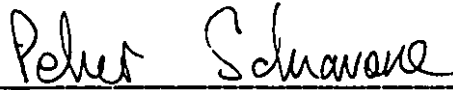
The undersigned certify that they have read, and recommend to the Faculty of Graduate Studies and Research, for acceptance, a thesis entitled Performance Prediction for Steamflooding Marginal Heavy Oil Reservoirs Using Horizontal Wells submitted by Luong T. Doan in partial fulfillment of the requirements for the degree of Master of Science in Petroleum Engineering.

_____

Professor S.M. Farouq Ali (Supervisor)

_____

Professor R.G. Bentsen

_____

Professor P. Schiavone (External Examiner)

_____

Professor J. Szymanski

Date _April 10, 96_

Công Cha Như Núi Thái Sơn,
Nghĩa Mẹ Như Nước Trong Nguồn Chảy Ra,
Một Lòng Thờ Mẹ Kính Cha,
Cho Tròn Chữ Hiếu Mới Là Đạo Con.

Ca Dao Tục Ngữ Việt Nam

Abstract

This study focused on experimental and theoretical modeling of horizontal wells in steam-flooding recovery of oil from marginal heavy oil reservoirs. Scaled experiments were performed to evaluate the effectiveness of a variety of recovery strategies for a homogeneous reservoir, and one with bottom water. Also included in this study were the effects of well shut-in, dipping reservoir and pattern inversions; that is, cross pattern flooding.

For the base case run, the theoretical analysis included calculations for the saturation profile and for the steam zone volume in the reservoir, and a heat balance calculation during the steamflood. Results of these experiments were then scaled-up to predict field ope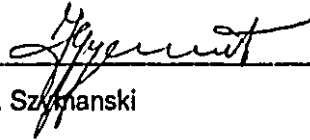rations and to determine the optimistic recovery. In addition, experiments were carried out also in an unscaled visual model. These experiments were intended to provide insight into the oil recovery mechanisms.

Based on experimental results and data analysis, the following were found: the dominant displacement mechanism in a thin, permeable and homogeneous heavy oil reservoir was the downward expansion of the steam at the top of the formation. The location of the horizontal wells affected the cumulative recovery significantly. The presence of a Neoprene sealant sheet resulted in an optimistic prediction of approximately 7.6%, after 0.8 PV of steam had been injected.

Acknowledgments

Table of Contents

iv

List of Tables

List of Figures

Nomenclature

a	thickness of the Neoprene sheet, [L]
b	thickness of the cap rock, [L]
C	specific heat, $[L^2t^{-2}T^{-1}]$
f_p	the amount of injected heat which is produced, dimensionless
f_{st}	steam quality, $[MM^{-1}]$
g	acceleration due to gravity, $[Lt^{-2}]$
h	enthalpy per unit mass, $[L^2t^{-2}]$, or convection constant, $[Mt^{-3}T^{-1}]$
J	mechanical equivalence of heat energy, dimensionless
k	permeability, $[L^2]$
k_h	thermal conductivity, $[MLt^{-3}T^{-1}]$
k_r	relative permeability, dimensionless
$k_{no.}^{\bullet}$	thermal conductivity of atmosphere, $[MLt^{-3}T^{-1}]$
L	length or distance, [L]
L_v	Latent enthalpy per unit mass, $[L^2t^{-2}]$
M	volumetric heat capacity, $[ML^{-1}t^{-2}T^{-1}]$
m	mass, [kg]
p	pressure, $[ML^{-1}t^{-2}]$
Q	heat, $[ML^2t^{-2}]$
$\dot{Q}$	rate of heat flow, $[ML^2t^{-3}]$
q	flow rate, $[L^3t^{-1}]$
r_w	effective wellbore radius, [L]
S	saturation, mass fraction
T	temperature, [T]
t	time, [t]
v	velocity, $[Lt^{-1}]$
V_s	steam zone volume, $[M^3]$
w	mass flow rate, $[Mt^{-1}]$
x	coordinate, [L]

Greek Symbols

α	thermal diffusivity, $[L^2t^{-1}]$
Δp	pressure difference between two point, $[ML^{-1}t^{-2}]$
ΔN	difference in the oil production interval, [ml]

ΔW difference in the water production interval, [ml]

β eigenvalues

ϕ porosity, dimensionless

μ viscosity, $[ML^{-1}t^{-1}]$

ρ density, $[ML^{-3}]$

ω slit width, [L]

∇ del. operator.

Subscripts

1,2,3   the zone containing steam, oil and condensate, respectively.

D   dimensionless

form   formation

inj.   injected

j   phase (oil, water or steam)

loss   refers to the heat loss to the cap and base rock

o   oleic phase

ob.   overburden

P   prototype

prod.   produced

R   reference variable used to obtain a dimensionless quantity

s   steam

w   water (unless otherwise specified)

Chapter 1

INTRODUCTION

Canada's heavy oil and oil sands deposits are estimated to contain as much oil as the conventional oil resources of the entire world. Heavy oil deposits, in particular those in southwestern Saskatchewan and southeastern Alberta, represent an attractive target for exploitation as the in-place heavy oils are mobile under reservoir conditions. These reservoirs are thin (5-10 meters of pay) and often in communication with an underlying water zone ("bottom water"). Primary recovery in these reservoirs typically amounts to less than 5% of the initial oil in place (IOIP). In a few cases, where the conditions are more favourable, the use of horizontal wells has increased primary recovery to 15-20% prior to water coning. This still leaves up to 80% of the oil in place unrecovered.

Steam injection has been tested in these reservoirs, but the combination of thin net pay and the existence of a bottom-water zone leads to excessive heat loss, as well as low sweep efficiency due to the diversion of injected steam away from the oil zone into the bottom water zone. Conventional steam injection recovery processes (such as cyclic steam stimulation and steamflooding using vertical wells) have proven to be unsuitable for the large majority of these reservoirs. Horizontal wells, on the other hand, hold promise to improve the recovery efficiency of the steam injection processes. One of the biggest advantages of horizontal wells is their extended contact with the reservoir, leading to a large increase in the flow rate.

In steamflooding thin heavy oil reservoirs, many factors such as shut-in, cross pattern flooding, thickness of the bottom water layer, and dip affect the recovery process. This study attempts to provide insight into the performance prediction of steamflooding a marginal heavy oil reservoir using horizontal wells, and looks at different steamflooding strategies for improving the recovery. These objectives are achieved experimentally using a scaled physical model. Interpretation of the experimental results includes a calculation for the saturation profiles, and steam zone volumes in the reservoir, and a heat balance calculation for the steamflood. Subsequently, the results from these experiments are scaled up, using the same set of scaling criteria, to predict field performance.

Chapter 2

STATEMENT of the PROBLEM

The application of horizontal well technologies to enhanced oil recovery processes has increased significantly in recent years. To understand fully the effectiveness of horizontal wells in thermal recovery processes, experiments using a scaled physical model are carried out. There were five main objectives of this experimental study.

1) Examine different steamflooding strategies for improving the recovery;

2) Determine the effect of shut-in, dip and bottom water thickness on recovery;

2) Investigate the dominant oil recovery mechanisms in the reservoir;

3) Estimate the distribution of reservoir fluids; that is, the saturation of steam, condensate and oil; and

4) Investigate the effect of the Neoprene sealant sheet on the heat loss.

The above objectives were achieved using experimental and theoretical methods outlined below.

2.1 Experimental Objectives

1. Experimental Apparatus Development

   a) Modification of horizontal wells used in previous studies;

   b) Modification to the injection and production ports to allow for a pattern inversion study;

   c) Modification to the scaled physical model for active bottom experiments; and

   d) Modification of an existing visual model to allow for steam injection.

2. Experimental Strategies

   a) Investigate the effect of shut-in, well locations and pattern inversion on the cumulative oil recovery;

   b) Investigate the effect of steamflooding steeply dipping homogeneous and bottom water reservoirs;

   c) Examine the dominant displacement mechanism; and

   d) Examine the effect of injecting gas during a steamflood to increase recovery

2.2 Theoretical Objectives

a) Interpret experimental results.

b) Calculate the oil saturations in each zone of a reservoir along with steam and water saturations.

c) Compare the steam zone volume obtained from experimental data with Neuman's steam override model, and Mandl and Volek's frontal drive model.

d) Develop a mathematical model to study the heat distribution for a typical experiment.

Chapter 3

REVIEW of the LITERATURE

3.1 Introduction

The use of horizontal wells for primary and secondary recovery of petroleum fluids (oil and/or gas) is becoming more widespread. The largely favourable responses obtained from various existing projects, coupled with the constant improvement in horizontal drilling technology and the corresponding reduction in horizontal drilling and completion costs, have encouraged increasing utilization of horizontal wells in the recovery of fluids from petroleum reservoirs.

The idea of drilling wells horizontally into a reservoir to increase the reservoir-wellbore contact area is not new. As early as 1919, attempts were made to drill horizontal drainholes from an existing vertical wellbore. Most of the early projects involving horizontal drainholes were unsuccessful, mainly because of the high cost and unreliability of drilling equipment. In the last 15 years, the depletion of the oil reserves in the United States and Canada has led to the introduction of new recovery technologies, including in particular horizontal well based technologies. In recent years, innovations in lateral drilling technology and tools have lowered the cost of horizontal wells, contributing directly to the widespread application of horizontal well technology.

Compared to a vertical well, a horizontal well enjoys several advantages including a higher productivity index, the ability to delay the breakthrough of unwanted fluids (that is, water and/or gas coning), and a higher probability of intersecting fracture networks in naturally fractured reservoirs. These advantages are discussed briefly in the next sections.

3.2 Productivity Index Increase due to Horizontal Wells

Vertical wells usually have only a small portion of their total length open to reservoir fluid flow. As the fluids move radially toward a vertical well, the area available for flow decreases; this leads to high flow velocities and pressure gradients. Most of the pressure drop occurs in the vicinity of the vertical wellbore. A horizontal well, on the other hand, provides a much larger area for the inflow of reservoir fluids due to its extended contact (through increased length) with the reservoir. Consequently, for identical flow rates, the

pressure drop in a horizontal well is lower. Therefore, the productivity index, which is defined to be the flow rate divided by the pressure drop, is much higher for a horizontal well as compare to a vertical well. This is illustrated in Figure 3.1.
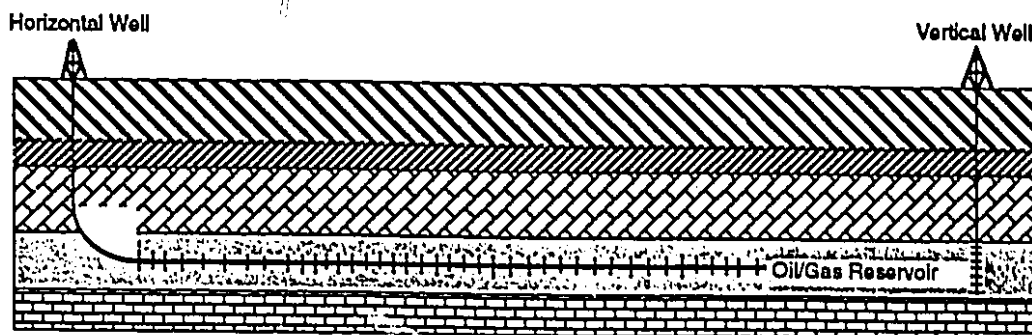
Figure 3.1: Horizontal well has more contact with the reservoir than vertical well in thin reservoirs.

Perrine[1] reported experimental data, using an electrolytic model, on productivity gains for a vertical well due to the presence of short horizontal drainholes connected with the vertical well. Several parameters were investigated including drainhole length, number and pattern of drainholes and well damage. Based on the experimental results, it was concluded that the drainhole length was most important in productivity gain. The increase in productivity was found to be directly proportional to the increase in the drainhole length. It was more effective in improving the productivity index than increasing the number of drainholes. The number and pattern of drainholes were found to have a lesser impact on the productivity gain than the length of each drainhole.

Giger, Reiss and Jourdan[2] provided mathematical equations for evaluating the productivity and water coning of horizontal wells. For a homogeneous and isotropic reservoir, an equation was formulated to compare the productivity indices of a horizontal well of length L and a fully penetrating vertical well of the same length. The horizontal well production rate was determined to be strongly influenced by vertical anisotropy, with higher rates achieved in the case of favourable anisotropy (as in reservoirs having vertical fractures). The authors also provided a formula to determine the critical production rate for a horizontal well. For multiphase flow, the authors determined that a horizontal well offers two advantages over a conventional vertical well: a smaller drawdown is required for identical flow rates, and the horizontal well can be placed optimally away from the oil-water contact.

Joshi[3] derived an analytical expression to calculate the steady state oil production rate for horizontal wells draining an elliptical drainage area. The influences of reservoir anisotropy, thickness, well drainage area and well eccentricity (that is, the well being positioned other

than at the centre of the reservoir) on horizontal well productivity were investigated. Water and gas coning tendencies of horizontal wells were also examined. Reservoir thickness, horizontal well length and reservoir anisotropy were found to be important parameters affecting the productivity of the horizontal well.

Karcher, Giger and Combe[4] reviewed previously derived formulas for horizontal well productivity. The authors also presented results obtained from a numerical model studying the areal sweep efficiency of horizontal wells in pattern floods. It was found that a horizontal well behaved like an artificial fracture when drilled along the lines of producers in a line drive-like pattern. As such, an areal sweep efficiency close to one was obtained.

Giger[5] developed equations for the pressure distribution and for steady-state flow into a given horizontal well using the theory of complex functions. By calculating the replacement ratio (the number of vertical wells required to drain the same area as a horizontal well), and by determining the ratio of areal productivity (ratio of productivity of same drainage area developed in one case by vertical wells, and in the other by horizontal wells), the author concluded that horizontal wells were highly suited for thin reservoirs. Also included in this study was a method for determining the optimum spacing of horizontal wells.

Ozkan and Raghavan[6] studied the performance of horizontal wells in bottom-water drive reservoirs. Analytical solutions were developed to study the pressure distribution in these reservoirs. The horizontal wellbore was represented mathematically by a line source, subject to either an infinite-conductivity or a uniform-flux boundary condition. It was concluded that the influence of anisotropy on horizontal well productivity was less significant than on vertical well productivity.

Babu and Odeh[7] developed an equation for determining the pseudo-steady state flow into a horizontal well. Two parameters were required in this equation: one to account for the effect of permeability anisotropy, location of the horizontal well and the relative dimensions of the drainage volume; and the other to consider the skin factor due to the restricted entry problem (the horizontal well length being less than the length of the drainage area). The authors concluded that the length of a horizontal well and its location in a drainage volume were the two most significant factors influencing well productivity.

Production forecasting methods were developed by Joshi[8] for four different types of reservoirs: homogeneous, naturally fractured, solution-gas drive and bottom-water drive. The methods were based on analytical solutions and correlations of numerical model results. Horizontal well performance was compared to that of stimulated vertical wells. Two conclusions were drawn: the use of a horizontal well was extremely effective for thin reservoirs and reservoirs with a high vertical permeability, and the productivity of a horizontal well exceeded that of a stimulated vertical well.

3.3 Suppression of Coning by a Horizontal Well

It has been determined that the use of horizontal wells often improves the recovery performance for reservoirs prone to water and/or gas coning by delaying the coning tendency. Horizontal wells, as explained above, reduce the pressure gradients in the vicinity of the wellbore, and consequently enable fluid production rates similar to those in the vertical well case for lower drawdown. Conversely, for a given drawdown a horizontal well could provide a much higher fluid production rate prior to coning than a vertical well. Another important reason is the capability of current lateral drilling technology to place a horizontal well at optimal horizons away from the oil-water contact and/or gas-oil contact. This is illustrated in Figure 3.2.
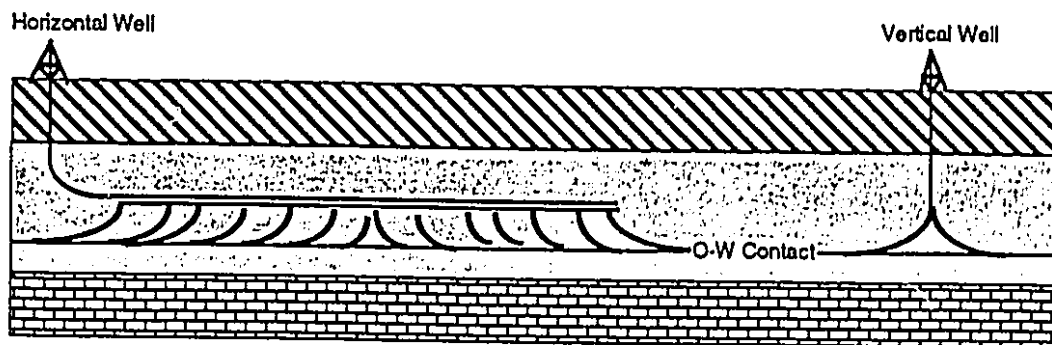
Figure 3.2: Water crests in horizontal well case, and water cones in vertical well case in reservoirs with water and/or gas coning tendency.

Chaperon[9] developed an equation to estimate the critical production rate of horizontal wells in anisotropic formations. The analysis, based on the work of Muskat[10], was for static and stable cones. By considering only flow in the plane perpendicular to the horizontal well axis, and by using static and dynamic equilibrium conditions the author derived an equation for calculating the critical fluid production rate per unit length of a horizontal well. The critical production rate per unit length of a horizontal well was found to be larger than that of a vertical well, and a function mainly of the horizontal transmissibility of the oil layer, and the distance between the horizontal well and the oil-water contact. In addition, the

critical production rate for horizontal wells was found to be not as susceptible to vertical permeability variation as that for vertical wells.

A semi-analytical approach to calculate cone breakthrough time for horizontal wells was developed by Papatzacos, Herring, Martinsen and Skjaeveland[11]. The oil-water contact and the gas-oil contact were treated as moving boundaries. Consequently, the shape and size of the cones became functions of both distance and time. An analytical solution for the standard Laplacian potential flow equation with a moving boundary was not possible; therefore, the resulting boundary-value problem was solved numerically. Three different cases were investigated: water coning, gas coning and simultaneous gas and water coning (two cones). The effects of water and gas viscosities, and different anisotropy ratios on the cone breakthrough time were also examined. Results generated compared closely with data obtained for the Helder field in the North Sea.

3.4 Intersection of Fracture Networks by a Horizontal Well

Naturally fractured reservoirs are usually modeled as composed of the matrix (which has large storativity but little or no permeability) and fracture networks (which, in contrast, have a small volume but very high permeability). As such, the fracture network serves as conduits for fluid flow from the matrix to the wellbore. In such a situation the productivity of a well is directly controlled by its intersection with the fracture network. In theory, a horizontal well can intersect several vertical fractures due to its horizontal orientation and length. A vertical well, on the other hand, can intersect at most one vertical fracture. Horizontal wells, as a result, have been employed extensively to exploit naturally fractured reservoirs worldwide. This is illustrated in Figure 3.3.
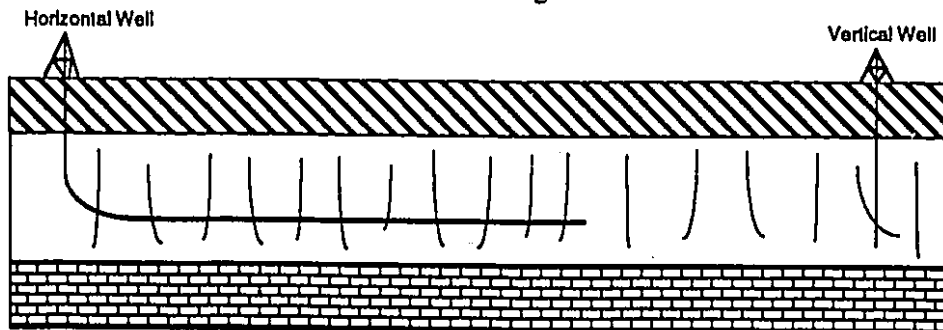
Figure 3.3: Horizontal well intersects multiple vertical fractures, vertical well intersects one vertical fracture.

According to a study by Sheikholeslami, Schlottman, Seidel and Button[12] horizontal wells drilled in the naturally fractured Austin Chalk reservoirs in Texas, depending on the length

of their horizontal interval, achieved productivities 2.5 to 7 times that of a typical vertical well. Bosio and Reiss[13] detailed the costs and productivity gains due to horizontal wells drilled in the Rospo Mare field. Typically, a Rospo Mare horizontal well costs about 50% more than a vertical well, and yet it achieved 4-6 times the productivity of the vertical well.

An extension of the above application of horizontal well technology is enhancement of the productivity of wells draining tight reservoirs by artificially creating vertical fractures around horizontal wells. Damgaard, Bangert, Murray, Rubbo and Stout[14] reported a project in the Danish Chalk, offshore Denmark, which utilized such artificially fractured horizontal wells. These fractured horizontal wells, about 40-50% more expensive than previously employed fractured vertical wells, attained productivities 4-6 times those of nearby fractured vertical wells.

3.5 Application of Horizontal Wells for Thermal Oil Recovery

Many heavy oil reservoirs in southeastern Alberta and Saskatchewan are thin (5-10 meters of pay), and are often in communication with a bottom-water zone. The heavy oils in these reservoirs are mobile under initial reservoir conditions, but the primary recovery typically amounts to approximately 5% of the initial oil in place (IOIP) before water breakthrough. In a few cases where conditions are more favourable the use of horizontal wells has increased the primary recovery to 15-20% prior to water coning. Conventional steam injection recovery processes, such as cyclic steam stimulation and steamflooding using vertical wells, have proven to be unsuitable for these reservoirs. The main reasons include excessive heat loss to the cap rock, and diversion of injected steam into the bottom water zone.

Horizontal wells, on the other hand, hold great promise for the recovery of heavy oils remaining in these marginal reservoirs. This is due primarily to the extended contact between the reservoir and a horizontal well, leading to higher productivity and sweep efficiency. In addition, horizontal wells can be placed optimally to delay gravity segregation and/or minimize heat loss to unproductive zones such as cap rock and bottom water zones. In Fort McMurray and Peace River, horizontal wells are drilled into the oil sand deposits to provide the initial communication channels necessary for steam injection into the reservoirs. Their extended contact area with the reservoirs enables accelerated heating of the reservoir, and mobilization of the bitumen.

The required well spacing in California heavy oil reservoirs often is very small (2-5 acres) in order to achieve reasonably high efficiency for conventional steam recovery processes such as cyclic steam stimulation and steamflooding. The small well spacing requirement is expensive, leading to high drilling costs as well as high operating and maintenance costs. Horizontal wells, on the other hand, can increase significantly the contact area with the reservoir; this leads to accelerated mobilization of the heavy oils, and hence a higher oil production rate. As a result, the economics of these operations can be improved substantially due to lower investment and accelerated payouts.

3.5.1 Steam Assisted Gravity Drainage (SAGD)

In the Steam Assisted Gravity Drainage (SAGD) process, as presented by Butler, McNab and Lo[15], two parallel horizontal wells were used in an oil sand pack. The upper horizontal well was the steam injector, while the bottom horizontal well was the producer. Steam was injected continuously into the sand, leading to the formation of a steam zone. As the steam moved upwards (by gravity) and sideways it condensed at the steam-oil interface, leading to heat transfer by conduction to the sand, and the oil mobilization ahead of the steam front. The mobilized oil and the condensate were drained by gravity downwards into the horizontal producer below the injector. The path of flow for the oil and condensate was along the edge of the steam zone interface, and opposite in direction to that of steam.

Material balances inside the steam zone were not considered. Rather, material balance was performed on the oil being heated at the interface and the oil being drained by gravity. Due to the high viscosity of bitumen, incompressible fluid flow was assumed. It is important to note that the model assumed conduction as the dominant mode of heat transfer, and the entire process was localized at the interface. Convective heat transfer ahead of the steam zone interface was not considered, and the mobility of the bitumen ahead of the interface was assumed to be zero. Of these assumptions the latter was acceptable, but the former was not. The rate of heating (melting) the bitumen in front of the interface at a later time was obviously smaller, due to the fact that heat had conducted into this region previously.

Butler and Stephens[16] modified the above model to eliminate movement of the interface away from the production well with time. The authors also extended the original theory to account for drainage into a series of parallel wells. An equation was derived to approximate the time required for the steam zone to move horizontally to the no-flow plane

between patterns, each of which included a horizontal steam injector and producer. Photographs of the steam zone, taken at different times during an experiment, illustrated the growth of the steam zone, as well as the gravity drainage of oil and condensate into the horizontal producer. Experimental results were found to be in reasonable agreement with those predicted from the modified theory.

In the above studies[15-16], the growth of the steam chamber in the vertical direction (that is, from the base to the top of the reservoir) was not considered. This led to some discrepancy between experimental and theoretical results in initial production periods during which the steam zone grew predominantly in the vertical direction, rather than sideways. Butler, Stevens and Weiss[17] considered both the vertical growth rate and the lateral growth rate of the steam zone as it gradually moved upwards. The authors assumed that the steam zone was circular in shape, with the horizontal well at its centre. The rate of growth of the steam zone was then postulated to be the rate of increase in its radius. An equation predicting the height of the steam zone as a function of time was derived. The agreement between scaled laboratory experimental results and this analytical model was reported to be good.

Griffin and Trofimenkoff[18] performed experimental studies of the SAGD process to support Esso Resources Canada LTD's Cold Lake horizontal well pilot. Experiments in scaled physical models, including both visual low-pressure models and high-pressure models, were designed according to the scaling group reported by Butler et al.[15]. Results from the visual-model experiments showed little steam override at the top of the reservoir. Production rates from the high-pressure model were substantially higher than the theoretically calculated values. The extra production was believed to have been due to displacement from end regions of the steam zone.

Edmunds, Haston and Best[19] reported results obtained in the SAGD pilot at the AOSTRA Underground Testing Facility (UTF) in Fort McMurray. The effects of anisotropy, heterogeneities, solution gas and capillary pressure on steam zone growth rate were examined. The steam zone growth rate was analyzed in terms of ceiling drainage (taking place at the top of the rising steam zone) and slope drainage (occurring at the sides of the sideway-spreading steam zone). A description was also given of the drilling and completion of the three pairs of horizontal injector-producer wells.

Butler and Petela[20] studied the steam zone expansion during the SAGD process. The steam zone was observed to grow, initially, downward between the horizontal injector and

producer, with the growth rate controlled by the pressure gradient and the thermal properties of the reservoir. Based on the assumption of single-phase flow for oil and steam condensate, the authors developed an analytical expression for the breakthrough time. In addition, several analytical expressions were developed to determine the advancement of the steam zone in a two-dimensional system.

Sugianto and Butler[21] attempted to study the effectiveness of the SAGD process in a bottom-water reservoir using a scaled visual model. The scaling groups used to build the model were similar to those established previously by Butler et al.[15]. The optimal recovery strategy determined from the experiments was to place the horizontal producer near the oil-water contact to ensure maximum drainage, and hence recovery of oil. To prevent water coning, the production pressure was kept approximately identical to or slightly higher than the pressure in the aquifer. The authors also noted that the thickness of the bottom water zone had a significant effect on cumulative recovery .

3.5.2 Steamflood

3.5.2.1 Scaled Physical Model Studies

Huygen and Black[22] investigated the effectiveness of different injection and production strategies using vertical and horizontal well combinations for steamflooding Athabasca oil sand. The investigation, based on scaled-model experiments, showed steamflood recovery performance being significantly dependent on geometry and communication between the injection and production well. The authors concluded that in the case of oil sands, communication between wells was necessary to provide initial injectivity. Horizontal wells were judged to be an effective means for providing this communication in the reservoir. Experimental recovery results were believed to be optimistic, as oil saturations in the model were higher than in the field. On the other hand, oil recovery results obtained from the experiments were deemed to be conservative, given the fact that the model horizontal permeability (relative to its vertical permeability) was lower than in the field.

Chang, Farouq Ali and George[23] reported results of scaled, low-pressure model experiments designed to study the effectiveness of different horizontal and vertical well combinations in steamflooding a bottom-water heavy oil reservoir. It was determined that the combination of a horizontal injector and a horizontal producer achieved the highest oil recovery in a homogeneous reservoir as well as in a reservoir with bottom water. In the

case of a reservoir having a thick bottom-water zone (bottom-water zone thickness being 50% of total pay) a horizontal steam injector was more effective than a vertical injector in preventing steam from going into the water zone.

Mathias, Doan, Farouq Ali and George[24] examined different strategies for steamflooding a reservoir having a thick bottom water layer (bottom water thickness of 50% of total pay). It was determined that there was an optimal horizontal well length beyond which oil recovery did not increase with horizontal well length. Strategies for steamflooding unfavourable and favourable stratified reservoirs were also investigated. In these cases horizontal well placement proved to be an important factor affecting sweep efficiency and oil recovery. Experimental production rates were scaled up using scaling criteria to predict field performance.

3.5.2.2 Numerical Simulation Studies

Dietrich[25] described a Kern River pilot in which eight ultra-short radius horizontal wells of varying lengths were drilled radially, in a spoke-like fashion, from a common vertical shaft. The horizontal wells were arranged in a spoke-like fashion, 45° apart from each other, and used for production. Poor oil response in the initial periods was attributed to the placement of the horizontal wells in a highly unfavourable reservoir environment. The termination of the pilots was followed by numerical studies to develop better operating strategies and to predict future potential. The main conclusion derived from the simulation studies was that horizontal wells can be effective for reducing steam override.

Rial[26] developed a simulator to examine the effectiveness of utilizing a horizontal steam injector in steamflooding a heavy-oil reservoir. The simulator was three-dimensional and three-phase. The distillation effect, temperature-dependent relative permeabilities and gravitational as well as with viscous and capillary forces were included in the simulator. The data used as input for the runs were representative of the Kern River field. A horizontal injection well was seen to achieve better areal sweep efficiency, as compared to a vertical injector. In addition, more heat swept through the grid system in the horizontal well case than in the vertical well case. For the Kern River prototype, up to 71% of the initial oil in place was recovered with the horizontal steam injector, compared to only 58% with the vertical steam injector for the same period of steam injection.

Jain and Khosla[27] examined the recovery performance of three combinations of vertical and horizontal wells in steamflooding Athabasca bitumen. The first combination had two 150-m long parallel horizontal wells separated by a distance of 60 m, the second combination had a 300 m-long horizontal steam injector in communication with a vertical producer, while the last combination had a 400 m-long horizontal producer positioned below two vertical steam injectors in communication with one another to create a heated plane over the horizontal well. In the first two configurations the steam drive process was modeled, while the SAGD process was modeled in the last configuration. The simulation results, obtained from a commercial simulator, showed that the last well combination achieved the highest oil production rates and the highest cumulative oil recovery.

The effectiveness of horizontal wells to reduce steam override in a mature steamflood, and prevent steam override in new operations was examined by Huang and Hight[28]. A thermal, three-dimensional, three-phase simulator accounting for gravitational, viscous and capillary forces, and temperature-dependent relative permeabilities was used. Both conductive and convective heat transfer were modeled. Reservoir properties for a typical California unconsolidated, heavy oil reservoir were used for the runs. For mature steamflood operations, horizontal wells were found to be effective in recovering oil in areas bypassed by steam. In new steamflood projects, horizontal wells not only improved but also accelerated oil recovery. In addition, they led to a reduction in oil saturation in blind spots from 60% to 30%.

Combe, Burger, Renard and Valentin[29] numerically investigated the steamflood performance improvements due to horizontal wells. Parameters studied included a wide range of fluid and reservoir properties, injection strategies, reservoir heterogeneity (that is, layered reservoirs) and spatial distributions of vertical and horizontal wells. It was concluded that the optimal strategy in layered reservoirs was to drill horizontal wells in different layers, rather than drill all wells in one layer. Also, horizontal wells were more effective in thin heavy oil reservoirs with low oil mobility.

In conclusion, horizontal wells can improve the recovery performance of conventional thermal recovery methods. Their most important contribution is to reduce steam override (gravity segregation) which results in better steam sweep efficiency. In addition, they offer high oil production rates, accelerated recovery and an improved oil-steam ratio.

3.6 Predictive Models for Steamflooding Performance

Over the years many models have been developed to determine the expansion of the steam zone volume, and hence the oil production rate. A discussion of several models is provided below.

3.6.1 Frontal Drive Models

Marx and Langenheim[30] presented the first study (1959) of oil recovery by steam injection. In this study, a relationship between the steam zone growth rate and the heat loss rate to the overburden and base rock was established. The front separating the steam zone and the unheated reservoir was assumed to be vertical. Heat transfer between the steam zone and its surroundings, including the cap and base rock, was by conduction. Heat flow from the steam zone into the liquid zone ahead of the condensation front was, however, not considered.

Mandl and Volek[31], in 1969, modified Marx and Langenheim's model[30] to account for heat transport from the steam zone into the condensate zone ahead of the front, which affects both the flow of condensate and the growth of the steam zone. Changes in the shape of the front as a function of time, and viscosity and density contrasts between the fluids were not incorporated into the model, due to their complexities. The heat balance, along with the mass balance equations, were applied to regions behind and ahead of the interface leading to a critical time, t_c. The critical time depended on reservoir thickness, temperature, steam quality, volumetric heat capacity, thermal conductivity and heat capacity of the overburden. It signified an important change in the mode of heat transfer across the condensation front. For time $0 < t < t_c$, the mode of heat transfer was predominantly conductive, while for $t \geq t_c$ the transfer of heat was predominantly convective. Correspondingly, two expressions were given for calculation of the steam zone volume (V_s).

$$V_s = \frac{Q_i M_s H_t^2}{4 k_{hob} M_{ob}(T_s - T_R)} \cdot F_1 \qquad (t < t_c)$$

and

$$V_s = \frac{Q_i M_s H_t^2}{4 k_{hob} M_{ob}(T_s - T_R)} \cdot F_3 \qquad (t \geq t_c)$$

where F_1, and F_3 were defined as,

$$F_1 = e^{t_D} erfc\sqrt{t_D} + 2\sqrt{\frac{t_D}{\pi}} - 1$$

and

$$F_3 = e^{t_D} erfc\sqrt{t_D} + 2\sqrt{\frac{t_D}{\pi}} - 1 -$$
$$\sqrt{\frac{t_D - t_{Dc}}{\pi}}\left\{ \left[1 + \frac{f_{sl} L_v}{c_w(T_s - T_R)} \right]^{-1} + \left(\frac{t_D - t_{Dc} - 3}{3} \right) e^{t_D} erfc\sqrt{t_D} - \frac{t_D - t_{Dc}}{3\sqrt{\pi t_D}} \right\}$$

In the above definition, the dimensionless time is given by,

$$t_D = \frac{4k_{hob}M_{ob}}{M_s^2} \cdot \frac{t}{h_t^2}$$

For $t < t_c$, Mandl and Volek[31] determined that the steam zone volumes for both models (that is, Marx and Langenheim's and Mandl and Volek's) were identical.

In 1978, Myhill and Stegemeier[32] developed a third frontal-drive model. The following assumptions were made. There was no vertical temperature gradient in the reservoir, the steam injection pressure and steam quality were constant, the heat losses from the steam zone to the overburden and base rock were conduction-dominated and the heat transfer inside the reservoir was by convection. A parameter for thermal efficiency, E_{hs}, was combined with expressions given by Mandl and Volek[31] to give the thermal efficiency of the steam injection process prior to steam breakthrough. The volume of steam required to be injected was then calculated from these parameters: E_{hs}, the heat contained in the steam zone, and the energy content of the steam.

3.6.2 Gravity Override Models

Van Lookeren[33] , in 1977, presented a gravity override model derived from segregated flow principles. He developed formulas for approximating the steam zone volume in both linear and radial steam drives, and found the shape of the steam zone to be dependent on the steam injection rate, pressure and effective formation permeability to steam. From

segregated flow principles, an expression describing the tilt of the interface; that is, the relationship between the height of the steam zone versus horizontal distance, $\partial h_{st}/\partial x$, was obtained.

$$\frac{\partial h_{st}}{\partial x} = \frac{\mu_{st} \cdot w_{st}(x_b)}{(\rho_o - \rho_{st})gh \cdot k_{st}\rho_{st} \cdot b \cos\alpha} \cdot (1 - M^*) + tg\alpha$$

where M^* is the pseudo-mobility ratio, defined by the following

$$M^* = \frac{\mu_o k_{st}}{\mu_{st} k_o} \cdot \frac{\rho_{st} w_o(x_e)}{\rho_o w_{st}(x_b)}$$

This pseudo-mobility ratio was obtained from a combination of the flow and material balance equations. It was noted that as the fluid viscosity increased, the interface became more vertical. Two dimensionless groups (A_{LD} and A_{RD}) were also defined to characterize the shape of the interface. The dimensionless groups were found to depend on steam injection rate, quality, density of fluids and steam viscosity. An expression for calculating the oil displaced from the steam zone was also given.

Neuman[34] presented a comprehensive gravity override model for a steam drive process. In this model, two important assumptions were made: steam rose quickly to the top of a permeable reservoir, and the horizontal pressure gradient in the steam zone was much less than the vertical pressure gradient of liquids which resulted from density variations. The time required for the steam to rise to the reservoir top was much less than the time required to heat the entire reservoir area. Continuing steam injection eventually led to the downward areal expansion of the steam zone, from the reservoir top towards the reservoir base. Parameters such as velocity of the steam-liquid interface, steam zone thickness, volume of oil displaced from the steam zone, steam injection rate required to sustain the growth of the steam zone and the additional oil displaced after termination of steam injection were calculated successively.

In the model presented by Miller and Leung[35] complete vertical overlay of steam zone, that is, 100% areal coverage, was assumed. In developing the model, the authors purposefully left out certain features to keep it simple. The production of oil from the reservoir was assumed to be dominated by conductive heating, and the production was proportional to the depth integral of $1/\mu_o$ in the oil zone. The temperature distribution of the condensate and

the oil zone beneath was determined using a one-dimensional, unsteady state heat conduction equation.

Kumar, Patel and Denbina[36] presented a model to predict the height of the steam zone. This model was a variation of Miller and Leung's[35] model. Two important assumptions were made: the injected steam rose to the top of the reservoir from the outset of a steamflood, and conductive heat transfer was the principal mechanism by which the oil underneath was heated. As heat propagated downwards into the oil column, oil viscosity was no longer a function of temperature alone; rather, it also became a function of distance and time of exposure to the heat flux. This model was different from Miller and Leung's[35] model in its consideration of the temperature distribution as a moving heat source, as well as the fact that there was no need to specify an oil production rate prior to steam injection. For cases of immediate steam override from the beginning of the steamflood the effect of convective heat transfer was considered minimal, due to counteracting gravitational and viscous forces. As such, conductive heat transfer remained the principal mechanism by which oil was mobilized.

3.6.3 Combined Frontal-Gravity Override Models

Jones[37] developed a semi-analytical model to predict the growth of the steam zone for a personal programmable calculator. This model was based on published studies by van Lookeren[33] and Myhill and Stegemeier[32]. The model considered all three production stages normally observed in the life of a steam drive project. The model achieved good prediction of the production rate for various reported field data. On the other hand, the model had to rely on several empirical equations to obtain a good match for the displacement process.

Farouq Ali[38], in 1982, presented a semi-analytical model for predicting the performance of a steamflood. Both frontal displacement and vertical displacement of steam during a steamflood were accounted for in this model which combined van Lookeren's[33] equation to estimate the reservoir thickness swept by steam with Mandl and Volek's[31] equation to determine the steam zone volume. Knowledge of these parameters enabled the average temperature ahead of the steam front, the oil viscosity and the oil production rate to be determined from material balance considerations. Empirical correlations were used for the relative permeability functions. The calculation was repeated iteratively to advance the

solution up to the time of steam breakthrough. This model accurately predicted the production rate for the Kern A River pilot project.

Chen and Sylvester[39] modified Farouq Ali's model[38] by incorporating fractional-flow theory to determine the oil saturation in the unswept zone. These authors compared their model with those of Jones[37], and Miller and Leung[35], and found good prediction for the oil production rate without requiring any empirical factors or adjustable parameters. The predictive capability of this model was found to be strongly dependent on the relative permeability relationships. As such, appropriate expressions for the relative permeabilities (k_{ro}, k_{rw}) were important for obtaining a good history match.

In conclusion, knowledge of the displacement mechanism in the reservoir is very important to the performance prediction of a steamflood. Inability to recognize this fact can lead to improper application of the predictive models presented above.

3.6.4 Material-Balance Application for a Steamflood

Peake[40] presented a simple steamflood material balance for both a two-zone and a three-zone reservoir model. The presence of an initial hydrocarbon gas saturation in the reservoir, pore volume change due to compressibility and a material balance for steam, condensate and oil were included in the analysis. Symmetric fluid flow between the injection and production wells, no steam flow from the control volume and insignificant steam production after steam breakthrough were assumed.

The material balance equations, derived by Peake[40], predict the oil and water production when fluid (oil, water and steam) saturations are known. In the reverse sense, the same material balance equations can be used to determine the fluid saturations – when accurate injection and production data are available – by solving a system of equations.

3.7 Steamflooding Dipping Reservoirs

As noted above, recovery strategies are highly dependent on reservoir geology. This is particularly true in the case of steam injection recovery processes. A brief discussion of the effects of reservoir geology on the steam injection recovery process is given below.

Steamflooding strategies for a steeply dipping reservoir are different from those for reservoirs having little or no dip. Repeated patterns, such as the inverted nine-spot or five-spot are commonly used in non-dipping reservoirs. In steeply dipping reservoirs, the location and elevation of the injectors and producers is often selected to take advantage of natural gravity segregation to improve sweep efficiency and thus oil recovery. From a physical and mathematical viewpoint the assumption of no-flow boundaries between patterns is not valid in the case of steeply dipping reservoirs. As such, allowance for fluid movement due to gravity has to be incorporated into the mathematical models.

Moughamian, Woo, Dakessian and Fitzgerald[41] used a three-dimensional, finite-difference steam injection simulator to study steamflooding a steeply dipping (53°) heavy oil reservoir in California. Sensitivity studies were made to select the best operating parameters. Based on the simulation results, the authors concluded that the most important parameter affecting cumulative oil recovery was the areal sweep efficiency. In addition, low oil recovery was obtained when the producers were aligned in a direct line-drive pattern with respect to the injectors. The sweep efficiency in this case was much less than when the rows of injectors and producers were staggered, with a row of injectors up-dip, and a row of producers down-dip.

An energy balance, including heat loss to the cap rock as a result of injecting steam up-dip, was not considered in this work. In addition, some inconsistencies arose in the comparison of results for the different patterns, and the calculated oil recovery was affected by the discretization schemes (11-point and 7-point).

Hong[42] used a compositional steamflood simulator to study steamflooding strategies in a steeply dipping reservoir, and to examine the recovery mechanisms in effect during a steamflood. The strategies studied included shutting in up-dip producers after steam breakthrough or occurrence of high steam-oil ratio (SOR), switching injectors and producers during drainage to maximize oil recovery and injecting a non-condensable gas (for example, nitrogen) to prevent steam cycling in the up-dip portions of the reservoir. It was determined that gravity drainage of the heated oil was the main production mechanism in steeply dipping reservoirs. As such, the location of the injectors and producers must be carefully chosen in order for oil production to be maximized. The following strategy was recommended: initiate the steamflood (in a line-drive configuration) with the injection of steam into the middle or lower portion of the reservoir, to be followed by shutting in the up-dip producers to prevent heat loss due to steam breakthrough or a high SOR, reducing

the steam injection rate to lower the SOR and finally injecting a non-condensable gas into the up-dip portions of the reservoir to prevent or reduce steam cycling effects.

3.8 Scaling Criteria

The experiments in this study were performed in a scaled physical model. Thus, a review of scaling principles in experimental studies of oil recovery processes is in order. Leverett, Lewis and True[43] were among the first investigators who applied scaling laws (viz. dimensional analysis) to model fluid flow in petroleum reservoirs. The dimensionless groups governing the water drive process were derived. Rapoport and Leas[44] examined the various parameters, through the use of scaling groups, involved in the displacement of light oil by cold water. Offeringa and van der Poel[45] also used dimensional analysis to obtain scaling criteria for their models designed to study oil recovery by solvent injection.

Geertsma, Croes, and Schwarz[46] pointed out that in general the set of dimensionless similarity groups obtained from dimensional analysis is larger than that obtained from inspectional analysis. However, the physical meaning of the similarity groups derived by dimensional analysis is generally less apparent than those derived by inspectional analysis. Rojas and Farouq Ali[47] combined dimensional analysis and inspectional analysis to derive all of the scaling groups governing the carbon dioxide/brine immiscible flooding of heavy oils.

Work dealing specifically with scaling of steam injection processes has been carried out by a number of researchers. Pujol and Boberg[48] found that accurate scaling of the capillary pressure was not crucial for recovery performance prediction for highly viscous oils. In these instances the ratio of capillary to viscous forces was so small that unscaled capillary pressures had little effect on oil recovery. On the other hand, capillary pressure had an important effect when the oil viscosity was less than 1000 mPa.s; not scaling the capillary pressure resulted in optimistic oil recovery. The heat input per unit volume of reservoir sand was determined to have the most significant influence on ultimate oil recovery.

Farouq Ali and Redford[49] examined scaling groups derived by various investigators for steam injection and in-situ combustion processes. They presented a comprehensive review of notable scaled laboratory thermal recovery studies. Kimber, Farouq Ali and Puttagunta[50] employed both dimensional analysis and inspectional analysis to obtain dimensionless similarity groups for steam and steam-additive injection processes. As a

result of the impossibility of satisfying all scaling criteria, sub-sets of scaling criteria were derived by the authors to scale individual mechanisms involved in the process, while neglecting others. In this work, geometric similarities were distorted (length, height and width ratios were different from each other) in order to satisfy the scaling criteria for reservoir fluids and porous medium properties.

Stegemeier, Laumbach and Volek[51] developed scaling criteria for low pressure models – which have been used by many investigators – to study the Mt. Poso and Midway Sunset steamflood projects. The authors used inspectional analysis to obtain the dimensionless similarity parameters. The steamflood experiments were carried out in these models at pressures below atmospheric pressure. The quantity of steam injected was found by these authors to be the most important factor affecting oil recovery performance.

Using a low pressure model – design based on the scaling criteria developed by Steigemeier et al.[51] – Kristoff[52] made experimental studies along with numerical studies of the Tangleflags steamflood. He found that the experimental results were in close agreement with field observations. However, numerical simulation results were different despite many adjustments of the reservoir description.

A model similar to the one used in this investigation was first designed by Proctor[53]. He applied the low pressure scaling criteria presented by Stegemeier et al.[51] and built the three-dimensional model that represented one-quarter of a five-spot in the Aberfeldy reservoir. This work was followed by Oracheski[54], Chang[55] and Matthias[56]. Oracheski[54] studied the effect of injecting a small solvent slug prior to steamflooding a bottom water reservoir. Chang[55] studied various strategies for steamflooding bottom water reservoirs having different thicknesses. Matthias[56] changed the injection system used in previous studies[53-55] and studied the application of horizontal wells to steamflooding bottom water reservoirs.

Doan, Farouq Ali and George[57] presented scaling criteria for flow in the vicinity and inside a horizontal well. Two criteria were derived: one for the flow from the reservoir into the horizontal well, and the other for the flow inside the horizontal well. Different types of horizontal well and horizontal well completion types were determined experimentally, with the results showing wellbore geometry having an influence on steam distribution and oil recovery.

Chapter 4

SCALING PARAMETERS and EXPERIMENTAL DESIGN

The use of physical models to study various transport phenomena and displacement processes has received considerable use in the petroleum industry. The models are often classified into three groups: partially scaled, fully scaled and unscaled. All "scaled" models are really partially scaled. Which group is not satisfied depends on practical considerations and on the desired modeling criteria. Perfectly scaled models are almost impossible to design and are also unnecessary. Unscaled models serve to observe phenomenon which may occur during a displacement process. The results are qualitative only; that is, they cannot be scaled up.

4.1 Attributes of Scaled Models

The use of scaled steamflood models have contributed significantly to the design, implementation and operation of many fields projects. They are one of the tools often used by engineers to determine: injection rate(s), pattern size and type, sensitivity studies for bottom water and performance prediction for a steamflood.

Conducting scaled model experiments to predict different injection and production strategies is not the only reasons why scaled model studies are important. They are also important because scaled physical models have the ability to retain the interaction between different physical processes and phenomena in the reservoir. As a result, one can gain insight into processes for which relationships are not known or are difficult to formulate.

Stegemier, Laumbach, and Volek[51] indicated that the Clausius-Clapeyron relation is one of the most important, and most difficult, relations to match precisely in a scaled steamflood model. When this relationship is not properly matched, the temperature and pressure in the steam zone will not correspond to each other. If this is the case, then the flow rates will not be scaled after steam breakthrough. The authors suggested that with sub-atmospheric pressures, the approximation is greatly improved.

4.2 Development of Scaling Parameters for the Low Pressure Model

A fully scaled model is usually difficult to design. This is attributed to the availability of materials and fluids having physical properties that satisfy all scaling requirements. Also, knowledge relating to reservoir description is often lacking. As a result, a compromise is made by using what is available and by seeing which parameters need to be scaled and which parameters can be relaxed. Now-a-days, most models used in laboratories are partially scaled. From here onwards, the use of the term "scaled model" implies a partially scaled model.

The design of the present low pressure steamflood model was based on the work published by Stegemier et al.[51]. The scaling of the horizontal well was developed by Doan et al.[57]. In the sections below, the technique for obtaining the dimensionless similarity groups is described briefly. The application of these groups to the scaled model is discussed in detail. Sample calculations for scaling up or down are illustrated also.

4.2.1 Unscaled Parameters

As mentioned earlier, complete scaling of different aspects of the steamflood process is not possible. In this study, the factors which were unscaled between the model and prototype were: 1) steam distillation of the crude oil, 2) capillary pressure and relative permeability, 3) thermal expansion and compression of the reservoir fluids and the matrix, 4) emulsification, 5) asphaltene flocculation and 6) specifications corresponding to the injection and production of a horizontal well (such as: pressure drop in the vicinity of and within the well-bore, skin factor, and perforation intervals).

4.2.2 Scaling Procedure

The scaling parameters are obtained by the following procedure. The derivation of the scaling groups starts with the derivation of the governing equation for fluid flow and heat transfer, in its most complete form. Next, they are put into a dimensionless form by dividing the dimensional variables m by a suitable reference quantity (m_R). Once, the dimensionless equations are completed, inspectional analysis is used to obtain the similarity parameters. For the majority of the physical models, it is almost impossible to satisfy all of the similarity parameters. Therefore, these groups are combined and/or modified, based on

engineering judgment, to obtain a new set of scaling parameters. These are generally matched between the model and the field prototype.

In the derivation of scaling criteria for the low pressure steamflood model, Stegemeier et al.[51] made the following assumptions:

1) Three phases may exist consisting of: an oleic phase, an aqueous phase, and a steam vapour phase (no volatile hydrocarbons).

2) There is no partitioning into or out of the oil phase (dead oil assumptions).

3) Rock compressibility and thermal expansion are negligible.

4) Darcy's and Fourier's equations are valid.

5) Capillary pressure effects are negligible.

6) The system is in local thermodynamic equilibrium.

7) Kinetic energy, potential energy and viscous dissipation energy are negligible compared with the thermal energy.

8) The enthalpy and internal energy are essentially equal for the oleic phase and for the aqueous phase, and are linear functions of the temperature.

9) The difference between the steam enthalpy and internal energy can be neglected.

10) The time rate of change of the specific steam enthalpy in the steam zone is negligible.

11) The internal energy of the rock is a linear function of the temperature.

12) The saturated steam temperature is the maximum temperature at any location.

13) Relative permeabilities depend exclusively on the saturations.

14) S_{orst} and S_{wc} are constant and uniform throughout the model.

15) Critical gas saturation for steam flow is assumed to be zero.

16) Changes in the density of the immovable water and residual oil are negligible.

From the list of assumptions made above, assumption 13 is the most serious. Relative permeabilities have been found to be temperature dependent. As a result of this assumption, the shape of the relative permeability curves based on the movable saturation between the model and the prototype further deviate from each other.

The formulation for the conservation of mass for oil and water (in both the liquid and vapour phase), the conservation of energy for the reservoir, Darcy's equation and Fourier's equation, the heat conduction in the cap and base rock and the constraints on the boundary

and initial conditions were given in Appendix A of Stegemeier et al.[51]. The dimensionless form of these equations is obtained as follows[51]

the conservation of mass for the oleic phase is:

$$\left(\frac{\phi_R S_R L_R}{v_R t_R}\right)\phi_D \frac{\partial(\rho_{oD}S_{omD})}{\partial t_D} + \nabla_D \bullet \left(\rho_{oD}\overrightarrow{V_{oD}}\right) = 0 \qquad \cdots\cdots \quad (4.1)$$

the conservation of mass for the liquid and vapour phase of water:

$$\left(\frac{\phi_R S_R L_R}{v_R t_R}\right)\phi_D \frac{\partial(\rho_{wD}S_{wmD}+\rho_{sD}S_{sD})}{\partial t_D} + \nabla_D \bullet \left(\rho_{wD}\overrightarrow{V_{wD}} + \rho_{sD}\overrightarrow{V_{sD}}\right) = 0 \qquad \cdots\cdots \quad (4.2)$$

the combined energy equation and Fourier's equation:

$$\left(\frac{\rho_{cR}C_{cR}}{\phi_R S_R \rho_R C_R}\right)\left[(1-\phi)\rho_R C_R + \phi(\rho_o C_o S_{ors} + \rho_w C_w S_{wc})\right]_D \frac{\partial T_D}{\partial t_D} + \phi_D\left(\rho_{oD}C_{oD}S_{omD}+\rho_{wD}C_{wD}S_{wmD}\right)\frac{\partial T_D}{\partial t_D}$$

$$+\left(\frac{L_{vR}}{C_R T_R}\right)L_{vD}\left[\phi_D \frac{\partial(\rho_{sD}S_{sD})}{\partial t_D} + \frac{v_R t_R}{\phi_R S_R L_R}\nabla_D \bullet \rho_{sD}\overrightarrow{V_{sD}}\right] + \left[\frac{v_R t_R}{\phi_R S_R L_R}\left(\frac{L_{vR}}{C_R T_R}+1\right)\right]\rho_{sD}\overrightarrow{V_{sD}}$$

$$\bullet\nabla_D(L_{vD}+c_{wD}T_D)+\left(\frac{v_R t_R}{\phi_R S_R L_R}\right)\left(\rho_{oD}C_{oD}\overrightarrow{V_{oD}} + \rho_{wD}C_{wD}\overrightarrow{V_{wD}}\right)\bullet\nabla_D T_D$$

$$-\left(\frac{k_{hR}t_R}{\phi_R S_R \rho_R C_R L_R^2}\right)k_{hD}\nabla_D^2 T_D = 0 \qquad \cdots\cdots \quad (4.3)$$

Darcy's equation:

$$\left(\frac{\mu_R v_R L_R}{k_R p_R}\right)\overrightarrow{V_{jd}} = \frac{k_d k_{rj}}{\mu_{jD}}\left[\nabla_D p_D - \left(\frac{\rho_R g_R L_R}{p_R}\right)\rho_{jD}\overrightarrow{g_D}\right] \qquad \cdots\cdots \quad (4.4)$$

the heat conduction in the cap rock and base rock:

$$\rho_{cD}C_{cD}\frac{\partial T_D}{\partial t_D} = \left(\frac{k_{hR}t_R}{\rho_{cR}C_{cR}L_R^2}\right)k_{hcD}\nabla_D^2 T_D \qquad \cdots\cdots \quad (4.5)$$

the upper and lower boundary conditions:

$$k_{hrD}\left(\frac{\partial T_D}{\partial n_D}\right)_r^{ub} = k_{hcD}\left(\frac{\partial T_D}{\partial n_D}\right)_c^{ub} \qquad \dots (4.6)$$

the mass injection rate:

$$\left(\frac{w_R}{\rho_R v_R L_R^2}\right)w_D = \pi d_D \int_0^{z_{tD}} \frac{1}{\cos\theta}\left(\rho_{wD}v_{wnD} + \rho_{sD}v_{snD}\right)dz_D \qquad \dots (4.7)$$

and the energy injection rate:

$$\left(\frac{w_R}{\rho_R v_R L_R^2}\right)\left[\left(\frac{f_{sR}L_{vR}}{C_R T_R}\right)f_{sD}L_{vD} + C_{wD}\Delta T_D\right]$$

$$= \pi d_D \int_0^{z_{tD}} \frac{1}{\cos\theta}\left[\rho_{wD}C_{wD}v_{wnD}\Delta T_D + \left(\frac{h_R}{C_R T_R}\right)\rho_{sD}v_{snD}h_{sD}\right]dz_D \qquad \dots (4.8)$$

Having established the dimensionless form of all pertinent equations and conditions relating to the steam injection process, the dimensionless parameters were simply the coefficients appearing in round brackets of these terms. Next, the independent dimensionless parameters were identified either from observation or by using the Buckingham Pi Theorem. With the independent parameters known, the scaling process can begin. However, as stated before, it was not possible to match all of these similarity parameters in a physical model. Therefore, based on engineering judgment, these parameters were modified and/or combined to form a number of reduced parameters, known as scaling groups (or parameters). The scaling parameters for the steam process are given in Table 4.1. Table 4.2 shows the scaling parameters for the prototype reservoir along with the reservoir properties.

4.3   Example of Scaling Prototype to Model Conditions

The prototype for the physical model represented one quarter of an 8-ha (20-acre), five-spot pattern of a typical moderately viscous oil deposit of the Aberfeldy field in Lloydminster, Saskatchewan. Currently, the prototype reservoir is being produced using vertical production wells only. Table 4.2 contains data for the prototype reservoir, and some of the more important data of the model reservoir.

In scaling, a single value of a quantity is often used to represent the whole field. This single value may not be characteristic of the whole field or the element of symmetry to be modeled as in the case of permeability. The permeability will vary throughout the field, but a single permeability was needed in the scaling calculations.

Table 4.1:   Scaling Parameter for Steam Processes (Modified from Ref. 51)

Number	Scaling Parameter	Name of Scaling Parameter
I	$\dfrac{p_R}{\rho_R g_R L_R}$	Poiseuille Number divided by Stokes Number.
II	$\left(\dfrac{f_{sR} L_{vr}}{C_R T_R} + 1\right) \times A^{\bullet}$	Modified Jacob Number + 1.
III	$\dfrac{f_{sR} \mu_{sR} \rho_R}{\mu_R \rho_{sR}}$	Ratio of steam pressure gradient to oil pressure gradient.
IV	$\dfrac{k_{hR} t_R}{\phi_R S_R \rho_R C_R L_R^2} \times A^{\bullet}$	Fourier Number or Peclet Number.
V	$\dfrac{\phi_R S_R \mu_R L_R}{k_R \rho_R g_R t_R}$	Stokes Number.
VI	$\dfrac{w_R t_R}{\rho_R \phi_R S_R L_R^3}$	Poiseuille Number divided by Modified Poiseuille Number.

The subscript 'R' denotes the reference variable used to obtain a dimensionless term

When $\phi \Delta S$ is not matched, A* takes on a value between unity and $\phi_R S_R \left(\dfrac{\rho_R C_R}{\rho_{cR} C_{cR}}\right)$.

--   If reservoir heating or heat production predominates, use unity.

--   If cap and base rock heating predominates, then use $\phi_R S_R \left(\dfrac{\rho_R C_R}{\rho_{cR} C_{cR}}\right)$.

Table 4.2: Scaling Parameters for the Prototype Reservoir

Field Property	Prototype Value	Model Value
Well Spacing	1/4 of 20 acre, 5-spot	1/4 of 5-spot
Length	141.4 m	0.8128 m
Net Pay Thickness	11 m	0.0632 m
Porosity	0.31	0.34 (average value)
Permeability	4.0 darcies	4498.5 darcies (scaled value)
Thermal Conductivity	0.002077 kW/m·K	0.003266 kW/m·K
Heat Capacity	2.1803 kJ/kg·K	2.3824 kJ/kg·K
Initial Fluid Saturations	$S_o = 0.73$ $S_w = 0.25$ $S_g = 0.02$	$S_o = 0.92$ $S_w = 0.075$ $S_g = 0.005$
Steamflood Residual Oil Saturation	$S_{or} = 0.15$ (estimated)	$S_{or} = 0.25$ (estimated)
Oil Density	993 kg/m^3	879.9 kg/m^3
Oil Viscosity	1275 mPa·s at 23.9°C 865 mPa·s at 32.2°C 220 mPa·s at 65.6°C 26 mPa·s at 135.0°C 1.3 mPa·s at 301.7°C	270 mPa·s at 22.9°C 238 mPa·s at 25.0°C 137 mPa·s at 35.0°C 123 mPa·s at 37.0°C 57.1 mPa·s at 52.0°C
Water Viscosity	0.891mPa·s at 25.8°C	0.891mPa·s at 25.8°C
Initial Reservoir Temperature	23.3°C	3.0°C
Initial Reservoir Pressure	3.45 MPa	0.0267 MPa
Production Pressure	0.345 MPa (gauge)	0.01397 MPa (abs.)
Steam Injection Pressure	3.345 MPa (gauge)	0.068 MPa (abs.) (scaled value)
Steam Injection Rate	100 - 150 m^3/D	212.0 ml/min (scaled value)
Steam Quality	0.70	0.11
Horizontal Wells		
Length		
Short	35.4 m (116 ft)	20.3 cm (8 inch)
Medium	53.1 m (174 ft)	30.5 cm (12 inch)
Long	70.7 m (232 ft)	40.6 cm (16 inch)
Outside Diameter	8.89 cm (3.5 inch)	4.75 mm (0.187 inch)

4.3.1 Length Scale

Although the selection of the length scale for the model was somewhat arbitrary, it was found that this factor was determined by the temperature-pressure relations and by the physical model size considerations. Stegemeier et al.[51] indicated that a successful match between the pressure-temperature relation for saturated steam was achieved if the size of the model was made as 'large' as possible. The question of how 'large' was determined by the practical constraints of cost and time necessary to pack, saturate, cool, clean and maintain the model.

The prototype length, L_P, for the element of symmetry was 141.4 m (463.9 ft). The length of the model was 0.813 m (32 inches). Hence, a length scale factor of 174 was used; that is,

$$\frac{L_P}{L_M} = \gamma(L) = 174 \qquad \qquad ..... \quad (4.9)$$

4.3.2 Model Production Pressure

In steamflooding, the pressure gradient (difference) between the steam zone and the reservoir was observed to be appreciable. Therefore the temperature-pressure relation for saturated steam must be scaled properly. It was suggested that when prototype pressures as low as 50 psia and typical length scales of 100 to 200 were present, the best match can be achieved by selecting the lowest possible production pressure. From a physical standpoint, the lowest pressure that can be maintained was about 1 psia (33 cm of mercury). With this limitation, the production pressure for the model was taken to be 13.79 kPa.

The scaling of the model pressure is given by the first scaling parameter in Table 4.1 as

$$\gamma(\Delta p) = \frac{\left(p - p_P\right)_P}{\left(p - p_P\right)_M} = \frac{\rho_P g_P L_P}{\rho_M g_M L_M} \qquad ..... \quad (4.10)$$

where the length scale was found previously. The ratio of the gravitational acceleration, $\frac{g_P}{g_M}$, was essentially unity. The density ratio, $\frac{\rho_P}{\rho_M}$, was assumed to be 0.9. With the value $\left(p_P\right)_M$ chosen at 13.79 kPa, and the production pressure of the prototype known to be 50 psia, a relationship between the model pressure and the field pressure was established.

$$p_M = 0.011567 + 0.006387 p_P \qquad \qquad \cdots \cdots \quad (4.11)$$

In carrying out the pressure scaling calculations, Table 4.3 was created. Several prototype pressures covering the range of scaling were tabulated along with their corresponding saturated steam temperatures T_S, and the enthalpy of water at steam temperature. The table also contains the calculated model pressures with corresponding steam saturation temperatures and other quantities yet to be determined.

4.3.3 Model Temperature

In order to obtain the best match between the model and prototype oil-viscosity, the model temperature should have the largest range of scaled values possible. With this in mind, along with the practical limitations, the lower limit was set at 3°C which is slightly above the freezing point of water.

To obtain a relationship between the model temperature and the temperature of the prototype, a corresponding temperature at one other point was required. Stegemeier et al.[51] suggested that it was best to take a value from the middle and the upper parts of the pressure-temperature relation for finding the temperature difference ratio. The reason cited was that most of the oil is produced when these temperatures were high.

Following this, the steady state injection temperature and pressure, 74°C and 45 kPa, were chosen. With the injection pressure of the prototype known to be 1.9 MPa, the corresponding steam temperature was found, from steam tables, to be 198.32° C. The criteria for scaling temperature is

$$\frac{(\Delta T)_P}{(\Delta T)_M} = \frac{\left(T_{inj} - T_I\right)_P}{\left(T_{inj} - T_I\right)_M} = \frac{\left(T_{sat} - T_I\right)_P}{\left(T_{sat} - T_I\right)_M} \qquad \qquad \cdots \cdots \quad (4.12)$$

The ratio of the left hand side yields:

$$\frac{(\Delta T)_P}{(\Delta T)_M} = \frac{198.32 - 23.3}{61.5 - 3.0} = 2.9918$$

Table 4.3:   Prototype and Model Scaling Values

Prototype Values							Model Values										
p	T_s	h_w	$C_w\Delta T$	L_v	ρ	μ_s	p	T_s	T_{sc}	h_w	$C_w\Delta T$	L_v	ρ	μ_s	f_s	$\frac{\mu_{oM}}{\mu_{oP}}$ cp/cp	$\frac{w'_a}{w_i}$
MPa *	C *	kJ/kg *	kJ/kg *	kJ/kg *	kg/m³ *	cp **	MPa Eq.4.22	C *	C Eq.4.24	kJ/kg *	kJ/kg *	kJ/kg *	kg/m³ *	cp **	Eq.4.37	Eq.4.39	Eq.4.38
3.45	241.73	1045.6	949.1	1757.9	17.346	0.0173	0.0336	71.80	76.00	299.3	286.7	2325.8	0.213	0.0109	0.051	4.12	0.8827
3.00	233.90	1008.4	911.9	1795.7	15.035	0.0171	0.0307	69.60	73.38	291.3	278.7	2334.9	0.195	0.0108	0.069	5.37	0.8689
2.5	223.99	962.1	865.6	1841.0	12.508	0.0168	0.0275	67.30	70.07	285.9	273.3	2336.4	0.177	0.0107	0.077	5.47	0.8646
2.00	212.42	908.8	812.3	1890.7	10.037	0.0165	0.0243	64.40	66.20	269.5	256.9	2347.8	0.157	0.0106	0.082	5.36	0.8658
1.50	198.32	844.9	748.4	1947.3	7.589	0.0160	0.0211	61.50	61.49	257.4	244.8	2354.9	0.139	0.0105	0.091	5.21	0.8620
1.00	179.91	762.8	666.3	2015.3	5.143	0.0153	0.0180	57.80	55.34	241.9	229.3	2364.0	0.118	0.0104	0.104	4.90	0.8559
0.50	151.86	640.2	543.7	2108.5	2.667	0.0141	0.0148	53.75	45.96	224.9	212.4	2373.9	0.099	0.0103	0.132	4.13	0.8372
0.345	138.36	582.0	485.5	2149.7	1.966	0.0135	0.0138	52.20	41.45	218.5	205.9	2377.6	0.092	0.0102	0.149	3.86	0.8232

* 'Fundamentals of Classical Thermodynamics', 3rd Ed., SI Version by G.J. Van Wylen and R.E. Sonntag (1985), Ref. 58

** $\mu_s = -5.46807e\text{-}04 + 6.8949e\text{-}06*T - 3.39999e\text{-}08*T^2 + 8.29842e\text{-}11*T^3 - 9.9706e\text{-}14*T^4$, Ref. 42.

$$T_M = 0.3342T_P - 4.7879 \qquad\qquad \cdots\cdots \quad (4.13)$$

4.3.4 Steam Quality

The steam quality inside the model is given by parameter II in Table 4.1. If reservoir heating or heat production predominates, Stegemeier et al.[51] suggested that the variable A* be $\phi_R S_R (\rho_R C_R / \rho_{cR} C_{cR})$. Hence, f_{sM} is given by

$$f_{sM} = \left(\frac{c_w \Delta T}{L_v}\right)_M \left\{ \left(\frac{f_{sI} L_v}{c_w \Delta T} + 1\right)_P \times \left[\left(\frac{\phi_P \Delta S_P}{\phi_M \Delta S_M}\right)\left(\frac{\rho_P C_P}{\rho_M C_M}\right)\left(\frac{\rho_{cM} C_{cM}}{\rho_{cP} C_{cP}}\right)\right] - 1 \right\} \cdots\cdots \quad (4.14)$$

Upon substituting the values for the steam quality at steady state steam injection conditions, the above expression yields

$$f_{sI,M} = \left(\frac{205.9 \text{kJ/kg}}{2377.6 \text{kJ/kg}}\right)_M \left\{ \left(\frac{0.7 \times 2149.7 \text{kJ/kg}}{485.48 \text{kJ/kg}} + 1\right)\left[\left(\frac{0.31 \times 0.62}{0.34 \times 0.85}\right)(1)(1)\right] - 1 \right\} = 0.149$$

4.3.5 Model Viscosity

In scaling the viscosity for the model, it was important that the oil production after steam breakthrough matches, as well as possible, with the prototype. It was found that in order to match the pressure gradient in the steam zone and the oil zone, the oil viscosity must be scaled according to parameter III in Table 4.1 as

$$\frac{\mu_{oM}}{\mu_{oP}} = \left(\frac{f_{sM}}{f_{sP}}\right)\left(\frac{\mu_{sM}}{\mu_{sP}}\right)\left(\frac{\rho_{sP}}{\rho_{sM}}\right)\left(\frac{\rho_{oM}}{\rho_{oP}}\right) \qquad\qquad \cdots\cdots \quad (4.15)$$

Upon substitution, the ratio of the viscosity becomes

$$\frac{\mu_{oM}}{\mu_{oP}} = \left(\frac{0.149}{0.70}\right)\left(\frac{0.01024}{0.01346}\right)\left(\frac{1.966}{0.092}\right)\left(\frac{1.0}{0.9}\right) = 3.845$$

The actual oil viscosity using physical viscosity measurements and reported field data was correlated using Andrade's equation. This resulted in the following equations:

$$(\mu_o)_P = 0.00080869 \times e^{\frac{4239.8}{T+273.15}} \qquad \cdots \cdots \quad (4.17)$$

$$(\mu_o)_M = 0.0000007782 \times e^{\frac{5140.9}{T+273.15}} \qquad \cdots \cdots \quad (4.18)$$

4.3.6 Time Scale Factor

The time scale factor is given as parameter IV in Table 4.1. If the heating of the cap rock and base rock were assumed to predominate, then the dimensionless scaling group is given by:

$$\frac{t_M}{t_P} = \left(\frac{k_{hP}}{k_{hM}}\right)\left(\frac{\rho_{cM}C_{cM}}{\rho_{cP}C_{cP}}\right)\left(\frac{L_M}{L_P}\right)^2 \qquad \cdots \cdots \quad (4.19)$$

where $\qquad k_{hM} = k_{granite} = 0.0030 \text{ kW/mK}$

$k_{hP} = k_{sandstone} = 0.002077 \text{ kW/mK}$

$\rho_{cM}C_{cM} = 2.3824 \text{kJ/kgK}$

$\rho_{cP}C_{cP} = 2.1803 \text{kJ/kgK}$

Substituting the above data into the time ratio yields

$$\frac{t_M}{t_P} = \left(\frac{0.002077}{0.0030}\right)\left(\frac{2400}{2242}\right)\left(\frac{1}{174}\right)^2 = 2.4572 \times 10^{-5}$$

The parameter t_M is the lab time and has units of minute. The parameter t_P is the time used in the field and it has units of years. By converting the appropriate units,

$$\frac{t_M}{t_P} = 2.4572 \times 10^{-5} \times 365 \frac{D}{year} \times 24 \frac{hr}{D} \times 60 \frac{min}{hr}$$

$$\frac{t_M}{t_P} = 12.92 \frac{min}{yr} \qquad \cdots \cdots \quad (4.20)$$

The above time ratio implies that for every 12.92 minutes of experimental time, the field equivalent time was one year. In other words, if the injection of steam or production of oil in the model was made for 12.92 minutes, the field equivalent time of injection or production would be 1 year.

4.3.7 Model Permeability

The scaling criteria for the permeability in the model is given as parameter V in Table 4.1.
It is

$$\frac{k_M}{k_P} = \left(\frac{\phi_M \Delta S_M}{\phi_P \Delta S_P}\right)\left(\frac{L_M}{L_P}\right)\left(\frac{\mu_M}{\mu_P}\right)\left(\frac{\rho_{oP}}{\rho_{oM}}\right)\left(\frac{t_P}{t_M}\right) \qquad \cdots\cdots \quad (4.21)$$

As can be seen from the above, the ratio k_M/k_P is dependent on temperature because the
ratio μ_M/μ_P is a function of temperature. However, it is impossible to scale the ratio k_M/k_P
if the temperature dependence is considered. As a consequence, a single value for the
permeability must be chosen, which implies that a single value for the ratio μ_M/μ_P must
also be used. The viscosity ratio was found to be most significant when steam
breakthrough occurred. The deviation in this ratio was also found around the vicinity of
the production well as the viscosity of oil was high compared to that of the displacing fluid.
For these reasons, the viscosity ratio was taken at the prototype steam injection temperature
of 240° C using equations 4.17 and 4.18. Upon substituting various ratios into equations
4.21, the permeability ratio yields:

$$\frac{k_M}{k_P} = \left(\frac{0.34\times 0.65}{0.31\times 0.60}\right)\left(\frac{1}{174}\right)\left(\frac{11.38}{3.16}\right)\left(\frac{1}{0.89}\right)\left(\frac{1}{2.4572\times 10^{-5}}\right) = 1124.48$$

Since the prototype has a permeability of 4 darcies, the permeability of the model is

$$k_M = 4497.9 \text{ darcies}$$

4.3.8 Horizontal Well

The scaling criterion for scaling down the size of a horizontal well was given by Doan et
al.[57] as

$$\left[\frac{\mu_o r_w^2 v}{JLk(\Delta p)}\right]_P = \left[\frac{\mu_o r_w^2 v}{JLk(\Delta p)}\right]_M \qquad \cdots\cdots \quad (4.22)$$

Rearranging the above expression for the radius of the horizontal well to be used in the
model gives:

$$r_{wM} = \left[r_{wP}^2 \frac{\mu_{oP}}{\mu_{oM}} \frac{L_M}{L_P} \frac{v_P}{v_M} \frac{k_M}{k_P} \frac{\Delta p_M}{\Delta p_P} \right]^{0.5} \qquad \ldots\ldots \quad (4.23)$$

By assuming that the flow velocity in the prototype was one-tenth of that in the model, and that the horizontal producer of the prototype had an OD. of 8.89 cm (3.5 inch), then:

$$r_{wM} = \left[4.445^2 \frac{3.16}{11.4} \frac{1}{174} \frac{1}{10} \frac{4497.9}{4.0} \frac{0.05459}{3.0} \right]^{0.5} = 0.254 \text{cm}$$

In this study, an aluminum tubing of 4.75 mm OD. was used for the horizontal well (either producer or injector), since 5.08 mm OD. tubing is not a standard size. This resulted in a 6.5% difference between the actual well size and the value determined by the scaling criterion. As a consequence, this led to a 12.6% difference in the assumed velocity ratio between prototype and model conditions. The scaling of the horizontal well length was straightforward as it was chosen similar to the model length ratio of 174. The length of the horizontal well used in the model was 18 inches long, which corresponds to a horizontal well that would be 79.553 m long in the field.

4.3.9 Steam Injection Rate

The ratio of the steam injection rates is given as parameter VI in Table 4.1. It is

$$\frac{W_M}{W_P} = \frac{\rho_{oM}}{\rho_{oP}} \left(\frac{L_M}{L_P} \right)^3 \frac{(\phi \Delta S)_M}{(\phi \Delta S)_P} \frac{t_M}{t_P} \qquad \ldots\ldots \quad (4.24)$$

Substituting the appropriate values into the expression above leads to:

$$\frac{W_M}{W_P} = \frac{0.89}{1.0} \left(\frac{1}{174} \right)^3 \frac{0.34 \times 0.65}{0.31 \times 0.60} \frac{1}{2.4572 \times 10^{-5}} = 0.00817$$

Since the steam injection rates in the prototype were between 100 - 150 m³/D, the injection rates for the model were between 0.817 - 1.2255 m³/D, for the entire field. This model represented one-quarter of a five-spot pattern; therefore, the rates were between 0.20425 - 0.306375 m³/D, or 141.8 - 212.7 ml/min.

Chapter 5

EXPERIMENTAL APPARATUS and PROCEDURE

5.1   Experimental Apparatus

In this study, two low pressure models were used. One was a scaled physical model, the other was a visual unscaled model. From the scaled physical model, the injection and production data were obtained after every 0.1 PV of steam had been injected. With the temperature and pressure recorded during the experiment, the temperature contours were generated. In the visual model, the oil recovery mechanism, and the dominant displacement mechanism that were speculated to occur in the physical model were carefully studied. The analysis included in this thesis is based on the data obtained from the physical scaled model combined with the insight obtained from the visual model. These two models were found to complement each other.

The experimental set-up for the scaled physical model is shown in Figure 5.1 As can be seen, the experimental apparatus consisted of four important sub systems: the scaled physical model and the injection, production and data acquisition systems. In the visual model, data acquisition was not used due to the sensitivity of Lucite to thermal stress. As such, holes on the walls of the model – required to hold the thermocouple in place – may lead to cracks; therefore, it was avoided. Instead, video recordings of the experiments were made.

5.1.1   Scaled Physical Model

The scaled physical model consisted of a fiberglass tray with dimensions: length – 81.28 cm (32 inches), width – 81.28 cm (32 inches) and height – 6.35 cm (2.5 inches). The prototype has the dimensions: length – 281.55 m, width – 281.55 m and height – 11 m. It represented one quarter of an eight hectare (20 acre) five-spot pattern. The scaling factor used between the model and the prototype was 174.

In order to locate precisely the position of the interface and the size of the steam zone, a total of 36 thermocouples were used to measure the temperatures inside the model, and four pressure transducers were used to monitor the injection and production pressures. Of the 36 thermocouples, four were placed at the four ports in conjunction with the four pressure
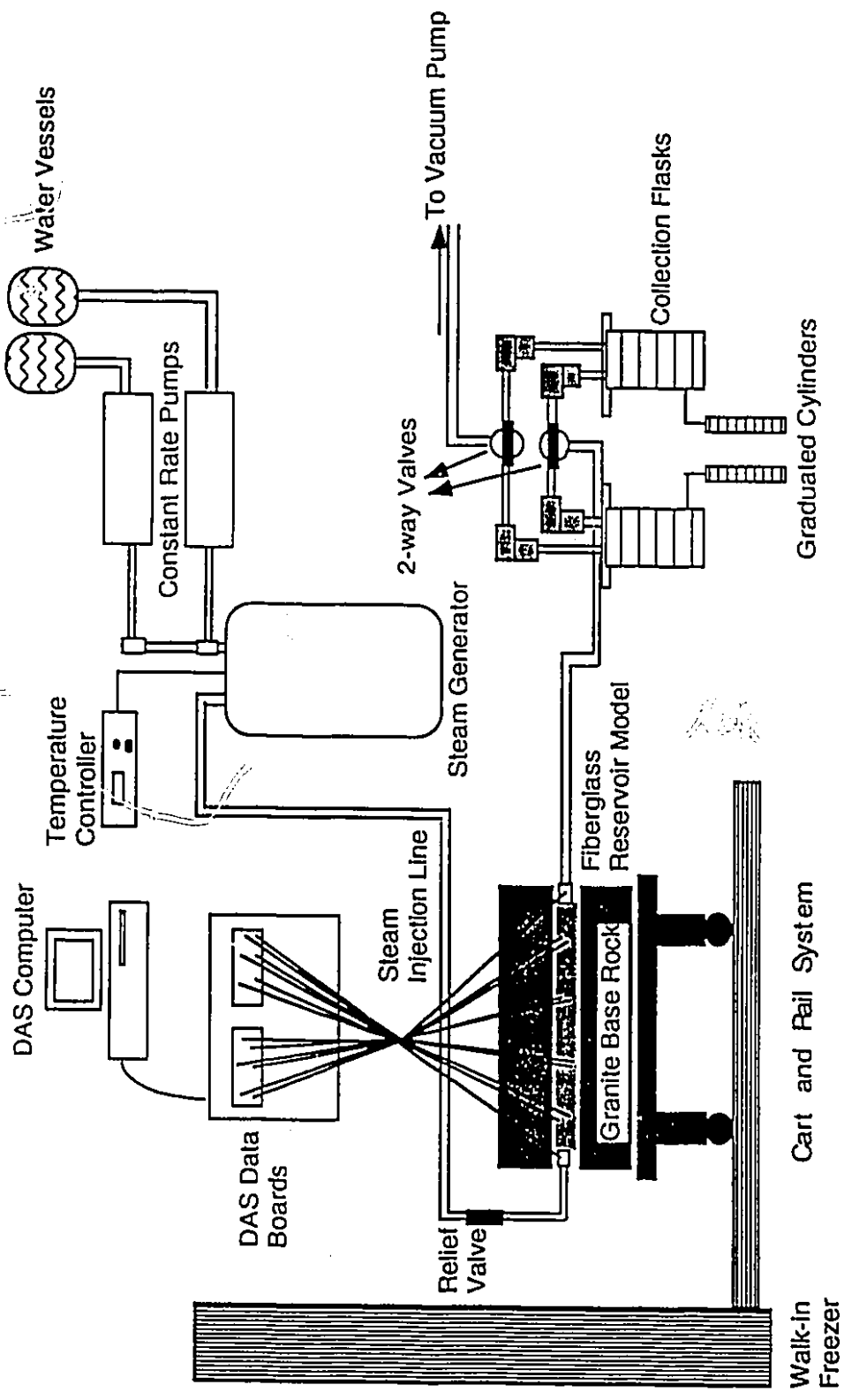
Figure 5.1: Steam Injection Experimental Apparatus.

transducers. The remaining 32 thermocouples, of which 16 were placed on the top layer and 16 on the bottom layer, were located strategically inside the reservoir to monitor the advancement of the steam zone.

The selection of fiberglass material to represent the model had several advantages. These included: low thermal conductivity, strength and inexpensive to build. The low thermal conductivity of the material satisfied the external /outer boundary conditions; that is, no heat flow across the boundary of the model and no heat transfer within the walls of the model. However, this fiberglass tray, due to its insulating nature, prevented heat loss to the underburden. The top and bottom granite blocks were used to simulate the overburden and underburden of the prototype. Granite was chosen because its properties, namely the thermal diffusivity, satisfied the scaling groups. Figure 5.2 shows the schematic overview of the physical model and one layer of thermocouples.

The total weight of the model and the granite blocks was about two and a half tons. Therefore a cart system, carrying the granite blocks and the scaled model on tracks, was designed to move the model from the refrigerating chamber to a location near the production system, where the experiment was carried out. The cart could also be tilted to about 45^0 to allow the even distribution of fluids during saturation. This also permitted experimental studies on steamflooding inclined reservoirs. The refrigerating chamber was required to fulfill the scaling criteria for the initial temperature condition of the model, which was 3^0C

5.1.2   The Visual Model

A visual model, that was used to study radial flow patterns of hot water into vertical wells, was re-designed to allow study of the displacement mechanism during a steamflood experiment. This visual model was made from Lucite, and it had the following dimensions: length (outer) 40.32 cm, (inner) 33.02 cm; height (outer) 40.32 cm, (inner) 33.02 cm; width (outer) 14.61 cm, (inner) 7.30 cm. Along with this model, two horizontal wells, one injector and one producer, were fabricated. The wells were made from sintered stainless steel material. The horizontal well had the following dimensions: inner radius - 4.76 mm, outer radius - 9.53 mm and length - 7.30 cm. The bulk volume of this visual model was found to be 8135 cm^3 (8.135 liter).

Lucite was very sensitive to physical and thermal stresses; therefore, care had to be taken in selecting a range of suitable operating conditions that were ideal for this material. The

Side View
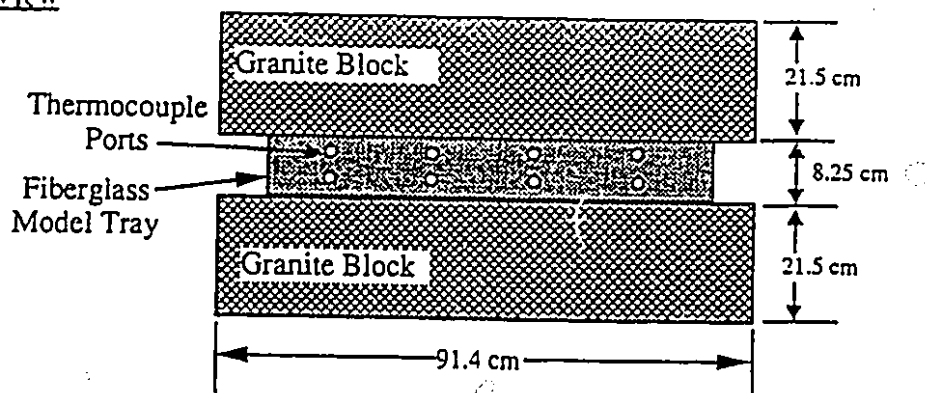
Plan View of the Model: Displays the Cap and Base Rocks and the Relative Level of the Upper and Lower Thermocouple Ports.
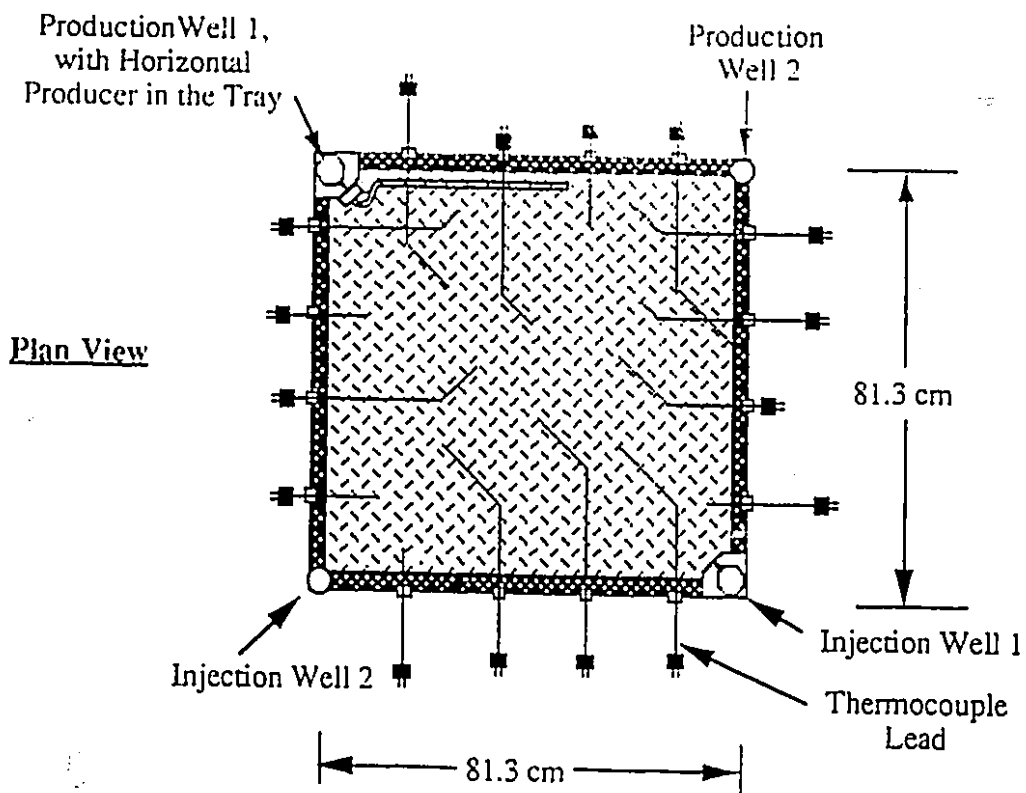
Plan View

This plan view illustrates the approximate positions of the top layer of thermocouples.

Figure 5.2 — Schematic Overview of the Physical Model and One Layer of Thermocouples.

temperature of the injected fluid was set at 77°C, while the injection rate was set at 22.5 cc/min. Lucite was a good insulator. As such, the heat stored inside the model was allowed to accumulate. This created some concerns about the thermal stresses on the inner walls of the model.

In the visual model, the following effects were observed from the condensation of steam on the inner walls: the dominant displacing mechanisms, the stability of the interface, the direction in which the steam zone was moving and the formation of a steam zone around the horizontal injection well.

5.1.3 Horizontal Wells Fabrication

A total of four identical horizontal wells, two injection wells and two production wells, were fabricated according to the scaling criteria derived by Doan et al.[57]. The wells were made from aluminum. Aluminum was chosen for the fabrication of the horizontal wells because it was inexpensive to purchase and easy to machine. The length of each horizontal well was approximately 45.7 cm, and the inner diameter was approximately 5 mm. The horizontal wells were perforated at 2 cm intervals, and the perforations were placed on both sides of the horizontal wells. Each perforation was 0.5 mm in diameter.

5.1.4 Injection System

From previous experimental studies, Matthias[56] indicated that a non-mixing system has a smaller steam quality range over the same boiler temperature range, thus giving a much better control of the steam quality. Following this advice, a non-mixing system was used in this study.

The injection system consisted of two-20 litre bottles containing water, two Milroyal pumps, a boiler and an insulated line. It was noted that the maximum capacity of one Milroyal pump was 200 ml/min. Therefore, to achieve a constant injection rate of 210 ml/min., two pumps were used. The rate settings on the pumps were: 130 ml/min. and 80 ml/min. The pumps, connected to the 40 liter aquifer, fed water to the boiler, which was set to generate steam at a temperature of 160°C. The line that was used to connect the boiler to the point of injection was heavily insulated to prevent heat loss in the line.

5.1.5 Production–Collection System

The production-collection system consisted of a vacuum pump, a pressurized discharge system and two traps. The efficiency of the vacuum pump, under experimental conditions, varied in accordance to the atmospheric pressure. However, this variation was minimal. In order to obtain proper experimental data, the proper use of the two traps along with the pressurized discharge system was extremely important. When this system was handled improperly, back pressures may be introduced into the model, and or reduce the 'strength' of the vacuum. The presence of the two traps allowed the collection of oil samples one at a time, and the pressurized discharged line allowed the collection of the samples from one of the traps.

5.1.6 Data Acquisition System

The data acquisition system consisted of a 486/66 personal computer equipped with a DAS–8 card, eight Exp–16 multiplexers, one ten-channel Validyne board and the Labtech Notebook™ Software package. The DAS–8 card served as an interface card to process data obtained from both the Exp–16 multiplexers and the Validyne board. The Exp–16 cards were connected to the thermocouples, which measured the temperature at various locations in the model. On the other hand, the Validyne board was connected to the pressure transducers, which monitored the pressure at the four ports. The software package recorded and processed all raw thermocouple and pressure transducer data in milli volts and converted them to real values of temperature (in °C), pressure (in kPa), and time (in seconds). The Labtech Notebook™ Software also controlled the sampling rate of pressures and temperatures; data was taken every 30 seconds. The experimental data were stored in ASCII file format, which was later read by Microsoft Excel™, and analyzed (in terms of temperature contour plots) by SURFER™.

In the visual model, experiments were recorded using an 8 mm camcorder. Subsequently, the displacement mechanisms were studied by watching a television screen. Pictures of the circular steam zone formed around the horizontal injector, during the experiment, were also recorded.

5.1.7 Model Fluids

The viscosity-temperature relationship for the refined oil used in the study and the prototype oil was given by Matthias[56]. It was found that the Faxam-100 oil gave the best match to the prototype oil in the low temperature range and hence it was selected to represent the prototype oil in the experiments.

In the visual model, the interface between the steam zone and the oil bank was difficult to locate because of the lack of contrast in color between the Faxam 100 oil and the steam. Therefore, the oil used in the experiment must be dark in color. Using the crude oil, that was available in the lab, was not a good idea because it left stain marks on the Lucite walls despite cleaning thoroughly with soap water. Since Lucite was sensitive to solvents like acetone and varsol, the stain marks were found to be embedded on the walls of the model. This led to the selection of transmission fluid for the displaced fluid. The 'dark red' color of the transmission fluid provided a sharp contrast at the interface; hence, the location and the stability of the displacement could be studied, and the movement of the front could be easily tracked. However, the disadvantage of using transmission fluid was its density; that is, it is a light oil.

Recently, a dye was found to change the color of the Faxam 100 oil from a light orange to a dark blue color. This color was found to provide excellent contrast between the oil bank and the steam front. The ability to use the same oil between the scaled physical model and the visual model was extremely important and advantageous. The reason was the establishment of a link between what was observed in the visual model to that which was thought to occur in the physical model.

5.1.8 Porous Media

The high absolute permeability of the scaled reservoir, as required by scaling criteria, was achieved with the use of glass beads having an average diameter of 3 mm (size 6-8 US. mesh). These beads were used for each of the experiments reported in this thesis. Subsequent to every experiment, these glass beads were thoroughly cleaned and reused for other experiments, as they were expensive.

5.2   Preparation of the Experimental Model

5.2.1   Packing Procedure

The size, weight, and shape of the model restricted the use of a vibrator to tightly and uniformly pack the glass beads inside the reservoir. The need for uniform properties throughout the pack was achieved with the use of a particle distributor. The application of the particle distributor concept to construct homogeneous reservoirs was introduced by Wygal[59]. He indicated that the particle distributor produced mechanically stable packs with uniform properties throughout, and often these packs were accurately reproduced.

In packing the model, the particle distributor was first carefully placed over the fiberglass tray, so that the sides were parallel to each other. Next, approximately four (4) pails of glass beads were poured through it. Once the beads completely filled the top of the modeled reservoir, the particle distributor was taken off and the remaining beads were scraped off.

5.2.2   Saturation Process

Once the model had been packed and sealed with the Neoprene sheet, the upper granite block was lowered to simulate the overburden. The two clamps were then tightened to the upper and lower granite blocks to prevent lifting of the model and cap rock during the experiment.

Before the saturation of the fluids was undertaken, the model was tilted to approximately 45° from the horizontal position to provide a stable gravity saturation front. Next, a vacuum was exerted on the entire model. This was essential if an even distribution of fluids in the model was to be obtained. In this model, there were separate injection and production ports that were used explicitly for saturation purposes. Again, this was necessary to provide an even distribution of fluids throughout the reservoir. Since this was a water wet system, the water was allowed to enter the model first. Once water entered the production system, a quick-connect was released to prevent water from encroaching farther. After the water sample was collected, the pore volume of the pack was determined. The pore volume was the amount of water accumulated in the model during the aforementioned process. Subsequently, oil was allowed to enter the model. Once oil was observed at the production end of the system, the saturation process was complete and the

encroachment of oil at the injection ports stopped. In the saturation process, it was assumed that the oil was incompressible. As such the amount of oil in the model was determined by the amount of water displaced. With the amount of water displaced being collected, the initial hydrocarbon saturation of the model could be found. Finally, the saturated reservoir was pushed into the cooler with a setting of 3^oC. Approximately 24 hours later, when the reservoir was at approximately 3° C, the steam injection experiments began.

5.2.3 Packing and Saturating the Visual Model

Before packing the visual model, the type of steam injection experiment was first determined, and the horizontal wells were put in place. With the same glass beads used in the scaled physical model, the visual model was packed. Here a particle distributor was not necessary. The beads were slowly and simply poured into the visual model. Once completed, slight vibrations were made to the model to ensure the pack was tight and firm. Next, the model was evacuated, and then saturated with water. With water seen in the production system, a quick connect at the lower plate was released to prevent further encroachment. Oil was then allowed to enter the model the same way water did. Again, once oil was seen at the production-collection system, the saturation process was completed. Since the purpose of these experiments was for studying the displacement mechanism, it was not necessary to satisfy the scaling criteria for the initial temperature condition in the model.

5.2.4 Preparation of a Bottom Water Model

The packing sequence in these bottom water experiments was quite different as compared to packing the homogeneous model. A solution of 5% (by weight) sodium chloride (NaCl) having 20% of the pore volume, was first mixed. With the model cleaned, the solution was poured directly onto the fiberglass tray. Next, the glass beads were packed on top of the bottom water layer. Once finished, the model was sealed and pushed into the freezer, set to operate at -17^oC. After the bottom water layer had frozen solidly, which was approximately 24 hours later, saturation of the model began. This saturation step was done in a similar manner to the saturation of the homogeneous model. Finally, the model was pushed back into the cooler with a temperature setting of 3^oC. The experiment began when the temperature inside the model was uniformly 3^oC.

5.3   Conducting Experiments

Once the temperature inside the model was at a uniform 3°C, the boiler was turned on along with the injection pumps. The injection rate was checked several times to ensure that it was in the range of 210- 212 ml/min. Approximately fifteen minutes after the boiler reached 160°C, the model was rolled out of the freezer, and connections of the thermocouples and pressure transducers were made. The data acquisition program was then activated, and read for approximately one minute. If the temperature readings were inconsistent, the change in the connection(s) was made. The vacuum pump was then turned on and the collection system, which consisted of the two traps, was evacuated along with the production line. With the injection and production ports selected, steam was introduced into the model by way of a quick connect. At the same time, the production system was activated along with the data acquisition system.

After every 0.1 PV of steam injected (CWE), the collection of fluids (oil and water) was switched from the first trap to the second one. Depending on the type of investigation, pattern inversions were often made during the experiment, and this required another person to help change the injection or production ports. The experiment ended after 2.1 PV of steam had been injected (CWE), unless specified otherwise.

5.4   Data Analysis

After an experiment, the collected samples of oil, water and emulsions were allowed to separate overnight. The volumes were then recorded, and the production history was analyzed. Analysis was based on four different curves : % of oil cut, % of cumulative oil recovery (% OOIP), instantaneous WOR and cumulative OSR versus the pore volumes of steam injected (CWE).

A commercial contouring package, known as SURFER, was used to analyze the temperature data. The SURFER™ gridding and viewing programs were used to generate the temperature contours. The gridding program had a sophisticated feature that can take irregularly spaced data and create a regularly spaced grid of any desired density. Once the data had been interpolated and gridded, its component was saved to a .GRD file. The program TOPO provided different options for a user to look at the content of the .GRD file, and to create the contour maps that were needed. A plotting subroutine was then called to print the contour map, which was stored as a .PLT file. SURFER™ also provides users

with a sub program called UTIL. This subroutine was extremely useful for determining the volume of a contoured surface, the cut and fill area, or a volume of a sliced contour.

Chapter 6

DISCUSSION of EXPERIMENTAL RESULTS

The objective of this study was to seek the optimal oil recovery from two different types of reservoirs: a homogenous reservoir, and a reservoir with a bottom water zone, using several steamflooding strategies in a scaled physical model. The effects of shut-in and dip on steamflooding performance were also studied. The results of these experiments were then scaled up to obtain insight into the displacement process in the field and to predict the performance of an actual steamflood. The following types of steamflooding experiments will be discussed: shutting-in the horizontal injectors and producers, injection into dipping reservoirs with bottom water, injection and production strategies to increase the volumetric sweep and gas injection with steam. This chapter also looks at the oil saturation profiles, calculated from the material balance equations (MBEs), along with the heat balance calculations during a steamflood. The discussion will be grouped according to the type of investigation, and where appropriate, comparisons will be made between appropriate experiments.

6.1   Presentation of Results

In this study thirty five runs were completed to study the displacement process together with the effects mentioned above. Of the thirty five runs, twenty five were done using the scaled physical model, while the remaining ten runs were conducted using a visual unscaled model. Figure 6.1 illustrates schematically the steamflooding and hot water flooding experiments performed. Table 6.1 summarizes the pertinent initial model properties, such as porosity and the initial fluid saturations, along with the oil recovery results. Both the production data and temperatures and pressures recorded during the run were used for analyzing the experiment. The injection and production data were used to generate the following curves: cumulative oil recovery, instantaneous water-oil ratio (WOR), oil cut and instantaneous steam-oil ratio (SOR) at various pore volumes of steam injected (CWE). The temperature and pressure data recorded during the experiment were used to draw temperature contours at various stages of the steamflood.
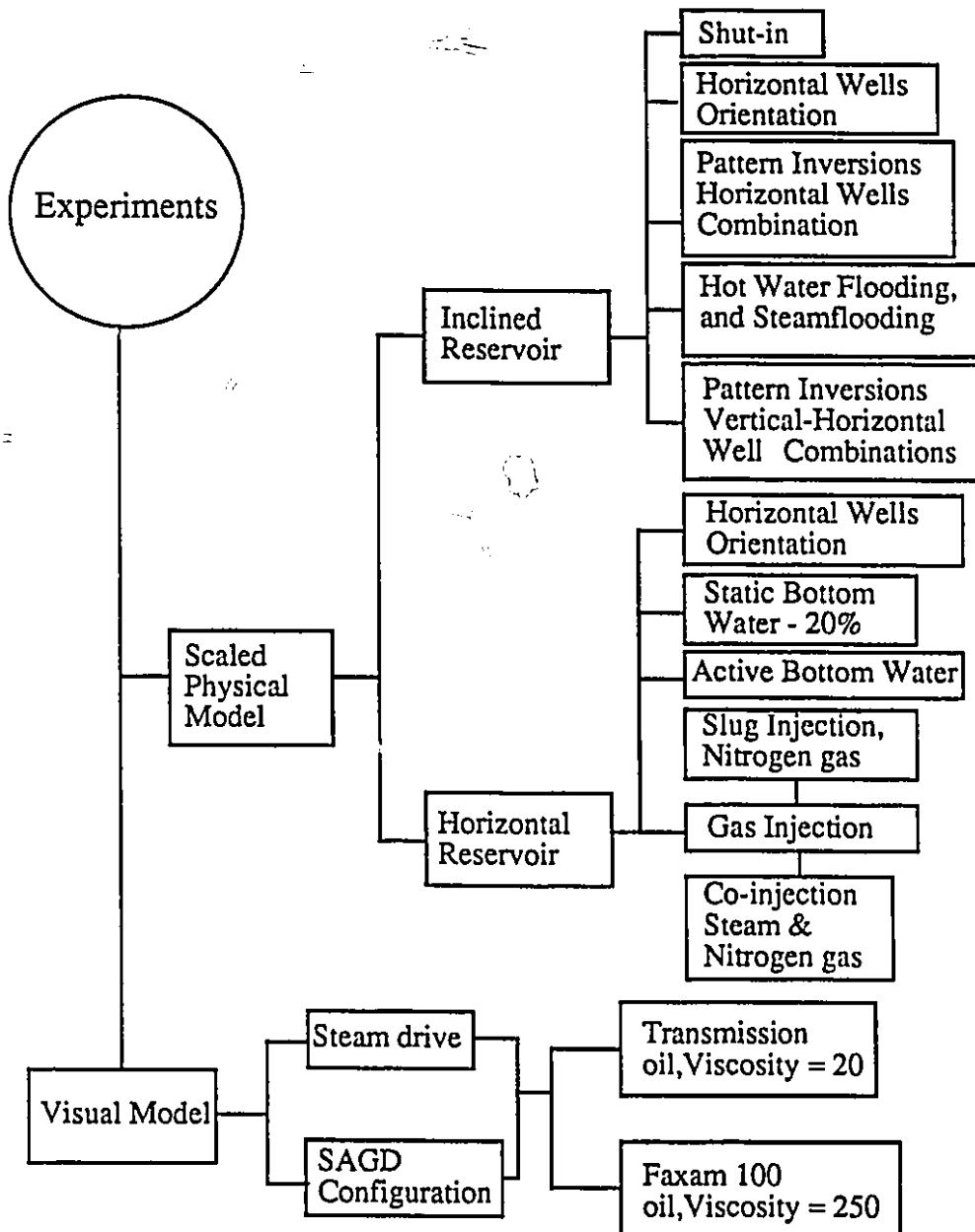
Figure 6.1: Overview of the Investigations Made from Conducting Low Pressure Model Experiments.

Table 6.1: Summary of Experiments Conducted in this Study

Run	Model Type	Process Type	Reservoir	Porosity %	S_{oi} %	BW Thickness	Cum Rec %OOIP	Cum. Inj. PV	Comments	Prod. Hist. Fig.	Temp Cont. Plot
Run 1	HM	SF with P.I.s	Inclined	34.0	89.9	None	61.4	2.159	Vertical and horizontal wells were used with pattern inversions to increase the cumulative recovery of a steamflood.	—	—
Run 2	HM	SF with P.I.s	Inclined	34.6	88.4	None	75.9	2.6	This experiment is identical to Run 1. However, the location of the HWs were different.	—	—
Run 3	HM	SF with P.I.s	Inclined	—	—	—	—	—	Misrun.	—	—
Run 4	HM	SF with P.I.s	Inclined	29.6	90.8	None	71.1	2.328	HWs were used at the injection and production ports. The effect of pattern inversions utilizing only HWs was studied.	—	—
Run 5	HM	SF with P.I.s	Inclined	34.1	90.0	None	67.4	2.5	HWs were used at the injection and production ports. The effect of shut-in was studied. The shut-in period was for 1.0 PV.	10	11
Run 6	HM	SF with P.I.s	Inclined	30.3	90.8	None	60.3	2.1	This run is similar to Run 5. However, the injection and production strategy subsequent to shut in was different	12	13
Run 7	HM	SF with P.I.s	Inclined	34.1	91.8	None	55.2	2.1	The effect of well location on the recovery was studied. The horizontal injectors and producers were placed diagonally, ie. NE-SW orientaion in the model	15	16

51

Run	Fluid	Process	Orientation						Description		
Run 8	HM	SF with P.I.s	Inclined	34.8	91.2	None	49.4	1.8	This run is similar to Run 7. However, the injection and production strategy were different.	17	18
Run 9	BW 5% NaCl	SF with P.I.s	Inclined	26.5	83.0	20.0%	52.4	2.1	The effects of steamflooding an inclined reservoir having a bottom water layer, and pattern inversions on such reservoir were studied.	23	24
Run 10	HM	SF with P.I.s	Horizontal	32.9	92.2	None	54.0	2.1	The HWs configuration of this experiment is similar to Run 7. The effects of dip, and pattern on the cumulative recovery were studied.	19	20
Run 11	BW 5% NaCl	SF with P.I.s	Horizontal	25.1	74.8	20.0%	36.6	2.1	The effect of steamflooding a horizontal reservoir having a bottom water layer was studied. Benefits of pattern inversions were also studied.	25	26
Run 12	HM	SF with P.I.s	Horizontal	30.4	90.3	None	56.5	2.1	Base Case experiment.	4	5
Run 13	BW 5% NaCl	SF with P.I.s	Horizontal	26.4	83.1	20.0%	41.2	2.1	The effect of raising the HWs above the oil-water contact was studied. Comparisons with Run 11 were also made.	28	29
Run 14	HM	SF with P.I.s and Gas (N$_2$) Injection	Horizontal	29.0	89.6	None	62.4	2.2	The effect of gas (N$_2$) injection (slugs) on the cumulative recovery, during steamflooding, was studied. The injection rate of gas was 544 mL/min.	30	31
Run 15*	HM	SF with P.I.s and Gas (N$_2$) Injection	Horizontal	31.8	90.3	None	45.8	2.2	The effect of co-injection of gas (N$_2$) and steam on recovery was studied. There was a leak present in this experiment.		

Run											
Run 16	HM	SF with P.I.s and Gas (N2) Injection	Horizontal	30.3	91.0	None	59.0	2.1	This experiment was a repeat of Run 15. This experiment was a success.	32	33
Run 17	Active BW 5% NaCl	SF with P.I.s	Horizontal	—	—	20%	—	—	The effect of active bottom water on the cumulative recovery of a steamflood was studied. A problem was encountered with the rate of water influx.	—	
Run 18	Active BW 5% NaCl	SF with P.I.s	Horizontal	—	—	20%	—	—	As in Run 17.	—	—
Run 19	Active BW 5% NaCl	SF with P.I.s	Horizontal	—	—	20%	—	—	As in Run 17.	—	—
Run 20	Active BW 5% NaCl	SF with P.I.s	Horizontal	28.95	89.6	20%	61.6	2.2	A leak in the model was detected after the experimental run.		
Run 21	HM	SF with P.I.s	Horizontal	32.01	90.85	—	49.61	2.1	The effectiveness of pattern inversions with vertical wells was studied. Pattern inversion intervals, sequence and configurations were identical to Run 12 (base-case).		
Run 22	HM	SF with P.I.s	Horizontal	—	—	—	—	—	Re-establishing experimental set-up after relocation.	—	—
Run 23	HM	SF with P.I.s	Horizontal	—	—	—	—	—	Re-establishing experimental set-up after relocation.	—	—
Run 24	HM	SF with P.I.s	Horizontal	33.50	90.76	—	49.49	2.2	Re-establishing experimental set-up after relocation.		

| Run 25 | HM | SF with P.I.s | Horizontal | 33.25 | 92.16 | — | 2.1 | Similar to experiment 12. The temperature distribution on the cap rock; i.e. the outer boundary condition, was established in this experiment. |

Legend:

BW	Bottom Water Model
HM	Homogeneous Model
PI	Pattern Inversions
SF	Steamflood

6.2 Fluid Injected: Steam versus Hot Water

There are two methods of determining whether the fluid injected is steam or hot water, in the case of a homogeneous reservoir. In the first method, the pressure and temperature data obtained during the experiment are used to determine whether steam or hot water was present. This is done by first generating a temperature contour plot at some specified period, then assuming that the pressure distribution between the injector and producer is linear. The temperature, and the corresponding pressure, at various locations inside the reservoir, are then checked with the steam tables to determine the nature of the injected fluid. In the second method, a plot of the cumulative injection − measured in cold water equivalents (CWE) − divided by the cumulative production (i.e. the ratio of CI/CP) versus pore volumes of steam injected is constructed. From the graph, observations are made to see whether the ratio is greater or less than one. When the ratio is less than one, that is the cumulative injection is less than the cumulative production, it is inferred that the injected fluid is expanding; hence, steam is present. When the ratio is equal to one, it is inferred that most of the steam has condensed, and the hot waterflooding is taking place. When the ratio is greater than one, the injected fluid is a compressible fluid, and the cumulative production is greater than the cumulative injection.

6.3 Stability of Steam Fronts

In waterflooding a heavy oil reservoir, water will breakthrough at the producer quite early. Hence, many pore volumes of water must be injected to lower the oil saturation to S_{or}, the residual oil saturation. The low displacement efficiency and volumetric sweep efficiency, obtained from waterflooding a heavy oil reservoir, are attributed to mobility ratio and viscous instabilities. The above effects are even more pronounced for the displacement of heavy oils by gas because the viscosity ratio of the displaced fluid to the displacing fluid is even larger.

The use of heat to reduce the viscosity of the heavy oil, and hence increase its mobility, has been widely accepted by the petroleum industry for many years. Among the different thermal recovery methods, steam injection is the most successful to date. This success is attributed to the unique steam properties. The steam displacement process has been found to be more stable, that is one that is not conducive to the formation and growth of viscous fingers, than the hot water displacement process. Small steam fingers, if formed, tend to

lose heat at relatively high rates, ultimately resulting in condensation and disappearance of the steam fingers[60].

6.4 Pattern Inversions, Cyclic Pattern, Parallel and Diagonal Injection – Production Strategy.

In this section, four different terminologies used for injection and production strategies – pattern inversions, cyclic pattern inversion and parallel and diagonal injection-production – are defined. Pattern inversion (also known as cross pattern flooding) is defined as a change in either the injection and/or production port(s) and hence pattern during a steamflood. The concept of pattern inversion is quite simple; however, a clear understanding of the mechanism involved is important. The idea behind pattern inversion is to expose as much, and as long as possible, the area where oil lies in the reservoir to steam displacement. Hence, the selection of a certain pattern, that is, injection-production strategy, and the time when a different pattern is used, becomes important. This strategy, together with the idea of re-saturating the flow channel/path of the fluids previously produced, is the basis of quick pattern inversion, and will be discussed later.

The diagonal injection-production strategy, and the parallel injection-production strategy are defined with the aid of the diagram below, Figure 6.2. The diagonal injection-production strategy refers to the location of the injector and producer on the diagonal and opposite to each other. The parallel injection-production strategy refers to having the injector and producer on parallel sides and opposite to each other.

Examples of a diagonal injection-production strategy include: injection at Port 1 and production at Port 4, or injection at Port 2 and production at Port 3. Examples of a parallel injection-production strategy include: injection at Port 1 and production at Port 3, or injection at Port 2 and production at Port 4

Cyclic pattern inversion (CPI) is defined as all possible sequential combinations that exist between one injector and one producer. This is illustrated in Figure 6.3. In the existing experimental set up, Ports 1 and 2 are the injection ports, while Ports 3 and 4 are the production ports. Therefore an example of a single pattern inversion cycle is shown in the diagram below. This sequence is:

    i)   Injection at Port 2, and production at Port 3;

    ii)   Injection at Port 1, and production at Port 3;

iii)   Injection at Port 1, and production at Port 4;

iv)   Injection at Port 2, and production at Port 4;

The sequence of the above injection/production strategies may not necessarily be in that order. The order may be different than the one suggested above.
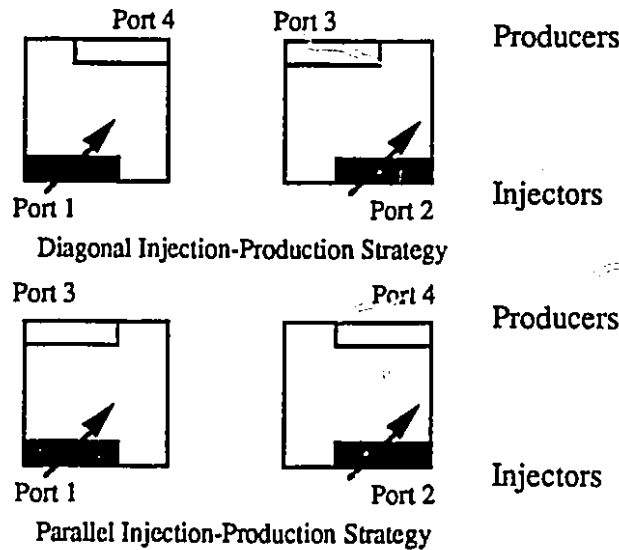
Figure 6.2:   Illustrates the definition of parallel and diagonal injection-production strategy
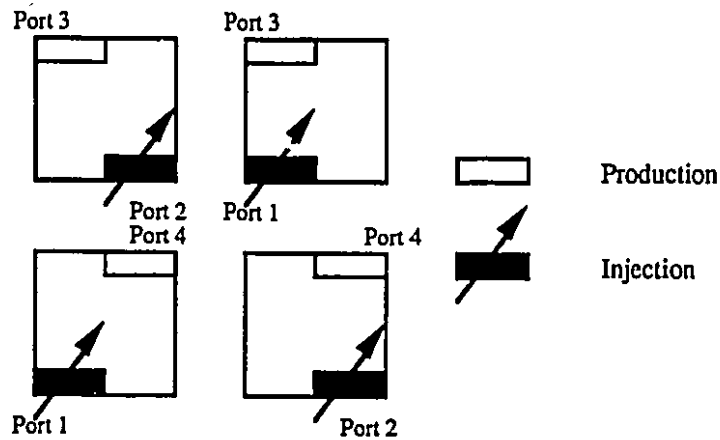
Figure 6.3:   Illustrates the use of cyclic pattern inversions

6.5   A Homogeneous Oil Reservoir, Base Case Experiment

This was a base case steamflood experiment with pattern inversions made using pairs of horizontal injectors and producers in a homogeneous horizontal reservoir. In this experiment, the glass bead pack representing the prototype had a porosity of 30.4% (pore

volume was 12755 ml), the initial oil saturation was 90.3% (or 11520 ml of oil), the steam injection rate was 210 ml/min. and the ultimate oil recovery was 56.5% of the initial oil in place (IOIP). Steam injection was utilized for 2.1 PV, and pattern inversions were made after 0.8, 1.2 and 1.6 PV of steam injection.

Figure 6.4 shows the production history of the experiment. From this figure, it was noted that the OSR curve decreased steadidily between the production period 0.5 to 0.8 PV. The use of pattern inversion was found beneficial as a stabilizing trend in the cumulative OSR curve was observed, that is, the decrement of the negative slope of this curve was less. The oil cut, at 0.1 PV subsequent to pattern inversion, was seen to increase also. It was noted that a higher oil cut was not seen instantaneously after pattern inversions because time was needed first to heat the oil in the vicinity of the injection port to make the oil mobile. The propagation of oil toward the producer resulted from both frontal displacement and vertical drive of segregated steam at the top of the formation. Figure 6.5 shows the temperature contours after 0.5, 0.85, 1.0, and 1.2 PV of steam had been injected. Figure 6.5 (a) shows a large volume of virgin oil located at the opposite diagonal, that is, at Ports 1 and 4. After 0.5 PV of steam was injected, the temperature contours showed the following: 1) steam breakthrough had almost occurred (the temperature of the fluids at the production was approaching steam saturation temperature), 2) steam override was evident (the upper temperature contours, $T \geq 60^{\circ}C$, traversed further inside the reservoir than the lower temperature contours) and 3) little interference (communication) between the injection and production wells was observed. To observe the interference effects and interference patterns, please refer to the temperature contours of Run 10, Figure 6. 20 (a).

On the top left–hand corner of the production history plot, Figure 6. 4, is an inset graph showing the ratio CI/CP versus the pore volume injected. As discussed earlier – in Section 6.2 – the graph provided another method of determining the state of the injected fluid for a specified injection period. On this graph, the ratio CI/CP was greater than one between the injection period 0-0.2 PV, implying that the injected fluid was hot water. After 0.2 PV of fluid had been injected, this ratio decreased to less than one, implying the presence of steam.

Theoretical analysis of the base run includes: a calculation for oil saturations – based on material balance equations, comparisons of experimental steam zone volumes with several steamflood models, and calculation of cumulative heat distribution during a steamflood. These three analyses are interrelated to each other; therefore, a precise knowledge of the
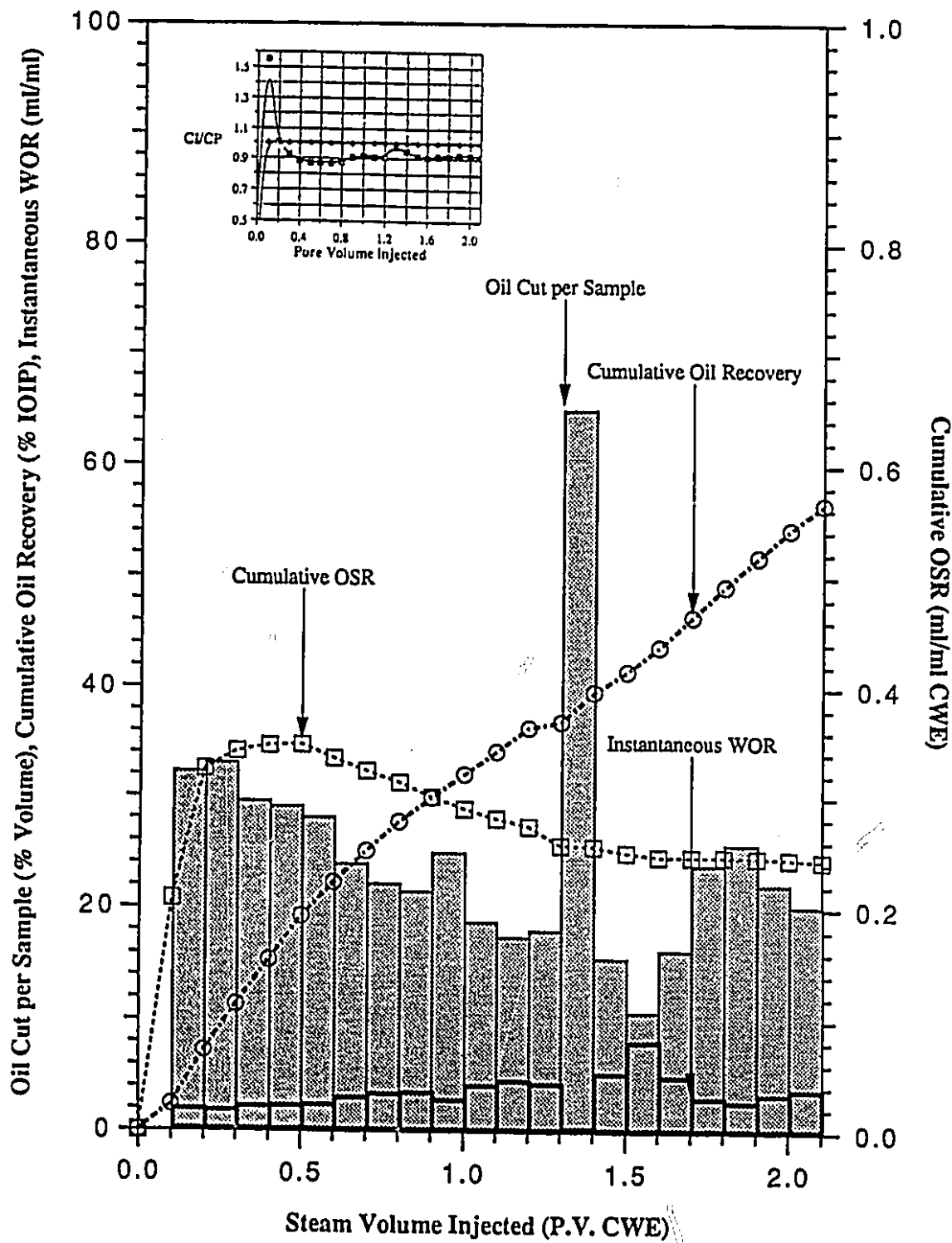
Figure 6.4: Production History of Run 12 (Base Case),
Steamflood with pattern inversions using pairs of horizontal injectors
and producers in a homogeneous, horizontal reservoir.
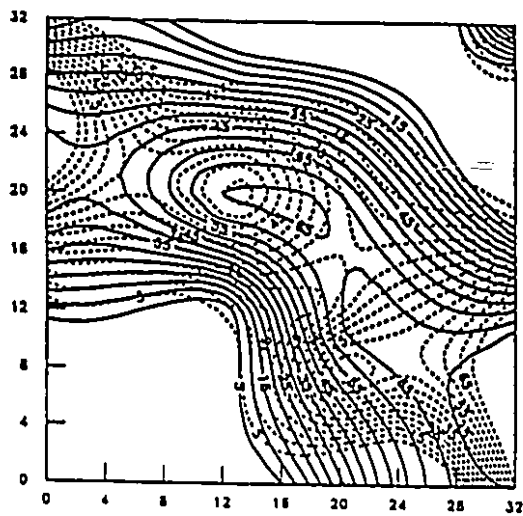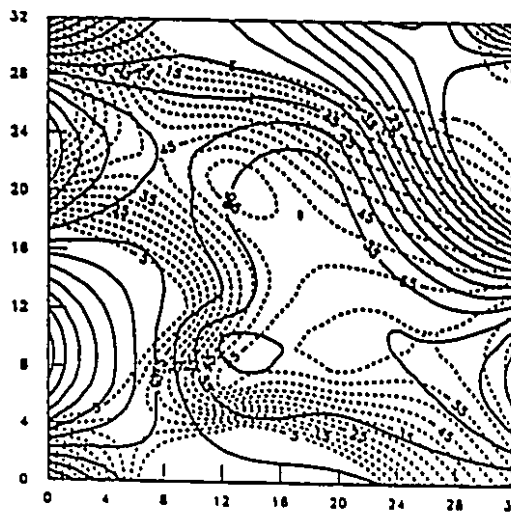
a) 0.50 PV (CWE) Inj.

b) 0.85 PV (CWE) Inj.
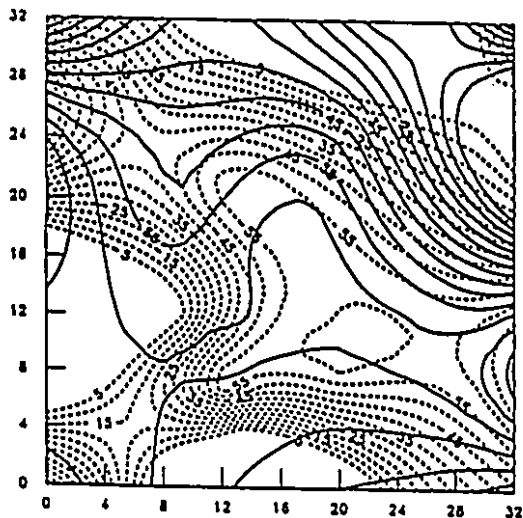
c) 1.00 PV (CWE) Inj.
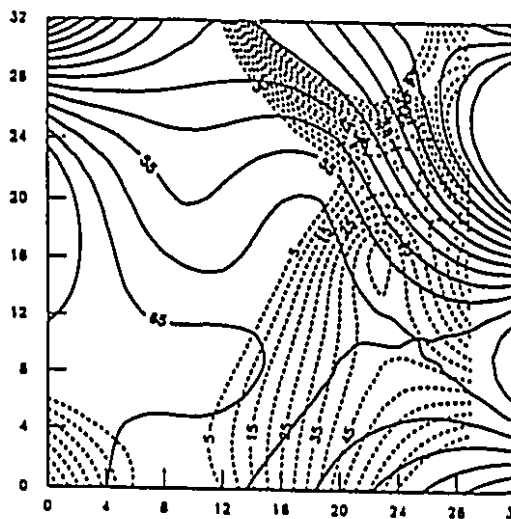
d) 1.20 PV (CWE) Inj.

Legend: ——— Upper Model Temperature, °C

— — — Lower Model Temperature, °C

Port 3   Port 4

Port 1   Port 2
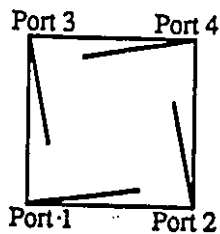
Homogeneous Model

Base Case Experiment

Legend:

Inj. for 0.8 PV using ports 2 and 3

0.4 PV	1 and 3
0.4 PV	1 and 4
0.5 PV	2 and 3

Figure 6.5:   Plan view of the temperature distribution inside the model along with injection and production strategy for Run 12.

fluids (oil, water and steam) saturations in the reservoir allows accurate determination of the steam zone, which leads to an accurate heat distribution (heat accumulation and heat loss) calculation. However, prior to making these analyses, knowledge of the dominant displacement mechanisms in the reservoir is important because it allows the heat loss process to be modeled in one dimension. These analyses are discussed in the next section.

6.5.1 Displacement Mechanisms

In interpreting the data to determine the dominant type of displacement mechanism, two questions were posed. They were as follows: if the reservoir was homogeneous, containing a connate or irreducible water saturation (S_{wi}) and an oil saturation, S_{oi}, then

> 1) why was a water cut present in the first sample collected, that is, after 0.1 PV of steam was injected, and
> 2) what did this fact tell us about the type of displacement, shape, or position of the steam interface inside the model ?

If a frontal drive model can be assumed, then according to the theory given by Mandl and Volek[31], steam condensate should not be present at the producer in the early stages of a steamflood experiment. The reason is that an oil bank is produced first, with condensate breakthrough occurring subsequently. After breakthrough, the water cut continues to increase, and in some cases steam breakthrough may occur.

From the discussion in the previous paragraph, it is obvious that the frontal drive model proposed by Mandl and Volek[31] cannot be assumed in these experiments. Therefore, a gravity override model, proposed by Neuman[34], is assumed. This assumption is supported by conducting experiments in the visual model, and from analyzing the temperature contours.

The visual experiments showed the segregation of steam resulting from density differences during a steamflood, thus contributing to a steam zone overlying the oil zone. From the temperature contours on Figure 6.5, it can be seen that vertical displacement of oil and condensate from the steam zone toward the horizontal production well was dominant in the recovery process. As mentioned in the previous section, prior to approximately 0.20 PV of steam injected, the state of the displacing fluid was hot water. During this stage, the shape of the interface appeared relatively vertical. After 0.2 PV had been injected, the formation

of a steam zone became evident. In the next 0.1 PV injection period, the interface between the steam–condensate remained relatively vertical, signifying a frontal drive. However, as injection continued, steam override became more pronounced, and the shape of the interfaces between the steam–condensate–oil was greatly tilted, as illustrated in Figures 6.5 (b) and (c). Eventually, as the flood matured, the energy present was more than enough to overcome the heat loss to the overburden. The result was an increase in temperature and advancement of the steam zone. At this stage, the interface appeared horizontal, and the production of the fluids resulted from the expansion of steam from the top of the reservoir.

This was supported by the observation made subsequent to the completion of the experiment, during the cleaning phase. In removing the Neoprene sealant sheet, the top of the modeled reservoir was observed to be 'clean', while the middle portion of the lower layer of the reservoir contained a large amount of residual oil along with the steam condensate. It was also observed that residual oil was present in the lower part of the porous pack near the two horizontal injectors. This implied the presence of frontal displacement. However, the vertical drive as a result of steam expanding from the top played a more dominant role. The temperature contours for the homogeneous base case experiment, Figure 6.5 (a), clearly illustrates the above observation. After 0.5 PV of steam had been injected (CWE), the lower temperature contour, $T = 5^\circ$ C, still remained at a distance less than 4 inches from the injector.

At this point, it is important to be aware of two factors that influence the resulting type of displacement (whether it is a frontal drive or gravity override). The two factors are permeability and heat loss. The vertical and horizontal permeabilities, k_v and k_h, in a formation will determine the dominant displacement mechanism. In this homogeneous model, as a result of the scaling criteria, the permeability of the glass beads pack was approximately 4500 darcies. This implied $k_v = k_h = 4500$ darcies. With the high permeability of the scaled porous medium, steam overriding the top of the reservoir was promoted. Equally important was the amount of heat accumulated in the model. The heat loss to the overburden was minimal due to the low thermal conductivity of the Neoprene sealant sheet. With the fiberglass tray representing the scaled model, the heat loss to the underburden was further restricted, due to the low conductivity of fiberglass. The low heat loss to the overburden and underburden increased the amount of heat stored in the formation. This effect, coupled with the high absolute permeability of the reservoir, created a condition where vertical displacement of fluids become more dominant as compared to frontal displacement. If the heat loss to the overburden were excessive, a

vertical drive would no longer be dominant, and the contribution of the frontal drive would have been more pronounced. In view of the above factors, the oil recovery is likely to be optimistic when this result is scaled up to a field project.

6.5.2 Fluid Saturation Profiles

With the aid of the temperature contour plots along with the pressure and production data, material balance equations (MBEs) were used to construct the saturation profiles of the fluids (steam, condensate and oil) present in the reservoir. In this procedure, a material balance for three zones was considered. These were: the steam zone (Zone 1), the hot water or condensate zone (Zone 3) and the virgin oil reservoir (Zone 2). Following Peake[40], two material balance equations (MBEs) were derived for the three zone reservoir. The first MBE was for the oil component, while the second MBE was for steam and water. In the MBE for the oil component, there were three unknowns: S_{o1}, S_{o2} and S_{o3}. Hence, to obtain the oil saturations in each zone, two extra equations were needed. In this work, the assumption that S_{o1} equals S_{orst} was made. As such, the three unknown saturations have been reduced to two. A second equation, required for the determination of S_{o2} and S_{o3}, was then formulated. It described the oil saturation inside the reservoir at any injection-production time. Having two equations, the two unknowns S_{o2} and S_{o3} were calculated. The water saturations for Zones 1, 2 and 3 were found by using the identity that the saturations in each zone added up to one. The full derivations and assumptions are shown in Appendix A.

From the production data along with the temperature contours and pressure data, it was observed that every steamflood experiment initially started as a hot water drive. Hence, the above MBEs were simplified to satisfy the two-zone hot water drive model. The derivation is presented in Appendix A. In this model, the first zone implies a hot water region, while the second zone signifies the virgin oil reservoir. The saturations S_{o1} and S_{o2} were obtained in a similar fashion, as described above.

With the oil saturations (S_{o1}, S_{o2} and S_{o3}) and steam saturation (S_{st}) known at various injection periods, the overall water saturation (S_w) is obtained and plotted. This information was valuable in determining the theoretical steam zone volume, the heat accumulation inside the model, along with the injection-production strategy; that is, pattern inversion and well combinations used.

A detailed calculation showing the construction of the saturation profile – for the oil phase – is presented in Appendix A. Figure 6.6 illustrates the graph of oil saturation profiles for Zones 1, 2 and 3. Initially, the oil saturation, S_{oi}, was 0.9031. For the first 0.2 PV of steam injected, the steam zone was not present. At this stage, the production of oil resulted from hot waterflooding. Therefore, there were two zones (Zone 1 – water and Zone 2 – oil) present in the reservoir. After 0.2 PV of steam was injected, the oil saturation in the oil zone decreased to 58.7%, and the oil saturation in water zone, S_{o1}, slightly increased to 25.1%. Physically, the increase in S_{o1} is expected because the advancement of the flood front exposed a larger volume of oil to steam. Since the sweep efficiency and displacement efficiency of a flood in a pattern are less than one, some oil is bypassed. This led to an increase in the oil saturation in the waterflooded zone. When the injection of steam continued beyond 0.2 PV, a steamflood was in operation. There were three distinct zones in the reservoir. These zones were the steam zone, the condensate zone and the oil zone. Figure 6.6 shows the oil saturation in the oil zone decreased most significantly, which was desirable, and the use of pattern inversions at 0.8 and 1.2 PV reduced the oil saturation in the condensate zone..

Figure 6.7 shows the saturations of the phases (oil, water and steam) at various injection times. In discussing this graph, it is important to recognize that the inversions in the pattern did not collapse the steam zone as illustrated at 0.9 and 1.3 PV. To clearly understand this effect, it was important to understand how the saturation of steam was obtained experimentally. As mentioned previously, the steam zone volume was taken as the difference between the cumulative amount of fluids produced and the cumulative amount of steam injected. This argument is valid if the reservoir is homogeneous and no gas saturation is present in the model. These two conditions are satisfied in this ba experiment. When pattern inversion was used, the volume of cold oil exposed pattern increased. As a result of the unfavourable mobility of the oil in the vicinity of the producer, the production of oil and water decreased. Hence, the cumulative production was misrepresented, and so was the steam zone volume.

6.5.3 Steam Zone Volumes

In Appendix B, steam zone calculations using both the Mandl and Volek[31] model and the Neuman[34] model are presented. The reason for the selection of these two models is the different representation of the dominant driving mechanism. As mentioned earlier, the Mandl and Volek[31] model was for a frontal displacement, while the Neuman[34] model was
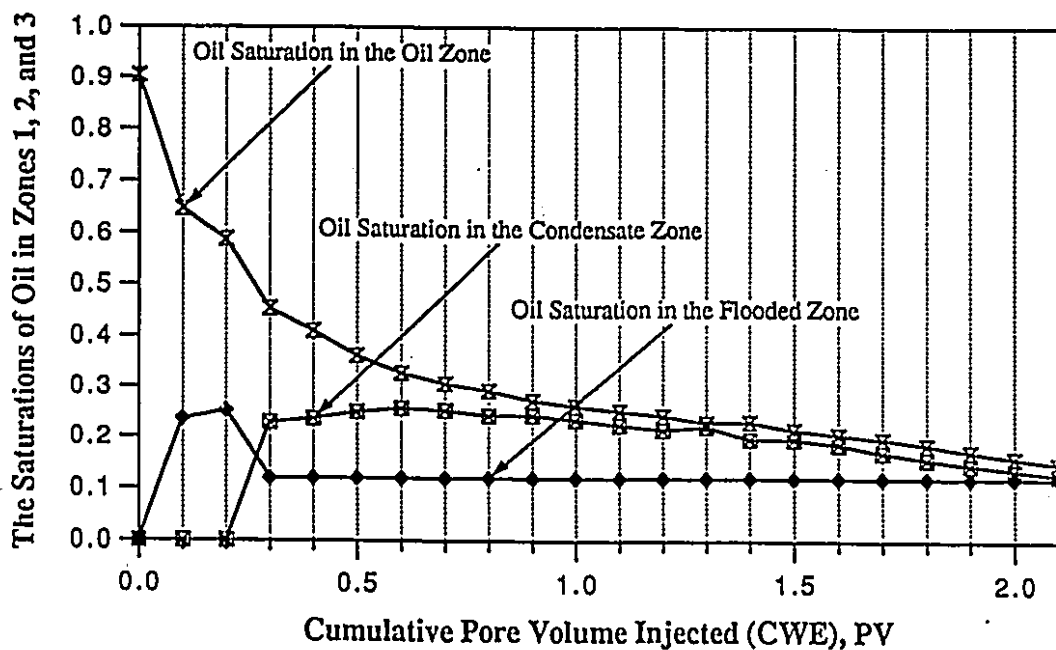
Figure 6.6:   The Saturations of oil in the oil, condensate, and steam flooded
               zones at various cumulative injection periods, for the base case run.
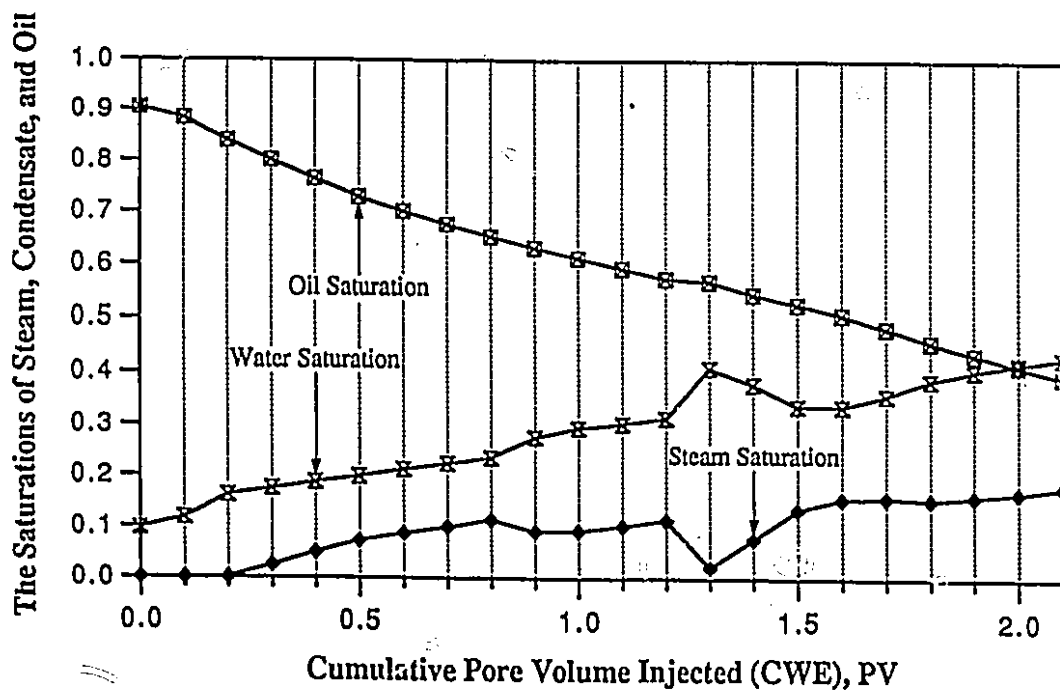
Figure 6.7:   The saturations of steam, condensate, and oil in the reservoir
               at various cumulative injection periods, for the base case run.

a gravity override model. In the frontal model, the critical time was first calculated to serve as a reference for determining the steam zone formula (expression) used. In the gravity override model, the height of the steam zone and the area covered by steam were calculated first. The steam zone volume was obtained by summing the area originally heated during each time increment multiplied by the steam zone thickness beneath an areal increment heated at that time. The graph of the Steam Zone Volume versus the Cumulative Pore Volume Injected for the Mandl and Volek[31]'s frontal displacement model, Neuman[34]'s gravity override model, and the experimental data is shown on Figure 6.8.

The calculation and comparison of steam zone volumes were done prior to pattern inversion as it was difficult to obtain these volumes subsequent to an inversion of pattern both experimentally and theoretically. Experimentally, the difficulties in determining the steam zone volume – as mentioned earlier – are attributed to the unfavourable mobility of cold oil exposed to the sweep pattern. This led to the misconception that the steam zone inside the reservoir collapsed. Theoretically, the equations given by Neuman to predict the steam zone volume could not be used because of the dependence of the parameter f_{pi} on the amount of heat injected, and produced. Also, the problem with resaturation of fluids, which was apparent with pattern inversions, were not considered by Mandl and Volek and Neuman for their work.

Figure 6.8 shows the experimental steam zone volumes matches well with Neuman[34]'s steamflood model. The accuracy of the prediction is attributed to the precise injection and production data, which implied the accurate use of the parameter f_{pi} in Neuman's steam zone expression. The differences in the steam zone volumes between experimental data and Neuman[34]'s model is attributed to the sweep efficiency of a pattern steam drive in the scaled physical experiment. On the other hand, the steam zone volume predicted by Mandl and Volek[31] showed a large discrepancy with those obtained experimentally. This difference was attributed to a single parameter, the thermal conductivity of the overburden, k_{hob}. The value k_{hob} used in the calculation of the steam zone volume was that for the Neoprene sheet.

6.5.4   Heat Balance

Heat balance calculations are probably the most important step in analyzing the economics of a steamflood. These calculations allow knowledge of the heat distribution inside the model along with the heat loss to the overburden and underburden, and the heat produced.
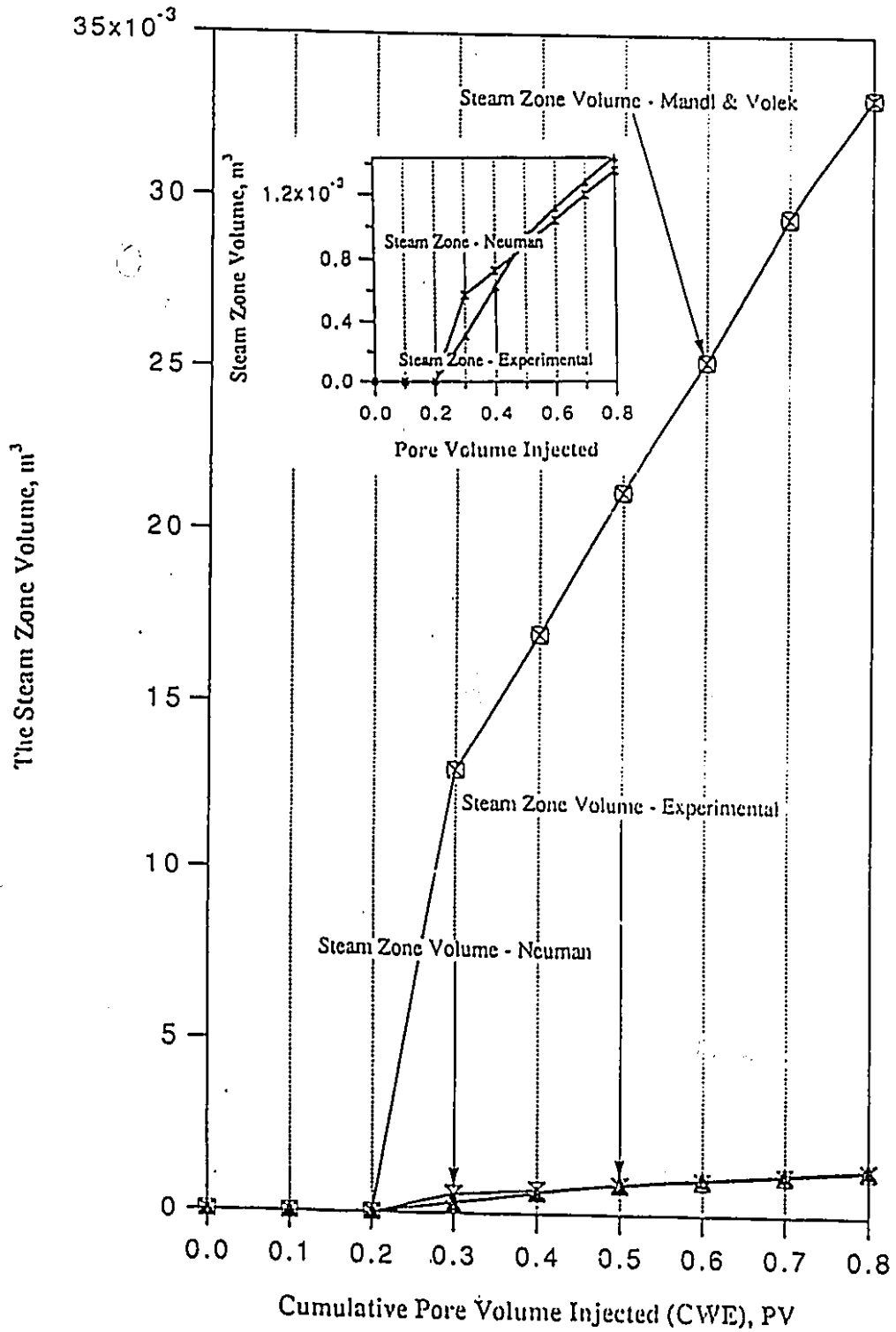
Figure 6.8   The steam zone volume obtained from Neuman's steam override model, Mandl and Volek's frontal drive model and experimental results.

In the following discussion, the term heat balance shall be referred to as the cumulative heat balance, not the instantaneous heat balance. The overall (cumulative) heat balance equation at any time, t, is given by:

$$Q_{inj} = Q_{production} + Q_{loss} + Q_{form} \qquad (6.1)$$

where

Q_{inj} — Amount of energy injected, (kJ)

$Q_{production}$ — Amount of energy produced, (kJ)

Q_{loss} — Amount of energy loss to the cap and base rock, (kJ)

Q_{form} — Energy accumulated in the formation, including the matrix (glass beads), and the fluids (oleic, aqueous, vapour), (kJ)

In this work, the amounts of heat injected and produced were obtained from the injection and production data. The heat injected at the end of any time t is given by the equation

$$Q_{inj.} = i_{st}\left(h_{inj} - h_{res} + f_{st}L_v\right) * t \qquad \ldots\ldots (6.2)$$

where

i_{st} = the mass flow rate of steam (kg/s),

h_{inj} = the enthalpy of saturated water (kJ/kg),

h_{res} = the enthalpy of water at the initial reservoir temperature (kJ/kg),

f_{st} = the quality of steam (dimensionless),

L_v = the latent heat of vaporization (kJ/kg),

t = the injection time (sec),

The cumulative heat contained in the fluids produced is given by

$$Q_{prod} = \sum_{i=1}^{n}\left\{\left(V_{w,i} \times C_{w,i} \times \rho_{w,i} + V_{o,i} \times C_{oi} \times \rho_{o,i}\right) \times \Delta T\right\} \qquad \ldots\ldots (6.3)$$

where

i = any production sample of oil and condensate.

n = total number of samples.

ΔT = the temperature difference between the initial reservoir temperature and the average temperature of production sample i.

C_w = the specific heat of water, kJ/kgK.

C_o = the specific heat of oil, kJ/kgK.

$$\rho_{w,o} = \text{The density of the water and oil, kg/m}^3.$$

The amount of heat accumulated in the model required a precise knowledge of the fluid saturations inside the reservoir, along with the steam zone volume and the condensate volume. The heat accumulated in the reservoir at any time t is given by

$$Q_{formation} = \sum_{k=1}^{m} V_{R,k} \times \left\{ \phi S_{o,k}\rho_{o,k}C_{o,k} + \phi S_{w,k}\rho_{w,k}C_{w,k} + \phi S_{st,k}\rho_{st,k}C_{st,k} + (1-\phi)\rho_{matrix,k}C_{matrix,k} \right\}$$

$$..... \quad (6.4)$$

where

m	= the number of temperature contours
k	= an incremental representation for any temperature contour,
$V_{R,k}$	= the volume corresponding to a temperature contour, (m^3)
ϕ	= the porosity of the glass beads reservoir, (dimensionless)
$S_{o,w,s,k}$	= the saturations for oil, water and steam for a given temperature contour k, (dimensionless)
$\rho_{o,w,s,k}$	= the density of the oil, water and steam for a given temperature contour k, (kg/m^3)
$C_{o,w,s,k}$	= the heat capacity of the oil, water and steam for a given temperature contour k, (kJ/kgK)
$\rho_{matrix,k}$	= the density of the matrix, (kg/m^3),
$C_{matrix,k}$	= the heat capacity of the matrix, (kJ/kgK).

The heat loss to the overburden and underburden is therefore found by rearranging Equation 6.1.

An analytical model, representing the cumulative heat loss, is also developed to verify the heat loss calculation made based on experimental data. As described in Section 5.2.1, a Neoprene sheet was used in this experimental set-up to prevent fluid leakage. As a consequence, the heat loss to the overburden is modeled by a composite heat transfer problem having two mediums: medium one (i=1) represents the Neoprene sheet and medium two (i=2) represents the granite cap rock. The temperature distribution in the Neoprene sheet and cap rock, as derived in Appendix C, are given by:

$$T_1(x,t) = \sum_{n=1}^{7} coeff_{T_{1n}} * \sin\left(\frac{\beta_n}{\sqrt{\alpha_2}}x\right) + \left[\frac{-k_2 h_3}{k_2 k_1 + h_3 k_1 b - h_3 a(k_1 - k_2)}\right](60x) + 70.... \quad (6.5)$$

and

$$T_2(x,t) = \sum_{n=1}^{7} coeff_{T_{2_n}} * \left[A_{2_n} \sin\left(\frac{\beta_n}{\sqrt{\alpha_2}}x\right) + B_{2_n} \cos\left(\frac{\beta_n}{\sqrt{\alpha_2}}x\right)\right]$$
$$+ \left[\frac{k_1 h_3}{k_2 k_1 + h_3 k_1 b - h_3 a(k_1 - k_2)}\right] * f_0\left(-x + a - a\frac{k_2}{k_1}\right) + 70$$

..... (6.6)

Therefore the cumulative heat loss is given by

$$Q_{loss} = -\int_{t=0}^{0.8PV} kA\frac{dT}{dx}dt$$

..... (6.7)

Figure 6.9 shows the temperature distribution at various penetrating distances and times inside both the Neoprene sheet and the cap rock. At times t = 100 and 600 seconds, the instability of the temperature distribution in the cap rock is observed. This implied that the solutions are not valid early in a steamflood. Appendix C presents the procedure and formula required to obtain the amount of heat injected, produced and accumulated. A derivation of the analytical solution to the heat loss problem, and sample calculations of the heat lost for the base case steamflood experiment are also illustrated in Appendix C.

In Run 12, after 0.8 PV of steam had been injected, the cumulative heat injected was 5367.3 kJ; the cumulative heat produced was 1583.9 kJ; and the heat stored in the formation was 3337.5 kJ. Therefore, the heat loss was found to be 595.6 kJ. From the analytical model, the heat loss was found to be 643.4 kJ. The difference in the two values of heat loss was approximately 7.4%. The small difference between these two values was attributed to the proper modeling of the heat loss process. Apparently, this also implied the proper calculation for the heat stored in the formation, and verified the dominating mode of displacement was gravity override.

6.6   Steeply Dipping Reservoir

Different strategies for steamflooding a steeply dipping reservoir were studied by Hong[42], who used a compositional steamflood simulator. The reservoir was represented by two-dimensional and three-dimensional grid models. The steamflooding strategies included: 1) Shutting-in the producer locating up-dip once steam breakthrough or a high steam to oil ratio (SOR) occurred, 2) Reducing the injection rate to meet economic constraints,
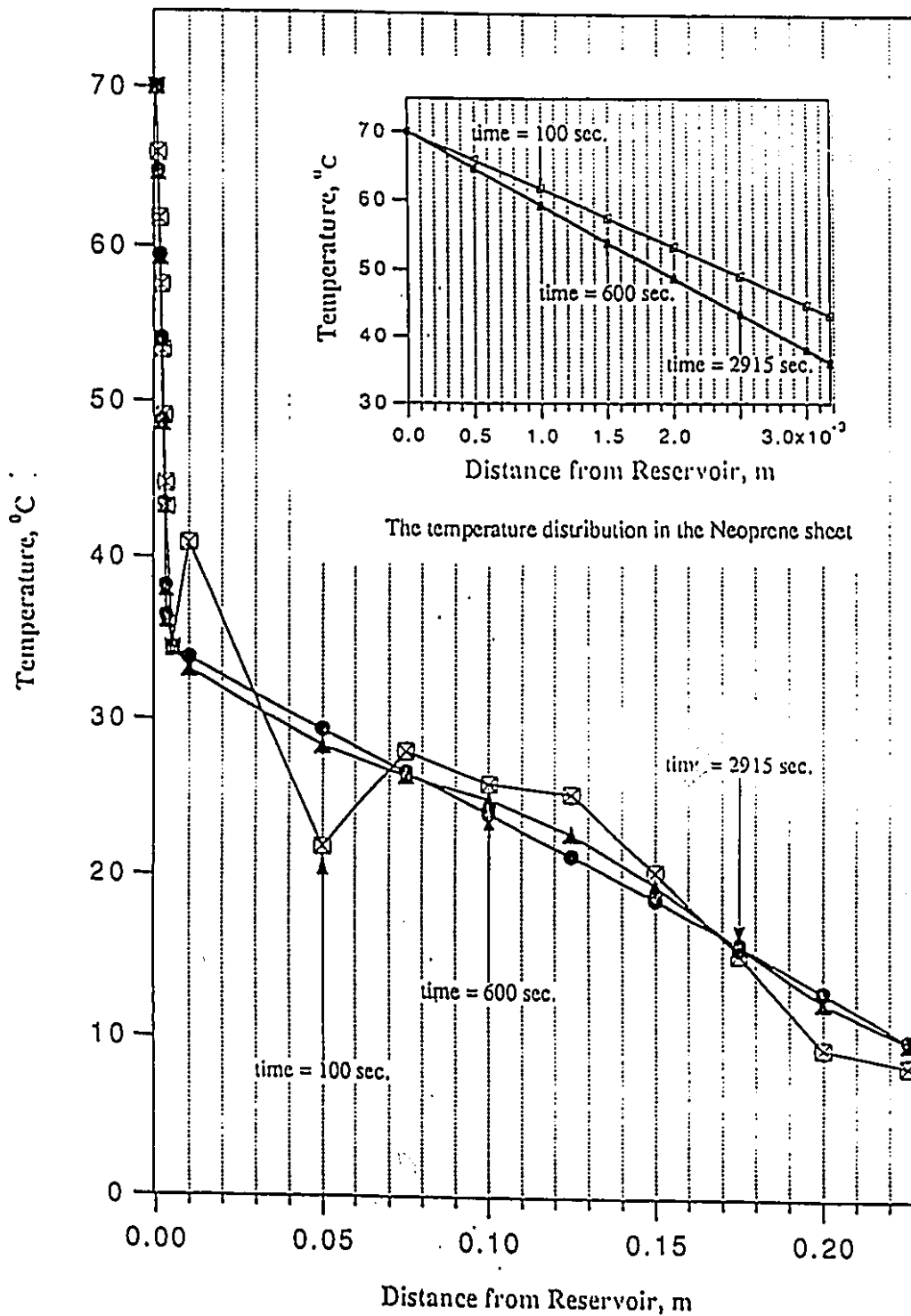
Figure 6.9: The temperature distribution in the Neoprene sheet and cap rock
after 100, 600, 2915 (0.8 PV) seconds.

3) Switching the injectors and producers during drainage to obtain maximum recovery, and
4) Injecting a non-condensable gas, such as nitrogen, to prevent steam cycling in the up dip
portions of the reservoir.

There are several important differences between the work in this thesis, and the work
reported by Hong[42]. In the study made by Hong[42], the reservoir was 30.5 m thick, the
injection of steam was from vertical wells, and there were several rows of vertical wells at
different elevations on the incline – hence covering several planes. In contrast, this study
consisted of a prototype reservoir that was 11 m thick (the thickness of the scaled model
was 2.5 inches) and the injection of steam and production of fluids were from horizontal
wells. The location of the horizontal wells used in these experiments is illustrated, as a
subset, on the temperature contour plots.

In several reported cases of steeply dipping reservoirs, steam cycling was observed. Steam
cycling is defined as the phenomenon where the injected steam rises to the top of the
reservoir, then condenses due to cooling, and subsequently, the condensed water falls
toward the bottom of the reservoir as a result of gravity. In the present experimental set-
up, the movement of condensed water towards the bottom of the reservoir could not be
observed; hence, definite conclusions cannot be made. However, in conducting experi-
ments using the visual model for a homogeneous reservoir, this effect was observed only
when the injection rate was sufficiently low. With the low injection rate, the rate of heat
injected required for the formation and maintenance of the steam zone was insufficient. As
a result, steam condensed and segregated.

6.7   Shut–In Experiments for Steeply Dipping Reservoirs

Due to economic or strategic reasons, and/or due to operational problems, some
steamflooding projects are being shut-in. In doing so, the operators are concerned about
the effect on recovery performance when steam injection is resumed. Hence, questions of
how to properly manage the oil reservoir prior to, and subsequent to shut-in arise.

In studying the effects of shut-in, two experiments were carried out. The collapse of the
steam zone which led to an increasing WOR was carefully studied. The time of continuous
injection prior to shut-in was an important parameter as the mechanism of the displacement
process was observed to vary depending on whether it was made before or after steam
breakthrough. In these two experiments, the injector was shut-in prior to breakthrough. In

doing so, the steam zone volumes prior to shut-in and re-injection were monitored easily and the data were manipulated more accurately.

The current experimental set-up made it extremely difficult to monitor the steam zone volume when the flood was shut-in after steam breakthrough. The reason was with only one pressure transducer and one thermocouple at the production port, it was not possible to observe steam condensing in the vicinity of the horizontal production well.

6.7.1 Shut-In and Pattern Inversions in a Dipping Reservoir

Experiment 5 involved the use of horizontal wells at the injection and production ports to study the effects of shut-in in steeply dipping (inclined) reservoirs. The porosity of the glass bead pack was 34.1%, the initial oil saturation was 90.0% and the rate of injection was 210 ml/min. with steam injection down-dip. In the experiment, steam was first injected for 0.7 PV. It was followed by a period of shut-in, equivalent to 1.0 PV of injection time, then steam injection was resumed. Pattern inversions were made after 1.1 PV, 1.5 PV and 2.0 PV of steam had been injected. Pattern inversions were made in an attempt to increase the areal and vertical sweep, thus increasing oil production. Figure 6.10 shows the production history of Run 5. From the inset graph of the ratio CI/CP versus the pore volume injected, it was observed that within the injection period 0–0.3 PV, the flood was a hot water drive. After this period, a steamflood was evident in the reservoir. The production history also shows that subsequent to re-injection, relatively high oil production was obtained. This was a result of the oil present prior to shut-in. Subsequent to re-injecting 0.1 PV of steam, the instantaneous water-oil ratio (WOR) increased by one order of magnitude. This increase was a result of the production of the steam condensate present in the reservoir during the shut-in period. The oil cut was also observed to increase as the injected steam supplied enough heat to overcome the heat loss and advance the steam front.

With the temperature data acquired during the experiment, the effect of shut-in was observed by constructing temperature contours at various times during the steamflood. Figure 6.11 shows the temperature contours for Run 5. Prior to making further discussion, it is important to note that the injected steam has two main purposes: 1) to supply the heat loss to the overburden and underburden occurring behind the steam front, and 2) to raise the temperature of the condensate zone to a new value of T_s.

Figure 6.10: Production History of Run 5,
Steamflood with pattern inversions using pairs of horizontal injectors
and producers for a homogeneous and inclined reservoir. Wells were
shut-in for an equivalent injection time of 1.0 PV (CWE) of steam
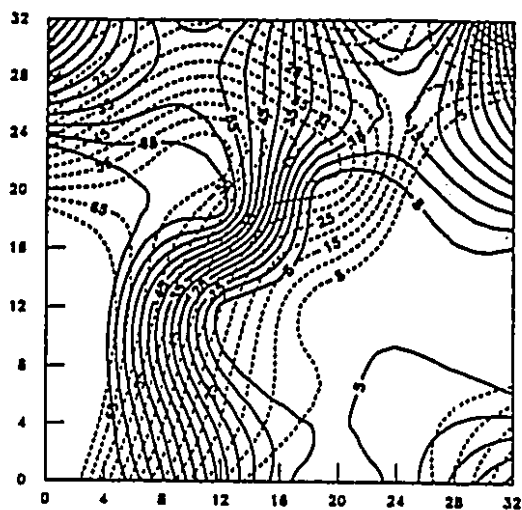
a) 0.50 PV (CWE) Inj.
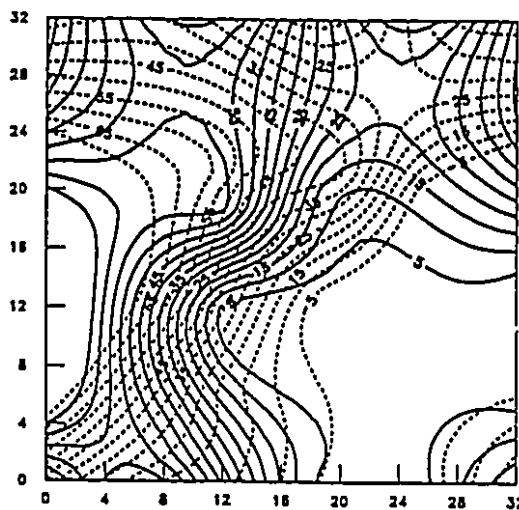
b) Start of Shut in
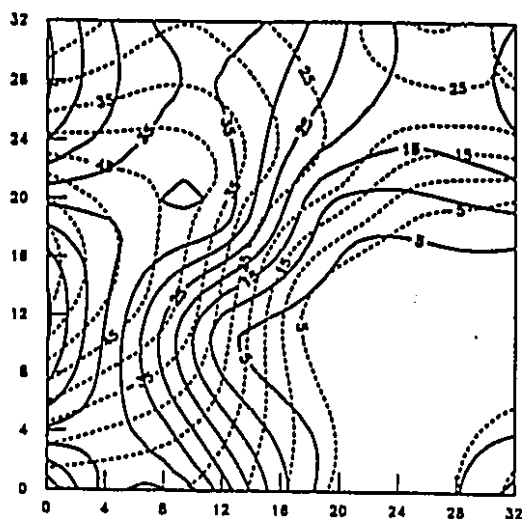
c) End of Shut in
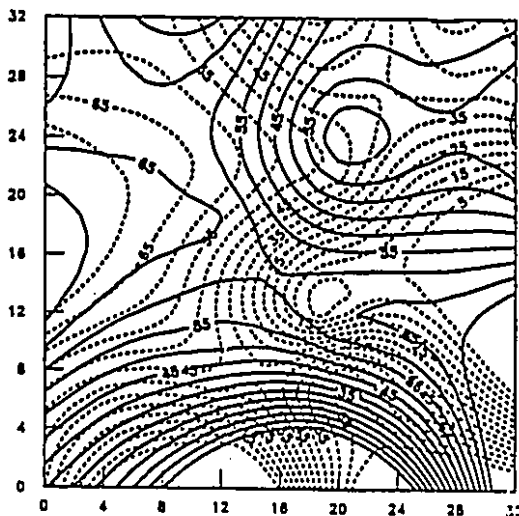
d) 1.30 PV (CWE) Inj.

Legend: —————— Upper Model Temperature, ° C

— — — Lower Model Temperature, ° C
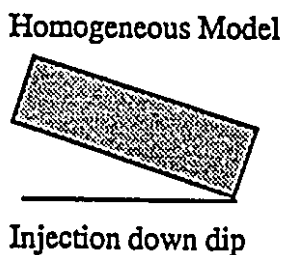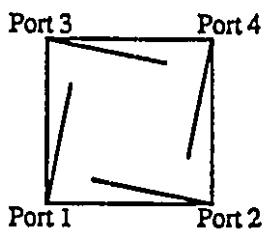
Port 3   Port 4   Homogeneous Model Legend:

Inj. for 0.6 PV using ports 1 and 4
Shut on time equivalent to 1.0 PV of injection

0.5 PV	1 and 4
0.4 PV	2 and 3
0.5 PV	2 and 4
0.4 PV	1 and 3

Port 1   Port 2

Injection down dip

Figure 6.11:   Plan view of the temperature distribution inside the model along
with injection and production strategy for Run 5.

When the injector was shut-in, the production rate was observed to decrease sharply. This was due to the reduction of both pressure and heat in the reservoir. The reduction in injection pressure resulted in a small driving force between the steam zone and the horizontal producer. The reduction in the injected heat contributed to the collapse of the steam zone, which reduced the amount of heat transferred into the oil zone ahead of the moving front, and consequently led to unfavourable mobility.

Shortly after shut-in, a small amount of fluid was produced over a short interval of time. There are two possible explanations. The first explanation is: as the injector is shut-in, the temperature and heat in the steam zone decreased leading to condensation. As a result of condensation, the pressure slightly increased giving rise to some fluid production. However, not long after, the pressure gradient between the reservoir and production well was so small that no production was observed. The second explanation is based on the production mechanism. In this low pressure model, the presence of a vacuum pump served two functions. The first function was as a pressure sink point where fluids were produced. The second function was to keep the pressure inside the model less than the atmospheric pressure. In using the vacuum pump, there was a tendency for fluids to be produced by the force of suction.

From observing the temperature contours, Figures 6.11 (b) and (c), that is, the period between the start of shut-in and re-injection, the steam zone volume was clearly seen to collapse which resulted in a larger volume of condensate, as compared with the base case run. The steam zone prior to shut-in was approximately 0.000534 m^3. Based on engineering judgment, the steam zone volume after shut-in was approximately 0.000209 m^3. Hence, as a result of shut-in, the steam zone collapsed by approximately 60%.

The experimental set up of Run 6 was similar to that of Run 5. The objectives of this experiment were to establish the repeatability of results obtained in Run 5, and to pin point the injection-production pattern giving the highest recovery. The porosity of the glass bead pack was 30.3%, the initial oil saturation was 90.8% and the injection rate was 210 ml/min. with steam injection down-dip. Steam was injected for 0.8 PV, followed by a period of shut-in, equivalent to an injection time of 1.0 PV. Pattern inversions were then made after 1.0 PV, 1.4 PV, and 1.8 PV of steam injected. The production data for this experiment (Run 6) is shown on Figure 6.12, while the temperature contour plots are shown on Figure 6.13.
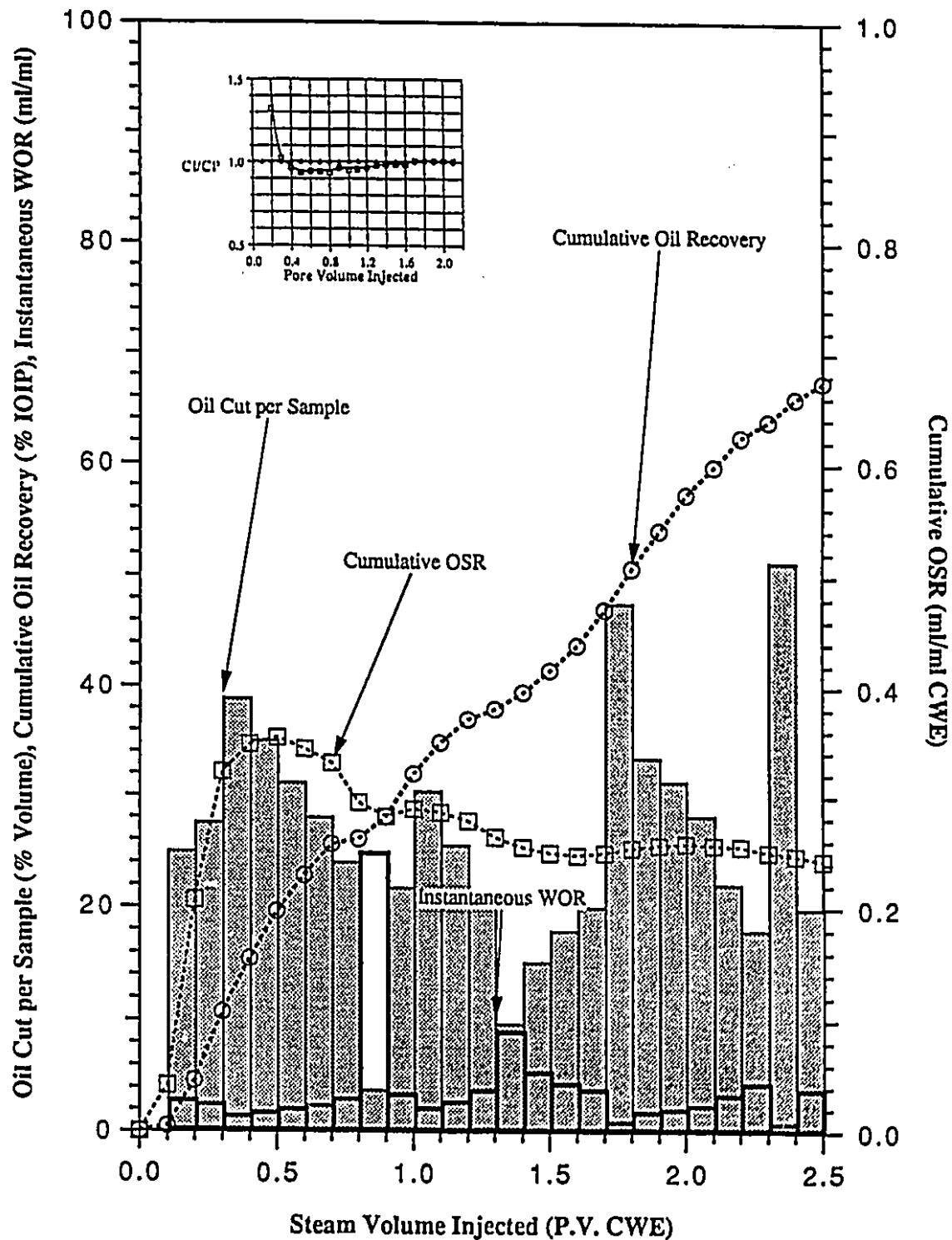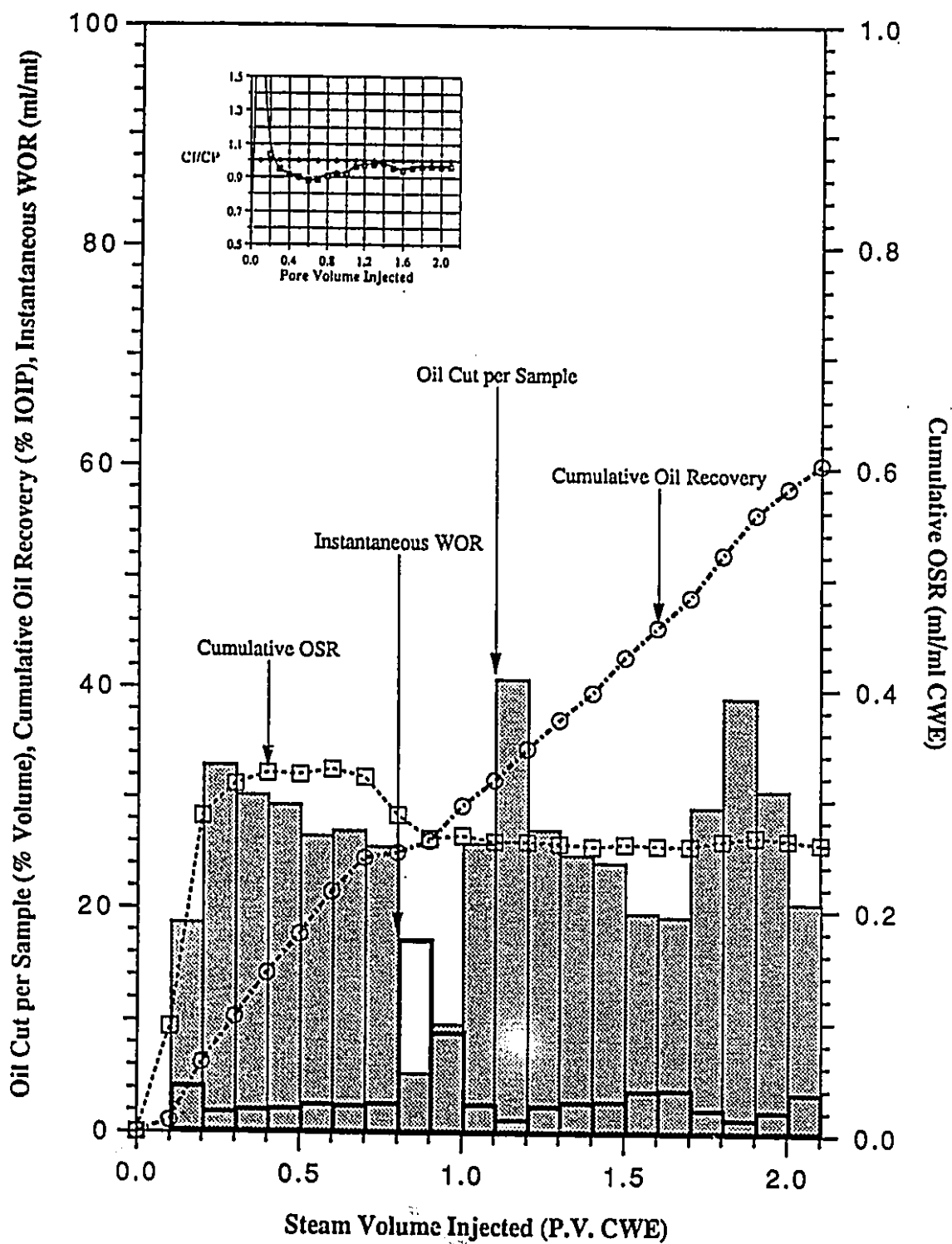
Figure 6.12: Production History of Run 6,
Steamflood with pattern inversions using pairs of horizontal injectors
and producers for a homogeneous and inclined reservoir. Wells were
shut-in for an equivalent injection time of 1.0 PV (CWE) of steam.

a) 0.50 PV (CWE) Inj.

b) Start of Shut in

c) End of Shut in

d) 1.30 PV (CWE) Inj.

Legend: ——— Upper Model Temperature, °C

— — — Lower Model Temperature, °C

Port 3   Port 4   Homogeneous Model   Legend:
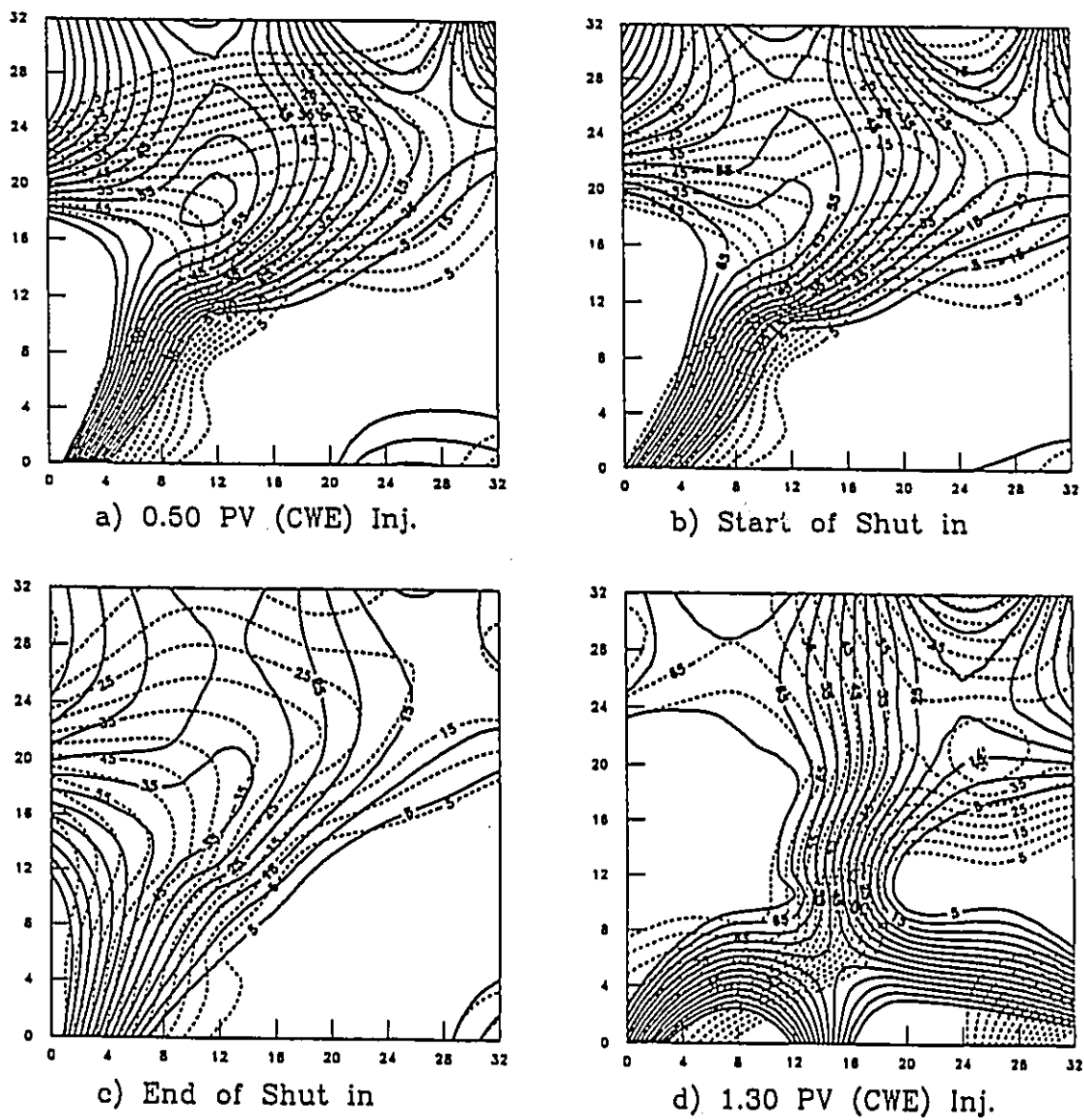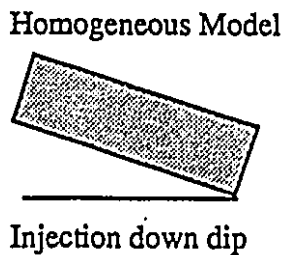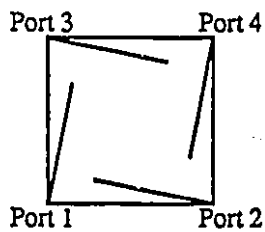
Inj. for 0.7 PV using ports 1 and 4
Shut on time equivalent to 1.0 PV of injection

0.3 PV	1 and 4
0.4 PV	1 and 3
0.4 PV	2 and 4
0.3 PV	2 and 3

Port 1   Port 2

Injection down dip

Figure 6.13:   Plan view of the temperature distribution inside the model along with injection and production strategy for Run 6.

The inset graph of the ratio CI/CP versus pore volume injected for both Runs 5 and 6 show that the steam zone present in Run 6 was larger than the steam zone in Run 5. This is the case because for identical injection period, the lower CI/CP ratio in Run 6 implied larger cumulative production which resulted from the expansion of the steam zone. Also, the formation of the steam zone occurred 0.1 PV earlier in Run 6. This was attributed to a lower initial pressure and higher initial temperature in the reservoir, and a tighter pack.

In Run 6, prior to shut-in, at 0.7 PV, the cumulative injection was 8904 ml. The cumulative production, on the other hand, was 10060 ml. The difference between the two is 1156 ml, and is attributed to the expansion of the steam zone. Therefore, the steam zone volume was approximately 0.001156 m^3 prior to shut-in. Based on engineering judgment, the steam zone volume prior to re-injection was approximately 0.0004314 m^3. Hence, as a result of shut-in, the steam zone collapsed approximately 63%.

Based on the heat loss calculation completed for the base case experiment, it was concluded that the heat loss in this model was much less than in the prototype (field). As such, a long duration of shut-in did not completely cause the steam zone to collapse. With large amounts of heat accumulated in the reservoir, the oil cut in Runs 5 and 6 reached a maximum value at approximately 0.4 PV after re-injection, that is, injection of steam after shut-in. This is evident from the inset graph of the ratio of CI/CP versus pore volume of steam injected, and from looking at the temperature contours on Figures 6.11 – 6.13 (b) and (c). Further discussion on the heat loss calculations and models is given in Appendix C.

The scaled up values corresponding to 0.4 PV, after re-injection, for Runs 5 and 6 are 2.11 years and 1.87 years, respectively. In field operations, such a long period of shut-in would have caused the steam zone to collapse completely because of larger heat loss to the overburden and underburden. Consequently, greater amount of heat, that is, a longer period of re-injection, would be required before oil production could be seen from the re-establishment of the steam zone.

Due to the storage of heat in the reservoir, the use of pattern inversions – subsequent to shut-in – for Runs 5 and 6 was found beneficial as the oil cut increased, and the cumulative OSR curve changed from a negative to a positive slope (trend).

6.7.2 Effect of Shut-in and Pattern Inversions on the Cumulative Oil Recovery

Figure 6.14 shows the cumulative oil recovery, and the oil cut per sample for Runs 5 and 6. It is interesting to note that the difference in the ultimate recovery for these two experiments was only 0.5%, in spite of the different times of pattern inversion, and different injection and production strategies used. The reason is the similar volumetric sweep efficiency in both runs.

In Run 5, the injection period between 1.1 and 1.5 PV of steam, with injection at Port 2 and production at Port 3, resulted in 6.7% incremental recovery. Subsequently, the injection of another 0.5 PV of steam with injection at Port 2, and production at Port 4, resulted in approximately 15.7% incremental oil recovery. The large difference in the cumulative recovery between the two patterns is attributed to two factors. The first factor is the depletion of oil in this pattern. The second factor is the existence of the steam condensate established in the middle part of the reservoir during shut-in, and the location of this condensate behind the oil bank. As a result, injection of steam in the diagonal pattern first displaced the oil present in the vicinity of the production port, then larger amounts of condensate were produced as the steam expanded. In Run 6, the use of a parallel pattern, viz. injection at Port 1 and production at Port 3, resulted in 10.3% incremental recovery, for 0.4 PV of steam injected. Subsequent injection of another 0.4 PV of steam, using a diagonal pattern, viz. injection at Port 2 and production at Port 4, resulted in 12.5% in incremental recovery.

Based on the discussion above, it was concluded that – subsequent to shut-in – the best strategy for steamflooding a reservoir would be to first use parallel then diagonal combinations of injectors and producers, provided a diagonal injection-production strategy was previously used. The reason, as can be seen from the cumulative recovery curve on Figure 6.14, is that it offered a more stable and balanced approach (the recovery for each pattern using the suggested strategy resulted in similar values). Also, by using this strategy, the production of the large volume of steam condensate in the middle of the reservoir, due to the collapse of the steam zone, was avoided partially.
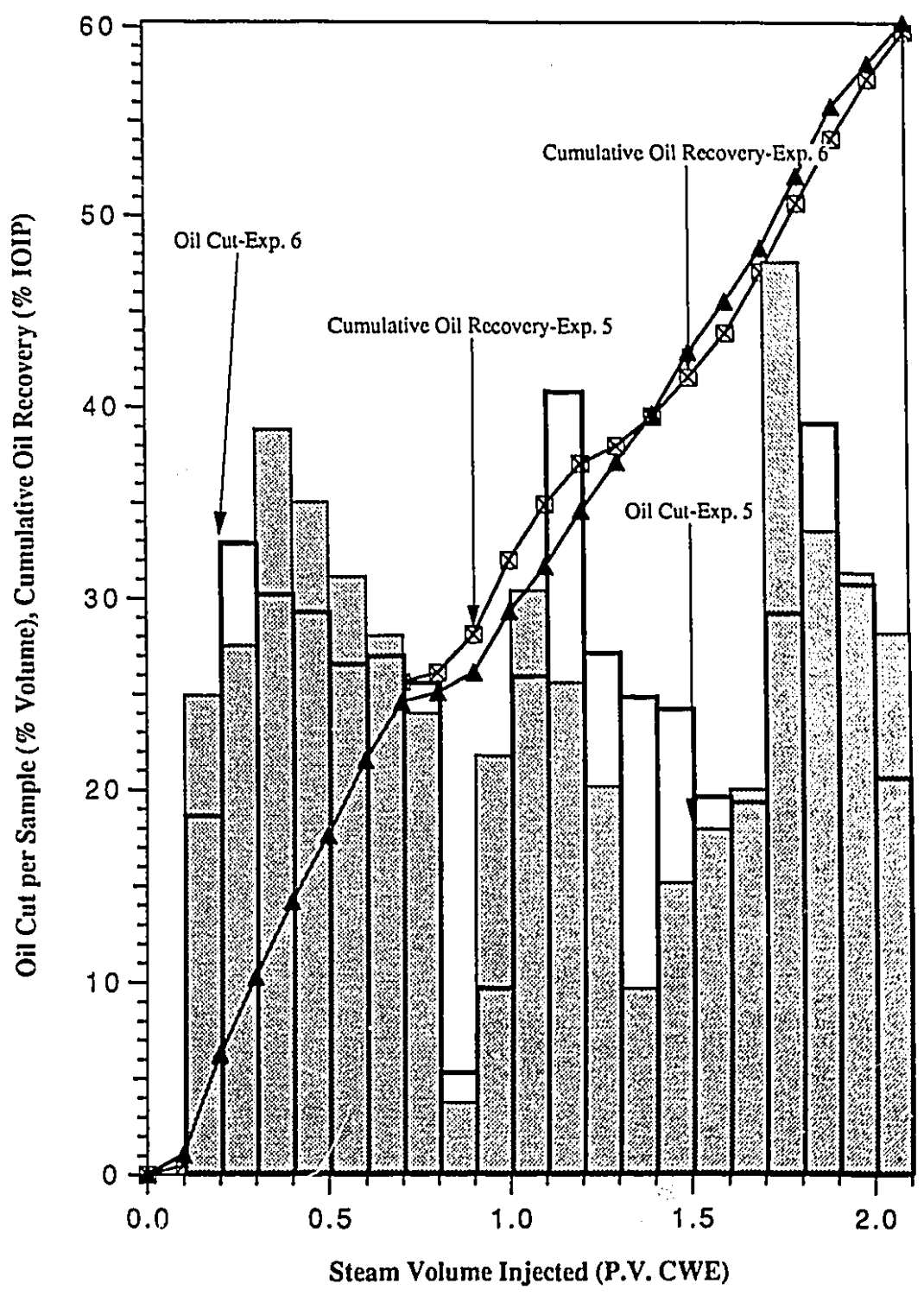
Figure 6.14: Cumulative oil recovery and oil cut for Runs 5 and 6.
The shut-in period is equivalent to 1.0 PV (CWE) of steam injection time.

6.8 Well Locations in Steeply Dipping Reservoirs

In this research, several effects which may lead to an increase in the cumulative oil recovery were examined. These included: 1) Well locations in a steeply dipping reservoir, 2) Dip, and 3) Pattern inversions in both the inclined and horizontal reservoirs. Two experiments, Runs 7 and 8, were carried out to study the effects of well location in a steeply dipping reservoir. Run 10 was carried out to study the effects of dip. This experiment – in every respect – was similar to Run 7, except for the inclination of the reservoir. In Run 10, the reservoir was in a horizontal position. Finally, the effectiveness of pattern inversions in either a horizontal or steeply dipping reservoir was analyzed based on the amount of oil recovered for a particular pattern.

6.8.1 Effect of Well Location and Dip on Cumulative Oil Recovery

The porosity of the glass bead pack, in Run 7, was 34.1%. The initial oil saturation was 91.8% and the rate of injection was 210 ml/min. Steam was injected down-dip for 2.1 PV, and pattern inversions were made after 0.7 PV, 1.2 PV, 1.5 PV and 1.9 PV of steam injected. In Run 8, the porosity was 34.8%, the initial oil saturation was 91.2% and the injection rate was identical to that of Run 7. The injection of steam was for 1.8 PV down-dip, with pattern inversions made after 0.6 PV, 1.3 PV and 1.7 PV of steam injected. The horizontal injection and production well configurations for Runs 7 and 8 are shown in Figures 6.16 and 6.18 along with the temperature contours, respectively. Figures 6.15 and 6.17 show the production histories for Runs 7 and 8, respectively.

From Runs 7 and 8, which were done for an inclined reservoir, it was found that the location of the pairs of horizontal injectors and producers was undesirable in two ways. First, the short distance between the tip of the injector and the producer caused the injected steam to channel rapidly to the producing well. Second, the horizontal producer and injector configuration did not expose as much of the reservoir to the steam front, as compared to other cases. Interference effects between the injection and production wells were appreciable and visible from looking at the temperature contours on Figures 6.16 and 6.18 (a). The interference effect is indicated by the circular region near the tip of the horizontal wells. The difference between this pattern and the pattern previously used resulted in a loss of approximately 5% in ultimate oil recovery, for the same pore volume of steam injected. From an economic standpoint, this horizontal injection-production

Figure 6.15: Production History of Run 7,
Steamflood with Pattern Inversions Using Pairs of Horizontal Injectors
and Producers (Wells Aligned Along Diagonals Between Corners of Pattern)
in a Homogeneous, Inclined Reservoir.

a) 0.50 PV (CWE) Inj.

b) 0.80 PV (CWE) Inj.

c) 1.20 PV (CWE) Inj.

d) 1.40 PV (CWE) Inj.

Legend: ———— Upper Model Temperature, °C

— — — Lower Model Temperature, °C

Port 3   Port 4   Homogeneous Model   Legend:

Inj. for 0.7 PV using ports 1 and 4

0.5 PV   2 and 4

0.3 PV   2 and 3

0.4 PV   1 and 3

0.2 PV   2 and 3

Port 1   Port 2

Injection down dip

Figure 6.16:   Plan view of the temperature distribution inside the model along
with injection and production strategy for Run 7.

Figure 6.17: Production History of Run 8,
Steamflood with pattern inversions using pairs of horizontal injectors
and producers (wells aligned along diagonals between corners of pattern) in
a homogeneous, inclined reservoir.

a) 0.50 PV (CWE) Inj.

b) 0.75 PV (CWE) Inj.

c) 1.30 PV (CWE) Inj.

d) 1.50 PV (CWE) Inj.
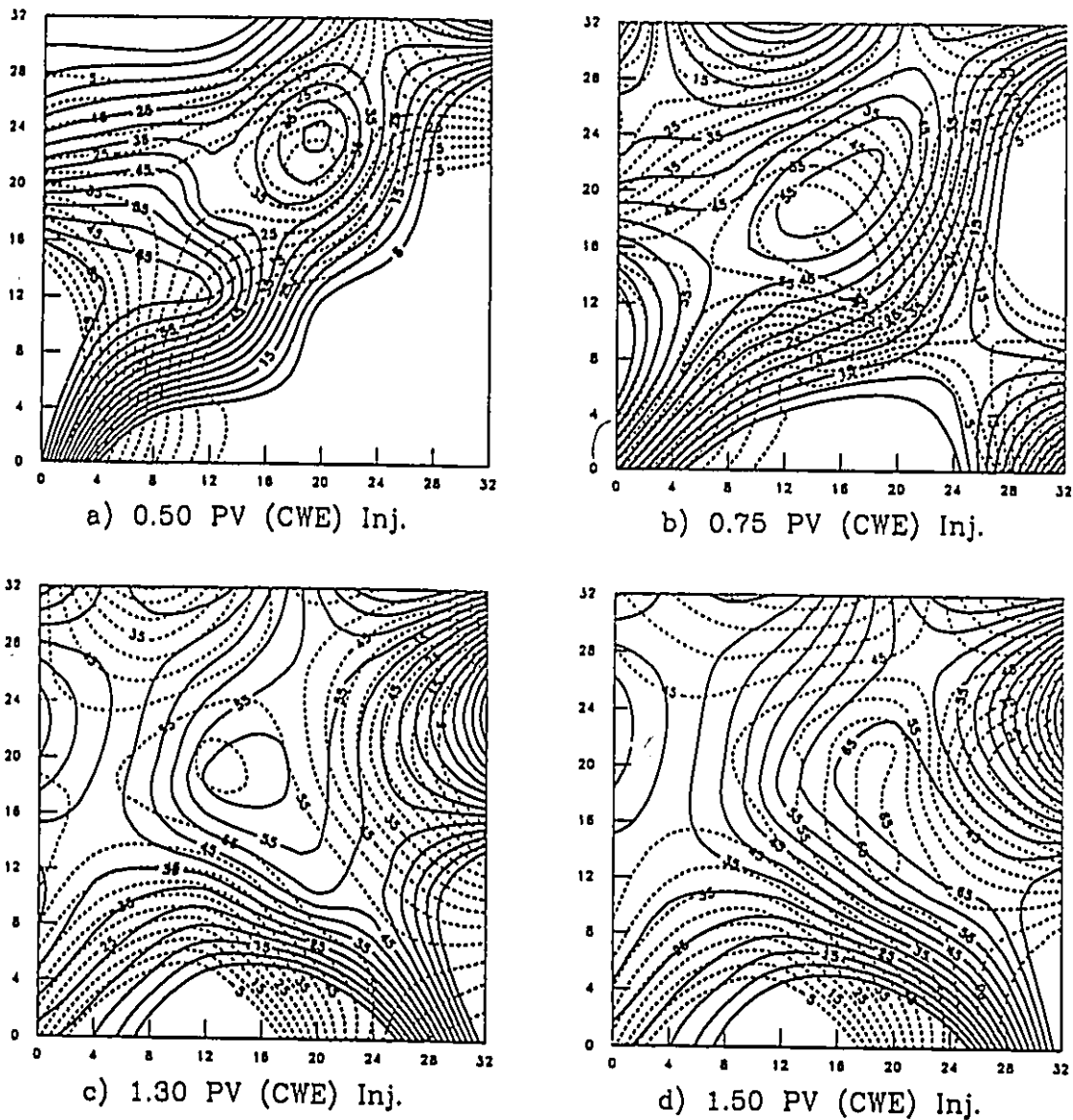
Legend: ———— Upper Model Temperature, °C

— — — Lower Model Temperature, °C
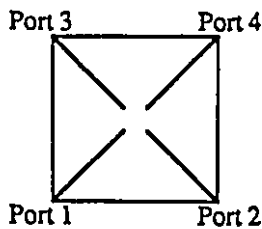
Port 3   Port 4   Homogeneous Model   Legend:
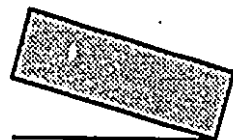
Inj. for 0.6 PV using ports 1 and 4

0.7 PV   2 and 3

0.3 PV   2 and 4

0.1 PV   1 and 3

Port 1   Port 2

Injection down dip

Figure 6.18:   Plan view of the temperature distribution inside the model along with injection and production strategy for Run 8.

well configuration was undesirable as a larger volume of steam was required to achieve a similar cumulative oil recovery for the base case experiment, Run 12.

Figures 6.15 and 6.17 show that Run 8 initially had a higher cumulative OSR and lower instantaneous WOR when compared to Run 7. The inset graph of CI/CP versus pore volume of steam injected, for Run 7, shows the flood was a hot water drive for the first 0.4 PV of steam injected. After this period, steam was present. In comparison, Run 8 started with a hot water drive for the first 0.2 PV of steam injected, and steam was present within the injection period of 0.2 to 1.5 PV. After 1.6 PV of steam was injected, both experiments indicated that the cumulative injected volume was larger than cumulative production. This was necessary to fill the voidage present, which resulted from the condensation of the previous steam zone expansion.

In Run 7, after 1.3 PV of steam had been injected, the total production was 2080 ml, of which 755 ml was oil. These two values greatly exceeded any of those observed previously. In the experiments conducted in an inclined reservoir, it was observed that after a pattern inversion was made, the maximum oil cut was obtained after a period of additional injection. However, in this experiment, a large amount of fluids were collected immediately after an inversion. The injection and production were at Ports 2 and 4, respectively. It was speculated that the oil in the vicinity of Port 4 was not being produced alone because time was required for the steam front to advance and displaced the oil. Most of the oil recovered in this sample probably resulted from the movable oil in the middle of the reservoir where the mobility of the fluids (steam, condensate and oil) are high. As a result, a diagonal pattern inversion caused the displacement of movable oil into the production path.

The above hypothesis is supported by the fact that the velocity of fluids was greatest in the diagonal direction from the injector to the producer. As can be seen from Figure 6.16, the temperature contours in the middle of the reservoir is observed to expand both areally, and vertically. The pressure data shows that a large pressure difference occurred between the injector and producer as the production port was switched from Port 4 to Port 3, while the injection was kept at Port 2. As a result of this large pressure gradient between the injector and producer, a high oil production rate, 305 ml/min., was obtained at the production well, whereas the injection rate, at Port 2, was at 210 ml/min. The reason for this regional pressure gradient was uncertain. Possibly the perforations of the horizontal production well were temporary plugged restricting the flow. Thus the pressure resulting from the

steam injection process was allowed to build up inside the model. Upon the re-opening of these perforations, restriction to flow was no longer present, and this led to a high rate of production.

In Run 10, the effect of dip on oil recovery was studied. The experimental set-up was similar to that of Runs 7 and 8, except that the reservoir was horizontal. Steam injection was utilized for 2.1 PV with pattern inversion made after 0.7 PV, 1.2 PV, 1.5 PV and 1.9 PV of steam injected. The porosity of the pack was 32.9%, the initial oil saturation was 92.2% and the injection rate was again similar to that in the previous experiments. Figure 6.19 shows the production history of Run 10. Figure 6.20 shows the temperature contours for this experiment.

Figure 6.21 shows the oil recovery curve for Runs 7, 8 and 10. After 1.8 PV of steam had been injected, the recovery of the initial oil in place (IOIP) for these three experiments was 50.4, 49.4 and 49.1%, respectively. The difference between the oil recovery for Runs. 7 and 8 was 1%, in spite of the different times of pattern inversion, and different injection and production strategies used. The reason for the similar oil recoveries was, once again, attributed to the equal volumetric sweep in these three experiments.

The difference in the displacement mechanism between the horizontal reservoir and the steeply dipping reservoir can be observed from the temperature contours. Based on the two figures, Figures 6.16 (a) and 6.20 (a), the degree of steam override was observed to have greater significance in a horizontal reservoir. This indicates that the frontal displacement of fluids from the injector to the producer played a greater role in the inclined reservoir.

The difference in the recoveries for the three experiments was less than 1%, after 1.8 PV of steam had been injected, despite the different pattern inversions and durations used, and despite reservoir dip. Therefore, it is concluded that the effect of well location-configuration is more important in the cumulative recovery of oil than the effect of dip for a thin and homogeneous reservoir having high permeability.
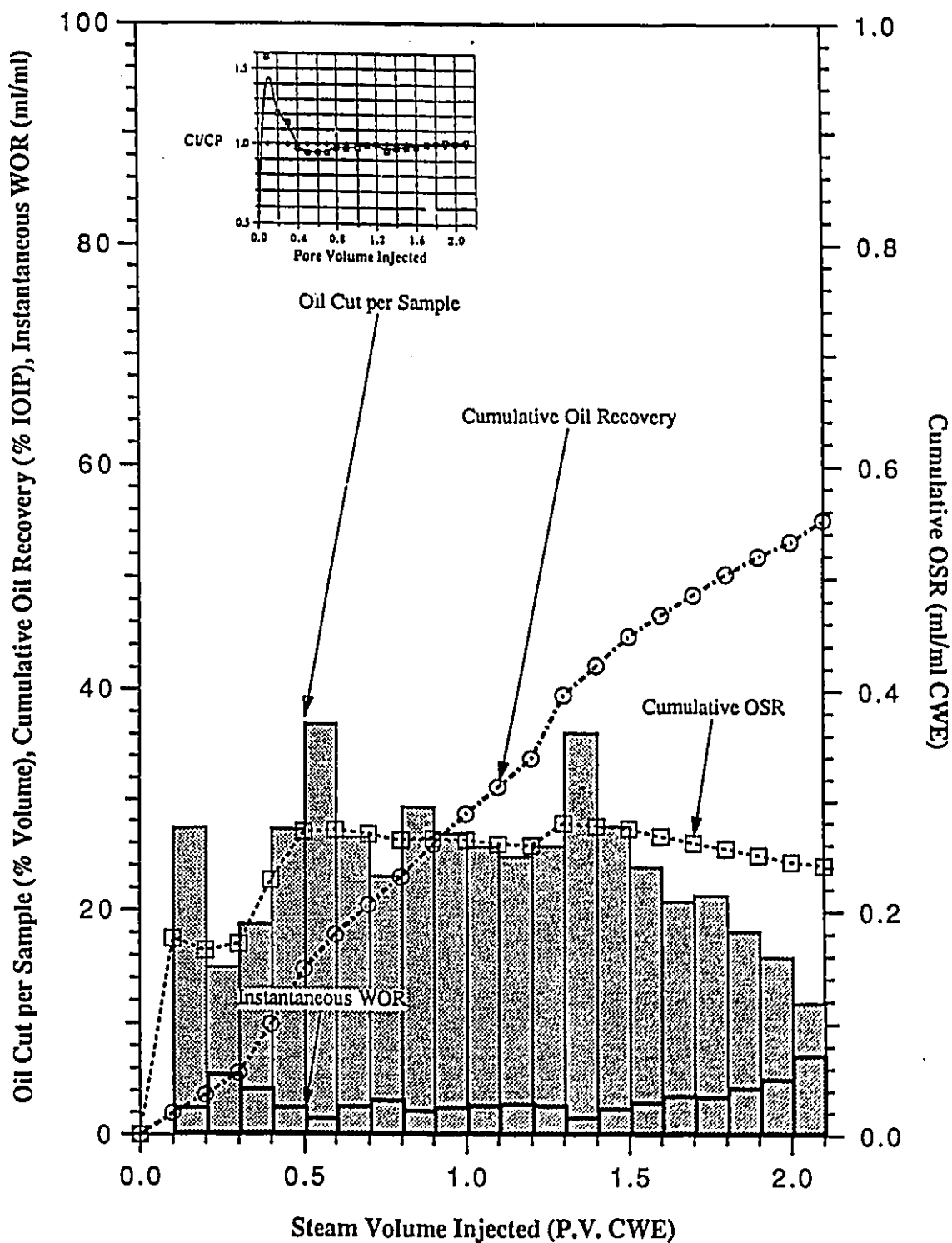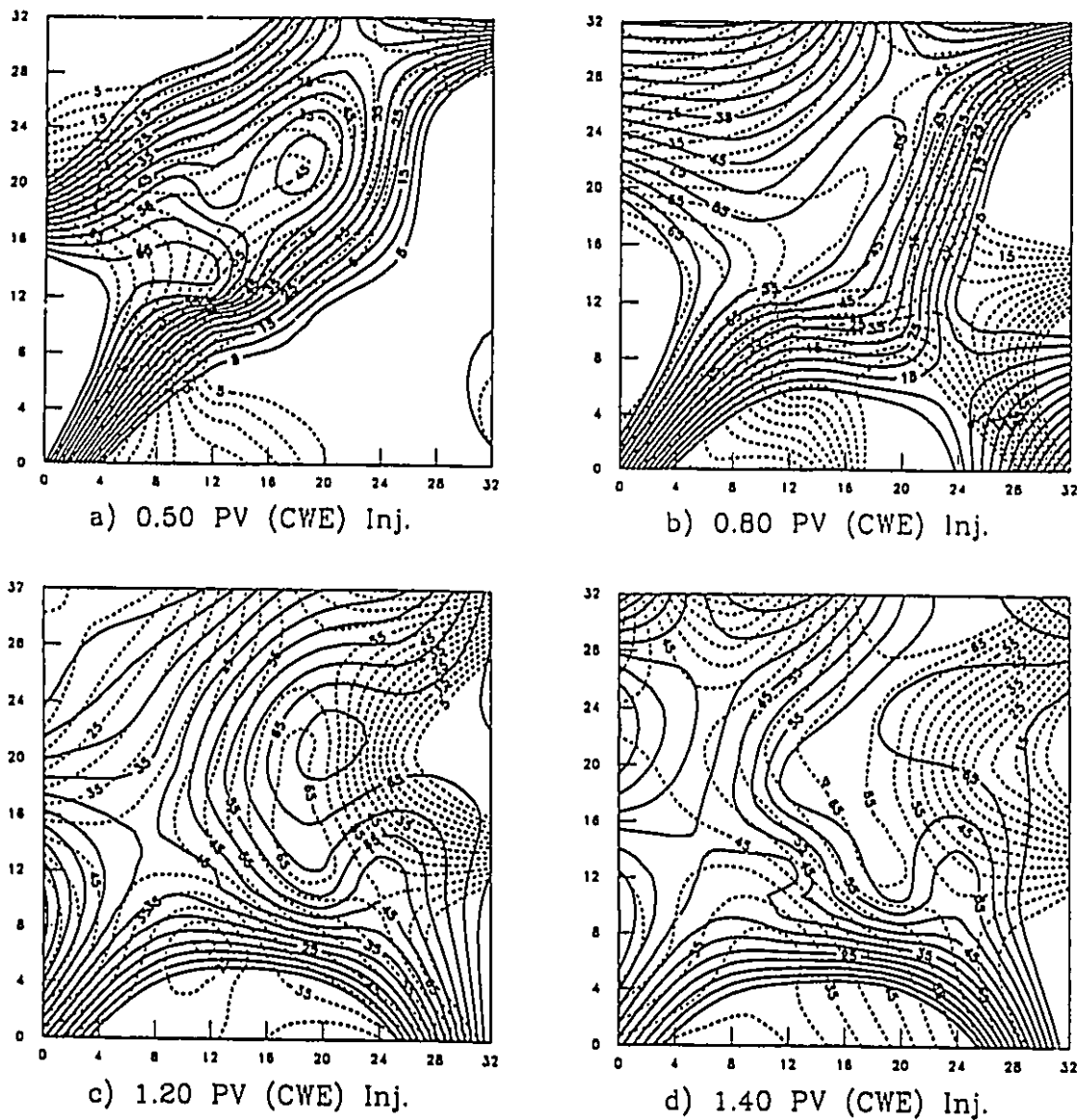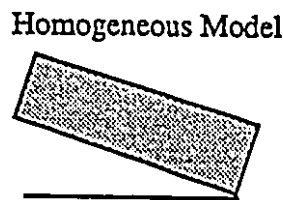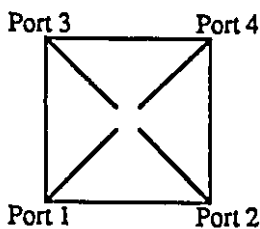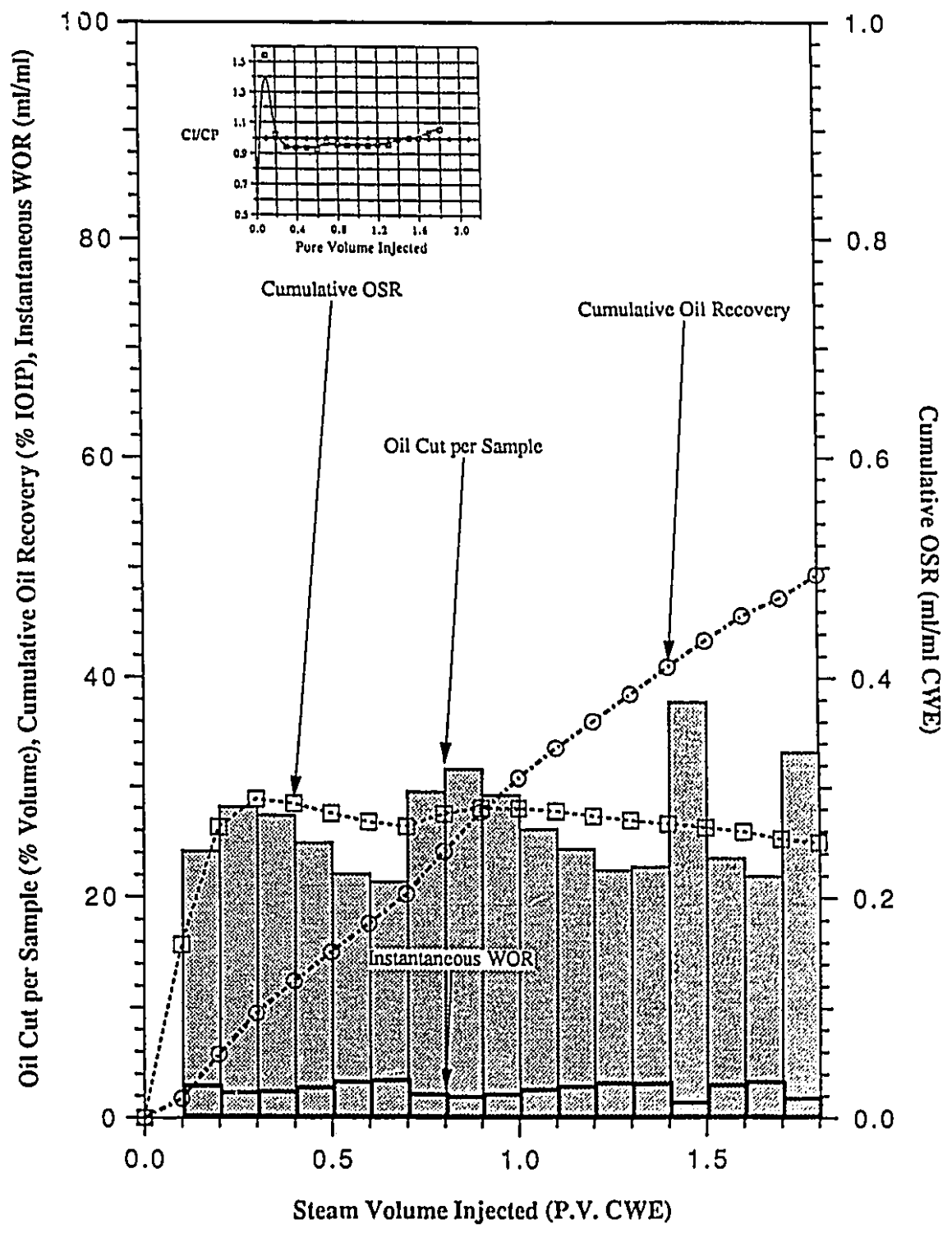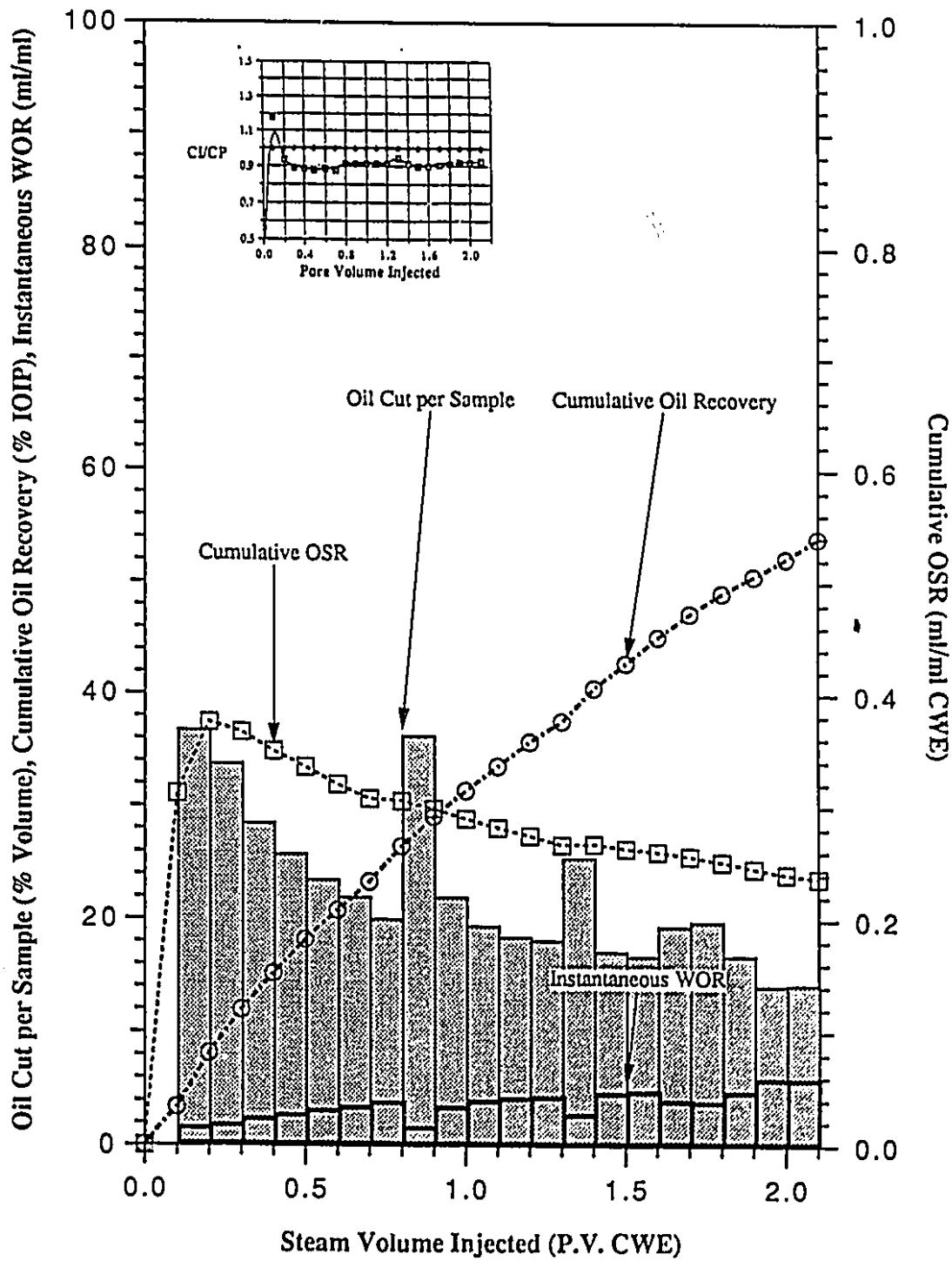
Figure 6.19: Production History of Run 10,
Steamflood with pattern inversions using pairs of horizontal injectors
and producers (wells aligned along diagonals between corners of pattern)
in a homogeneous, horizontal reservoir.
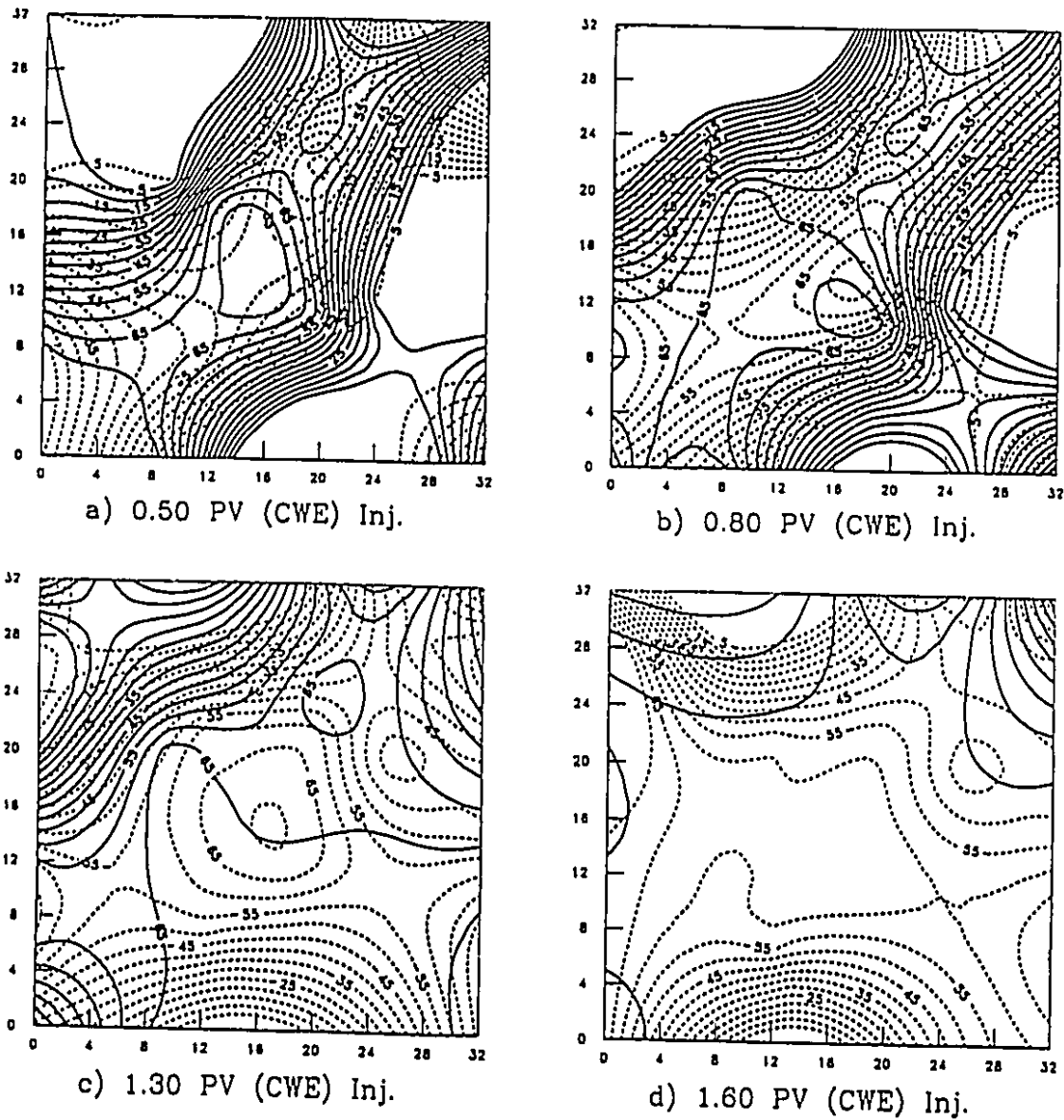
a) 0.50 PV (CWE) Inj.

b) 0.80 PV (CWE) Inj.

c) 1.30 PV (CWE) Inj.

d) 1.60 PV (CWE) Inj.

Legend: ——— Upper Model Temperature, °C

— — — Lower Model Temperature, °C

Port 3   Port 4

Homogeneous Model

Port 1   Port 2
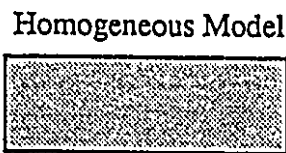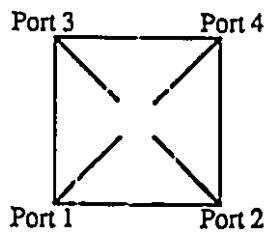
Legend:

Inj. for 0.7 PV using ports 1 and 4

0.5 PV	2 and 4
0.3 PV	2 and 3
0.4 PV	1 and 3
0.2 PV	2 and 3

Figure 6.20: Plan view of the temperature distribution inside the model along with injection and production strategy for Run 10.
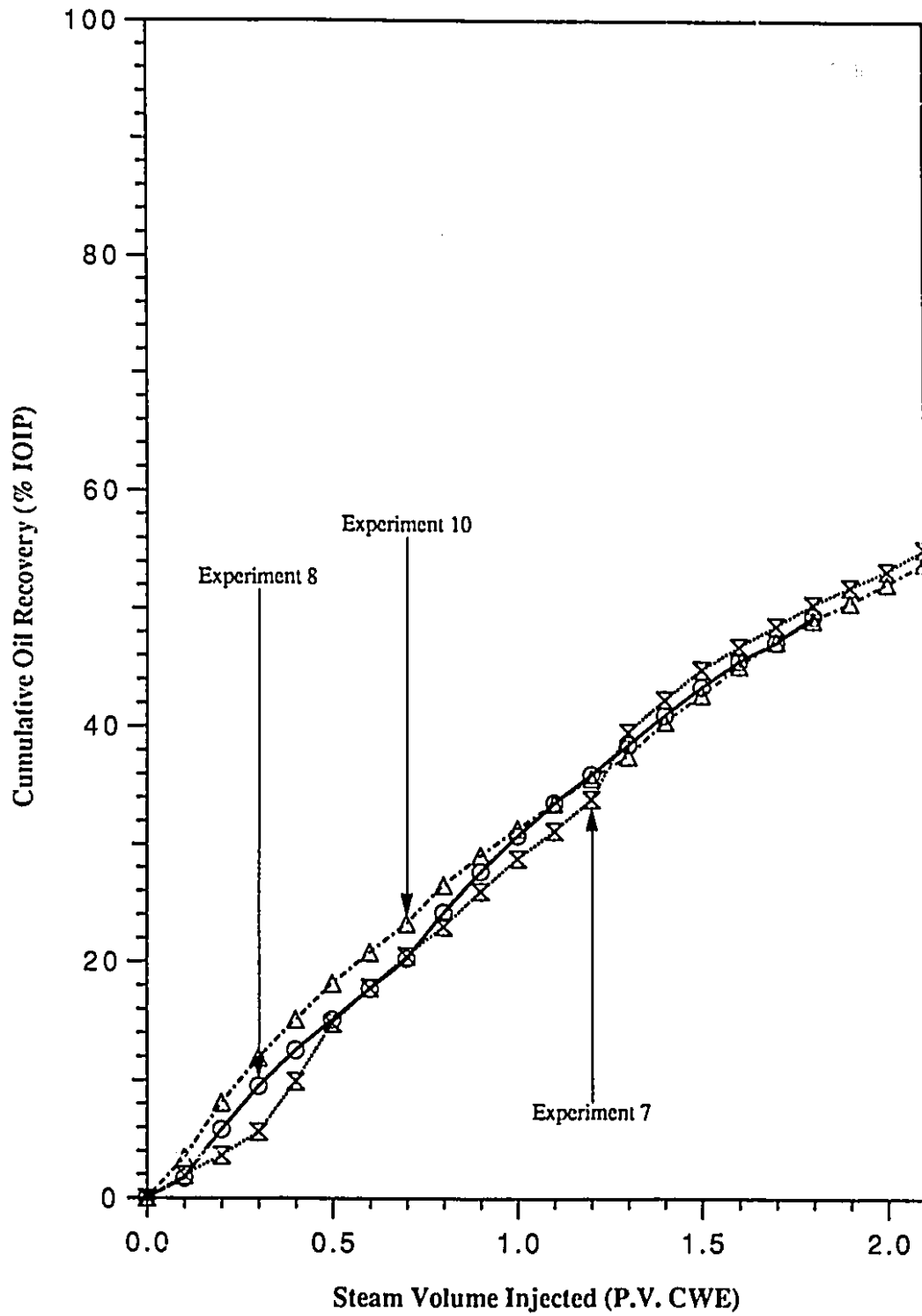
Figure 6.21: Cumulative oil recovery versus the cumulative PV of steam injected
for Runs 7, 8 and 10. In Runs 7 and 8, the reservoir is homogeneous
and steeply dipping. In Run 10, the reservoir is homogenous and horizonal.

6.8.2 Effectiveness of Pattern Inversions in Horizontal and Steeply Dipping Reservoirs

In Run 7, it was found that both the time when pattern inversion is made, and the use of the parallel injection production strategy were undesirable. In this experiment, after injecting 0.7 PV of steam at Port 1 and production at Port 4, an additional 0.5 PV of steam was injected at Port 2 with production at Port 4 resulting in a recovery of 33.9%. In Run 8, the injection of 0.6 PV of steam using the same well pattern as Run 7, with an additional 0.6 PV of steam using the diagonal injection/production strategy, that is, injection at Port 2 and production at Port 3, resulted in a recovery of 36.1%. After injecting 1.2 PV of steam, the cumulative oil recovery in Run 8 was 2.2% more. The reasons for the higher cumulative recovery in Run 8 were: 1) a larger distance of separation between the tip of the injector and producer, which reduced steam channeling between the two, and 2) the area exposed to the sweep was considerably larger. Hence, the strategy of Run 8 was considered to be more desirable.

As mentioned above, cumulative oil recovery curves for the three experiments were very similar. However, the oil cut curve for Run 10 was different from the other two runs. The oil cut in Run 10 was initially high, then it decreased gradually. After pattern inversions, the oil cut increased once again. In Runs 7 and 8, the oil cut was initially low, and gradually increased to the maximum value, then decreased. The use of pattern inversions to increase the area exposed to the steam front was found beneficial for all three runs. In Runs 7 and 8, pattern inversions changed the negative slope of the OSR curve to a positive trend. While in Run 10, pattern inversions made the negative slope of the OSR curve decrease less.

Based on the OSR curves, the use of pattern inversions was more significant – on the performance of a steamflood – for an inclined reservoir than it was for the horizontal reservoir. One explanation for this was in the inclined model, the steam volume advanced at a slower rate, due to the work against gravity, compared to the horizontal reservoir. This led to a better sweep, and a later breakthrough time. In the horizontal model, the steam front traveled at a greater velocity, therefore earlier breakthrough occurred, and hence the sweep efficiency was less.

From Runs 7 and 8, it was observed that the cumulative recovery, and the oil cut for both experiments were similar, when one cyclic pattern inversion was made after 1.8 PV of

steam was injected. In general, for any given set of experiments having similar set-up and horizontal well configurations, the ultimate oil recovery will be similar after injecting for one cycle – with no repeat in pattern – utilizing all possible horizontal injection/production well combinations. However, the correct sequence of injection and production strategy used enabled higher recovery for a shorter injection time, that is, quicker recovery. A shorter period of injection implies a lower operating cost.

It was found that if a different injection port, but the same production port was used after pattern inversion, the oil cut was high. This was true if the interference between wells, that is, communication between injector and producer, were minimal, and the reservoir was homogeneous. For example, if the first sequence utilized injection at Port 1 and production at Port 4, then injection at Port 2 and production at Port 4 should be used in the second sequence. This resulted in an increase in cumulative recovery. When this procedure was applied to the last two pattern inversion sequences in any experiment, higher recovery was obtained, provided that the oil available in the given pattern had not yet been produced.

In comparing the effectiveness of parallel and diagonal injection-production strategy, a question was posed: if identical injection periods were allowed, which injection-production strategy, that is, parallel or diagonal, will provide higher oil recovery. The answer was found to depend on the location of injectors and producers in a reservoir. If the horizontal injectors and producers were assumed to be located parallel to the pattern (quarter of a five-spot pattern) boundary then based on experimental results, the following conclusion was reached: If the injection period was short, for example, 0.2 or 0.3 PV, then the parallel injection and production strategy should be used because it provided a quicker production response. If the injection period was longer, for example, 0.6 or 0.7 PV, then the diagonal injection and production strategy should be used. The reason is it allowed a larger volumetric sweep of oil but on the other hand a slower oil production response.

6.9   Steamflooding a Reservoir Having a Static Bottom Water Layer

In this research, steamflooding of a reservoir with a static bottom water layer was studied by conducting three scaled physical experiments, where the thickness of the bottom water layer was 20% of the net pay. In the first of these experiments, the strategy for steamflooding a steeply dipping reservoir containing a static bottom water layer was studied. In the second experiment, a steamflood was carried out for a horizontal reservoir underlain by a bottom water layer. In both experiments, the horizontal injectors and

producers were located in the middle of the formation (near the oil water contact). In the third or final experiment, a steamflood was carried out with horizontal injectors and producers elevated further from the oil-water contact, that is, increased stand-off.

6.9.1 Steeply Dipping Reservoir - Horizontal Wells Located Near the Oil-Water Contact

In Run 9, attempts were made to study different steamflooding strategies on a thin, inclined reservoir underlain by bottom water. For this experiment, a steamflood was carried out with pattern inversions using horizontal injectors and producers for an inclined reservoir having 20% net-pay bottom water. The porosity of the glass beads pack was 26.5% and the initial oil saturation was 83.0%. The injection rate was 220 ml/min. and pattern inversions were made after 0.8 PV and 1.8 PV of fluids had been injected. Oil recovery began after 0.3 PV of steam had been injected. The instantaneous oil production and oil cut reached a maximum value of 440 ml and 27.9% at 0.5 PV, respectively. The overall recovery, after 2.1 PV of steam had been injected, was 52.4%.

Figure 6.22 shows the experimental set-up, along with the location of the reservoir fluids (oil and bottom water), in the inclined reservoir, prior to the start of this experiment. Figure 6.23 gives cumulative oil recovery, instantaneous WOR and oil cut versus the pore volume of steam injected (CWE). Figures 6.24 (a) to (d) show the temperature profile of the reservoir after 0.5 PV, 0.8 PV, 1.0 PV and 1.5 PV of steam had been injected.
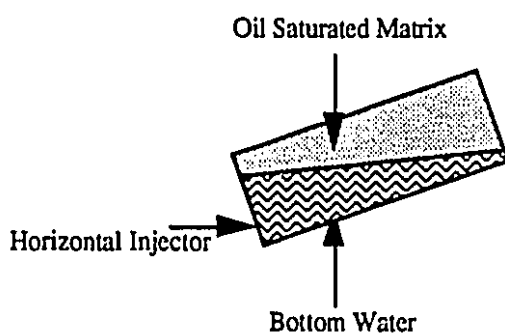
Figure 6.22: Position and location of the bottom water layer along with the horizontal injector in an oil saturated model representing Run 9.

Figure 6.22 shows the horizontal injection wells submerged in the bottom water layer from the start of steam injection. Initially, formation of the steam zone was suppressed as most

Figure 6.23: Production History of Run 9,
Steamflood with pattern inversions using pairs of horizontal injectors
and producers in an inclined reservoir with 20% net-pay bottom water.
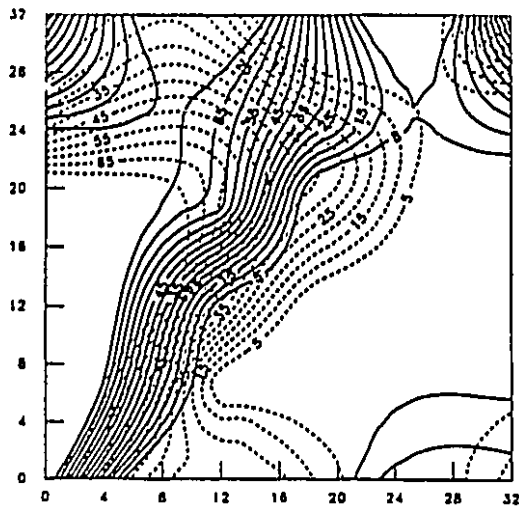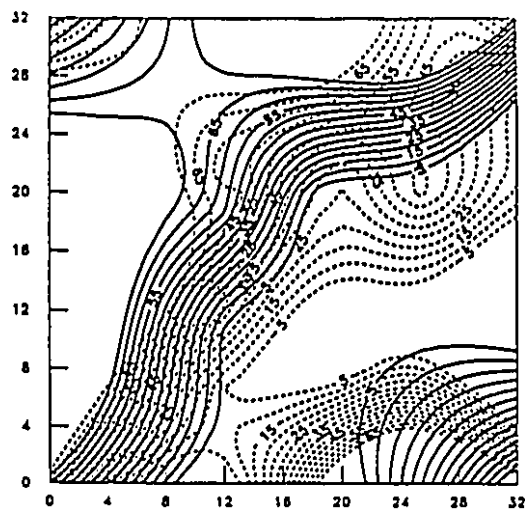
a) 0.50 PV (CWE) Inj.

b) 0.80 PV (CWE) Inj.
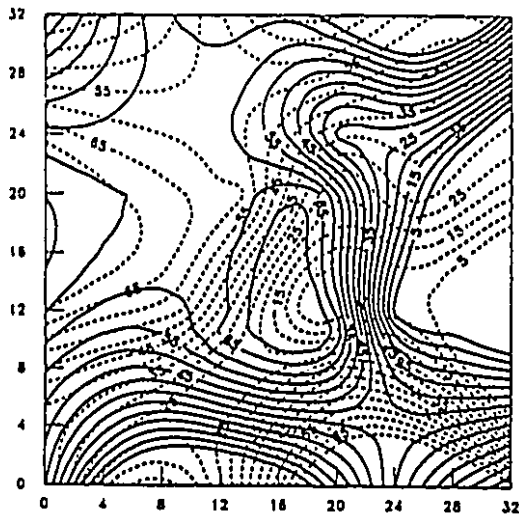
c) 1.00 PV (CWE) Inj.
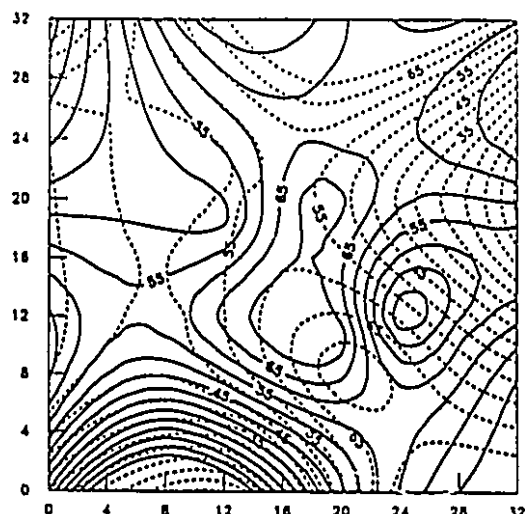
d) 1.50 PV (CWE) Inj.

Legend: ———— Upper Model Temperature, °C
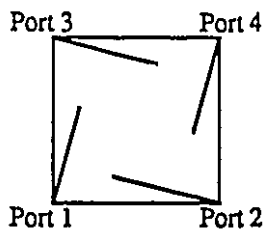
— — — Lower Model Temperature, °C

Port 3   Port 4   Bottom Water Model   Legend:
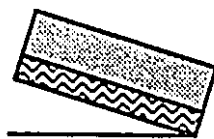
Inj. for 0.8 PV using ports 1 and 4

1.0 PV   2 and 4

0.3 PV   2 and 3

Port 1   Port 2

Injection down dip

Figure 6.24:   Plan view of the temperature distribution inside the model along with injection and production strategy for Run 9.

of the injected heat went into heating the bottom water formation. This was verified by observing the temperature contours, shown in Figures 6.24 (a) and (b). After 0.5 PV of steam had been injected, the temperature and pressure at Port 1 were 79.8°C and 62.1 kPa, respectively. From steam tables, these values indicate that hot water was the state of the fluid injected, and also the state of the displacing fluid in the model. This is so because the pressure distribution – which was assumed to be linear between the injector and producer – and the corresponding temperature contours were checked with values from steam tables. After 0.8 PV of steam had been injected, the pressure and temperature at the injection port were 22.1 kPa and 82.4°C, respectively. These values implied the presence of steam at the injector. However, after checking the pressures and corresponding temperature contours, it was determined that steam was not yet present inside the model. Hence, the flood – up to this point – was still a hot bottom water drive. After 1.0 PV of steam had been injected, the temperature and pressure at Port 2 were 78.3°C and 30.8 kPa, respectively. These values implied the presence of steam at the injector. From Figure 6.24 (c), the upper temperature contour, $T = 65°C$, was observed to traverse farther inside the formation (glass bead pack) as compared to the lower temperature contour, implying steam override.

In the early stages of the flood, the lower temperature contour, $T = 65°C$, was seen to advance farther inside the reservoir than the upper temperature contour. In this process, the injected heat first heated the bottom water, and subsequently heat was transferred from the bottom water to the lower portion of the oil layer by conduction. This increased the temperature of the oil, reducing its viscosity. As a result, the mobility ratio became more favourable and the hot water displaced the oil toward the producer. After 1.0 PV of steam had been injected, the amount of energy present in the reservoir became sufficient for the establishment of a steam zone, as illustrated in Figure 6.24 (c). Beyond this stage, the recovery of oil was greatly contributed by the expansion of the steam zone.

In thin reservoirs, the presence of thick bottom water, for example, above 20% net pay, was found to be undesirable. Properties of water, when compared to oil, include higher specific heat and higher mobility. A high mobility water layer provided a flow channel between the horizontal injector and producer. With the least resistive flow path present, the injected steam – which carries energy – channeled into the bottom water layer. Since the specific heat capacity of water (C_w) is higher than the specific heat capacity of oil (C_o), larger amounts of heat were stored in the bottom water zone. As a result, the oil at the top of the reservoir remained immobile (as the viscosity of oil is still high), and the oil cut at the

producer for the first 0.2 PV of steam injected was zero. This, consequently, led to lower cumulative oil recovery as compared to the base case run.

From looking at the cumulative oil recovery and the oil cut curves, in Figure 6.23, pattern inversions were beneficial. The cumulative oil recovery curve increased after pattern inversion was made at 0.8 PV. Subsequently, after 1.1 PV of fluids was injected, the oil cut for this pattern reached a maximum. At this stage, it was noted that the oil cut did not instantaneously increase the oil cut after a pattern inversion. The time required to first heat the bottom water layer was the reason.

As mentioned earlier, most of the injected heat initially channeled into the bottom water zone, and a steam zone formed only at later stages. Considering these factors, the horizontal wells should be located away from the oil-water contact. As such, the time and the distance the injected steam – which carries heat – has to traverse into the bottom water zone are delayed (prolonged).

6.9.2 Horizontal Reservoir with Horizontal Wells Located Near the Oil–Water Contact

In Run 11, attempts were made to study the effects of bottom water on the performance of a steamflood in a horizontal reservoir. The porosity of the glass bead pack was 25.1%, the initial oil saturation was 74.8% and the injection rate was 198 ml/min. In this experiment, pattern inversions, using pairs of horizontal injectors and producers, were made after 1.1 PV and 1.6 PV of steam injected. The reservoir was underlain by a 20% net pay bottom water layer. The injection of the first 0.5 PV of steam produced no oil. The cumulative oil recovery was 36.6%, after 2.1 PV of steam had been injected. Figure 6.25 shows the production history of this experiment.

Figure 6.26 shows the temperature contours for Run 11, indicating only a small steam zone was formed. A major portion of the heat injected channeled into the bottom water layer. The remaining thermal energy carried by the overriding steam to the top of the reservoir was not sufficient to promote further growth of the steam zone volume. This is evident from the upper and lower temperature profiles of Figure 6.26 (a). Since the injected energy can neither promote the growth of the steam zone nor maintain the temperature of the steam zone at T_s, condensation occurred. This is indicated by the small width between the contours for $T = 65^oC$ and $T = 5^oC$. From Figures 6.26 (a) and (b), the following was
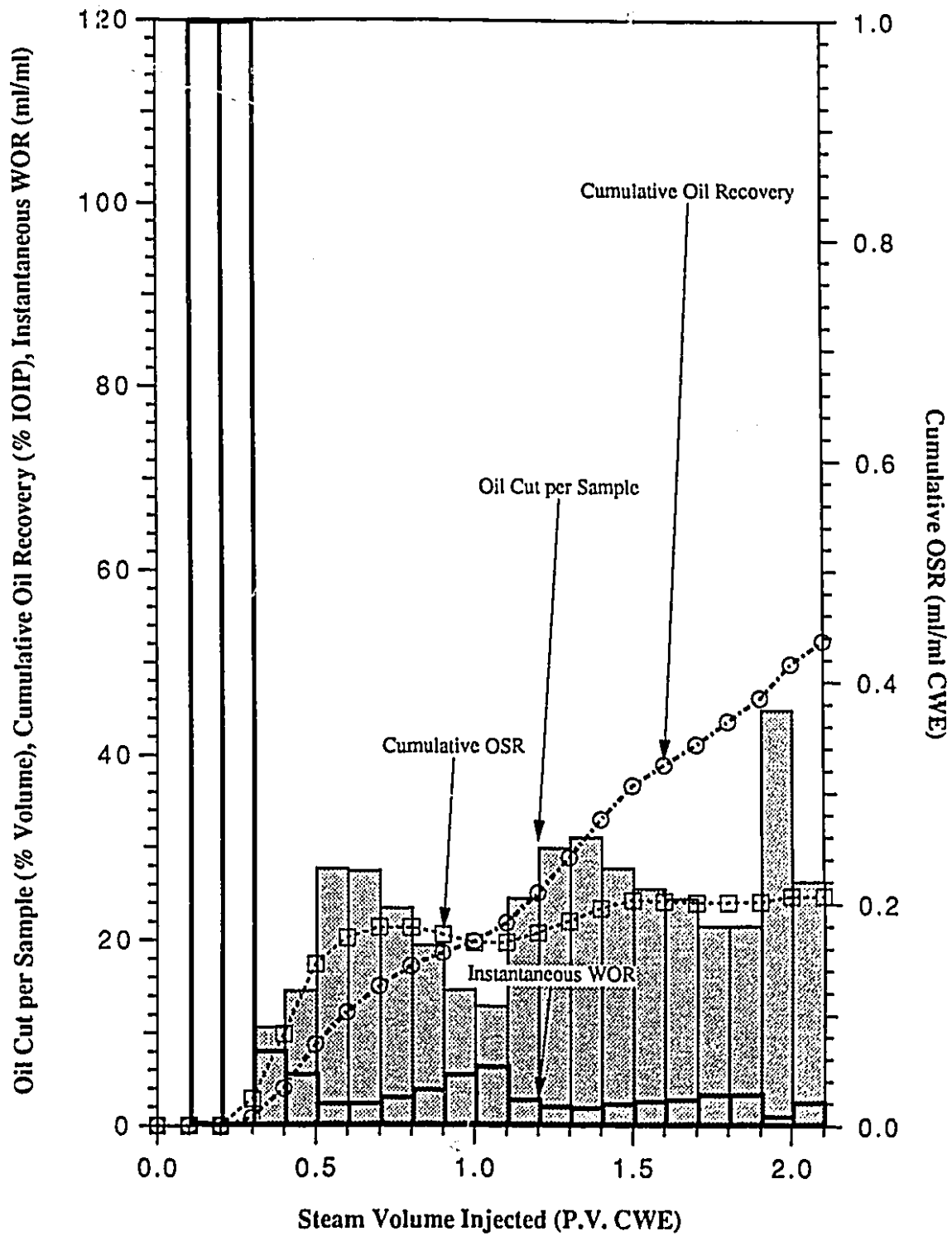
Figure 6.25: Production History of Run 11,
 Steamflood with pattern inversions using pairs of horizontal injectors
 and producers (wells located at the oil-water contact) in a horizontal
 reservoir having 20% net-pay bottom water.
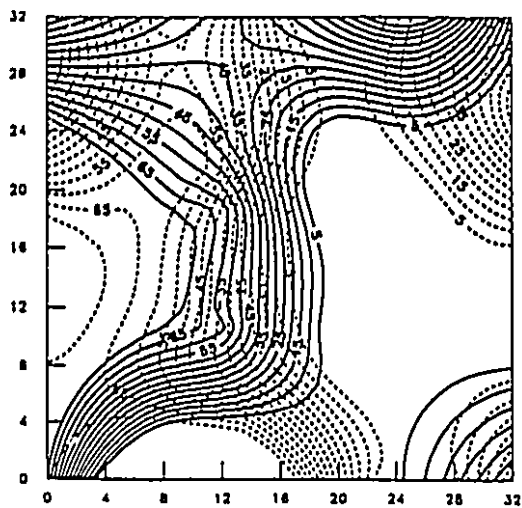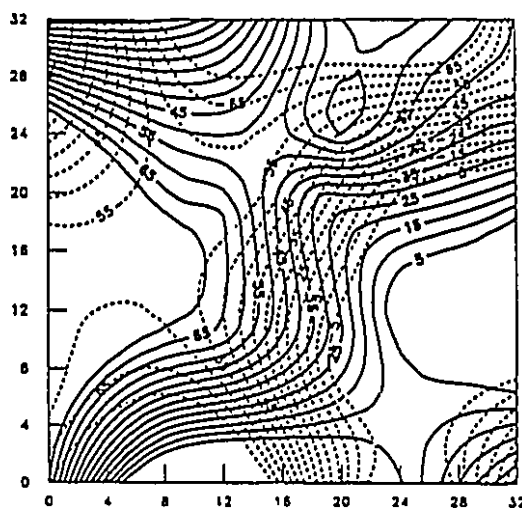
a) 0.50 PV (CWE) Inj.
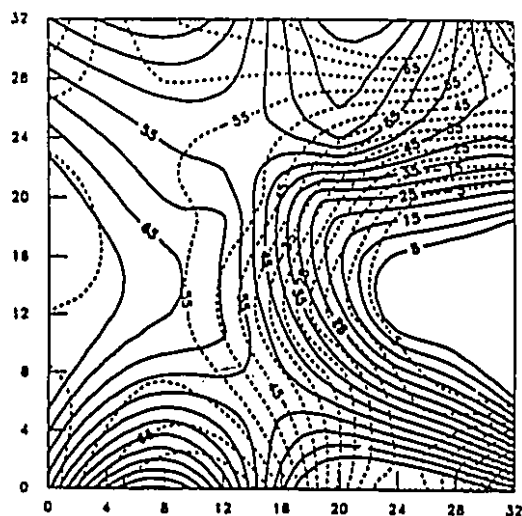
b) 1.00 PV (CWE) Inj.

c) 1.20 PV (CWE) Inj.

d) 1.70 PV (CWE) Inj.

Legend: ———— Upper Model Temperature, °C

— — — Lower Model Temperature, °C

Port 3   Port 4

Bottom Water Model
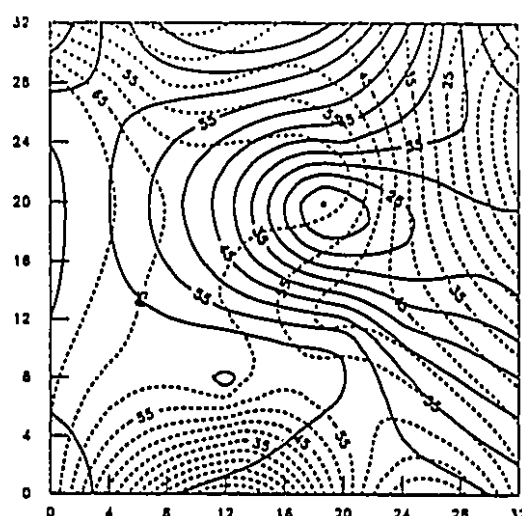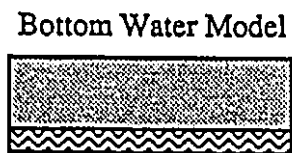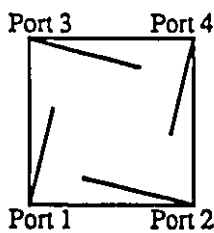
Legend:

Inj. for 1.1 PV using ports 1 and 4

    0.5 PV   2 and 3

    0.5 PV   1 and 3

Port 1   Port 2 Wells Located heat O-C Contact

Figure 6.26:   Plan view of the temperature distribution inside the model along with injection and production strategy for Run 11.

observed: the upper temperature contour, $T = 65^{\circ}C$, remained virtually at the same location during the injection of 0.5 to 1.0 PV of steam. However, the bottom temperature contour, $T = 65^{\circ}C$, traversed further inside the reservoir during the same injection period. This observation showed that a large amount of steam was used for heating the bottom water layer, with large amounts of condensate being formed. Because of the high conductivity of the bottom water layer, oil was bypassed and a large volume of steam condensate continuously flowed towards the producer. This resulted in a higher percentage of oil remaining inside the reservoir; that is $S_{or} = 0.634$. Also, as can be seen from the production history plot, the water oil ratio (WOR) was higher, and the OSR was lower than the base case run.

For an oil reservoir with static bottom water, the stand-off of the horizontal injectors and producers from the oil-water contact is important. In this experiment, the position of the horizontal injection and production wells was located just above the oil-water contact. As a consequence, the injected steam – which carries heat – channeled into the bottom water layer. Since the specific heat capacity of water is higher than the specific heat capacity of oil, larger amounts of heat are stored in the bottom water layer. This led to zero oil production during the first 0.5 PV of steam injected.

Figure 6.27 shows the graph of cumulative oil recovery for Runs 9, 11 and 13. A comparison of Run 9 with Run 11 showed remarkable differences in the cumulative oil recovery and also in the trend of the oil cut, and instantaneous WOR. The ultimate recovery, after 2.1 PV of steam had been injected, for the two experiments, differed by approximately 16%. The oil cut was much less in Run 11, and there was essentially no peak in the oil cut curve. Upon pattern inversion, the percentage of oil cut decreased in Run 11, while in Run 9, the oil cut increased.

In the context of the above discussion concerning the location of the horizontal producers and injectors with respect to the oil-water contact, four experiments were carried out using an unscaled visual model. From these experiments, an effective cylindrical steam zone volume – around the horizontal injector – was observed. Therefore, in thin oil reservoirs, where a thick bottom water (above 20 % net pay) layer is present, raising the horizontal injectors and producers may not be feasible because in trying to avoid wasting heat to the bottom water layer, the problem of heat loss to the overburden will be encountered.
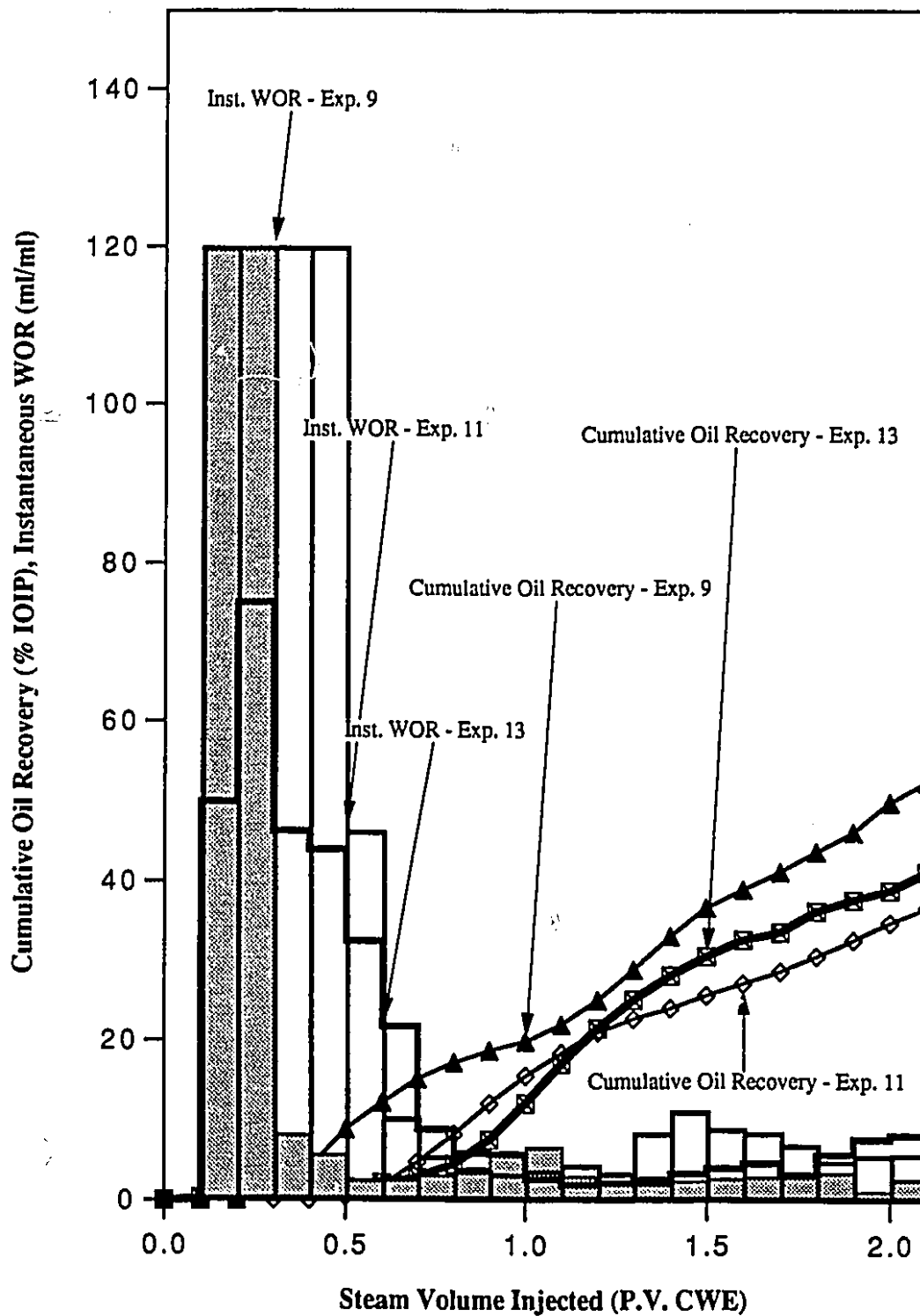
Figure 6.27: Cumulative recovery and instantaneous WOR versus PV of steam injected for Runs 9, 11 and 13. In all three runs, the reservoir has a 20% net-pay bottom water layer. Run 9 is steeply dipping, while Runs 11 and 13 are horizontal.

The presence of a thick bottom-water layer was detrimental to cumulative oil recovery, as was evident in this experiment (Run 11). The Neoprene sealant sheet and the fiberglass tray are good insulators, therefore the heat loss to the overburden and underburden was small. As a result, heat was allowed to accumulate in the reservoir to promote further growth of the steam zone. Yet, in this experiment, the formation of the steam zone was minimal for reasons mentioned above. In field operations, the steam zone volume and hence oil recovery are expected to be lower than the scaled-up values because of greater heat loss to the cap rock and base rock. Therefore, the economics of this type of reservoir may not be promising.

Production data showed that using diagonal pattern inversions in a thin horizontal reservoir with more than 20% of bottom water present was undesirable for three reasons. First, the steam zone, although not large, was already present. Any attempts to change the pattern would expose new cold water zones which will have to be heated, resulting in a waste of energy. Second, the use of a diagonal pattern would result in the cold oil being displaced into the path where favourable mobility already exists, temporarily blocking the pore space. Finally, the mobility of the oil and water mixture was favourable in the middle and in the vicinity of the production ports.

6.9.3 Horizontal Reservoir - Horizontal Wells Elevated Above the Oil-Water Contact

In Run 13, the effect of raising the horizontal injectors and producers in a 20 % net pay bottom-water layer was studied. The horizontal injectors at Ports 1 and 2 were 5.5 cm and 5.4 cm, respectively, from the bottom of the reservoir. While the horizontal producers at Ports 3 and 4 were located at a distance of 4.5 cm and 5.2 cm from the bottom of the reservoir, respectively. The first pattern inversion was made quite late in the experiment, after 1.6 PV of steam had been injected. Subsequently, various quick pattern inversions were made at 0.1 PV intervals. The porosity of the glass bead pack was approximately 26%, the initial oil saturation was 83.1% and the injection rate was at 210 ml/min. . The production history of this experiment is shown in Figure 6.28. Figure 6.29 shows the temperature contours for Run 13. From the production history plot, the peak oil cut was observed between 1.1 and 1.2 PV of steam injected, and the slope of the cumulative oil recovery curve was observed to increase after 1.0 PV of steam injected.
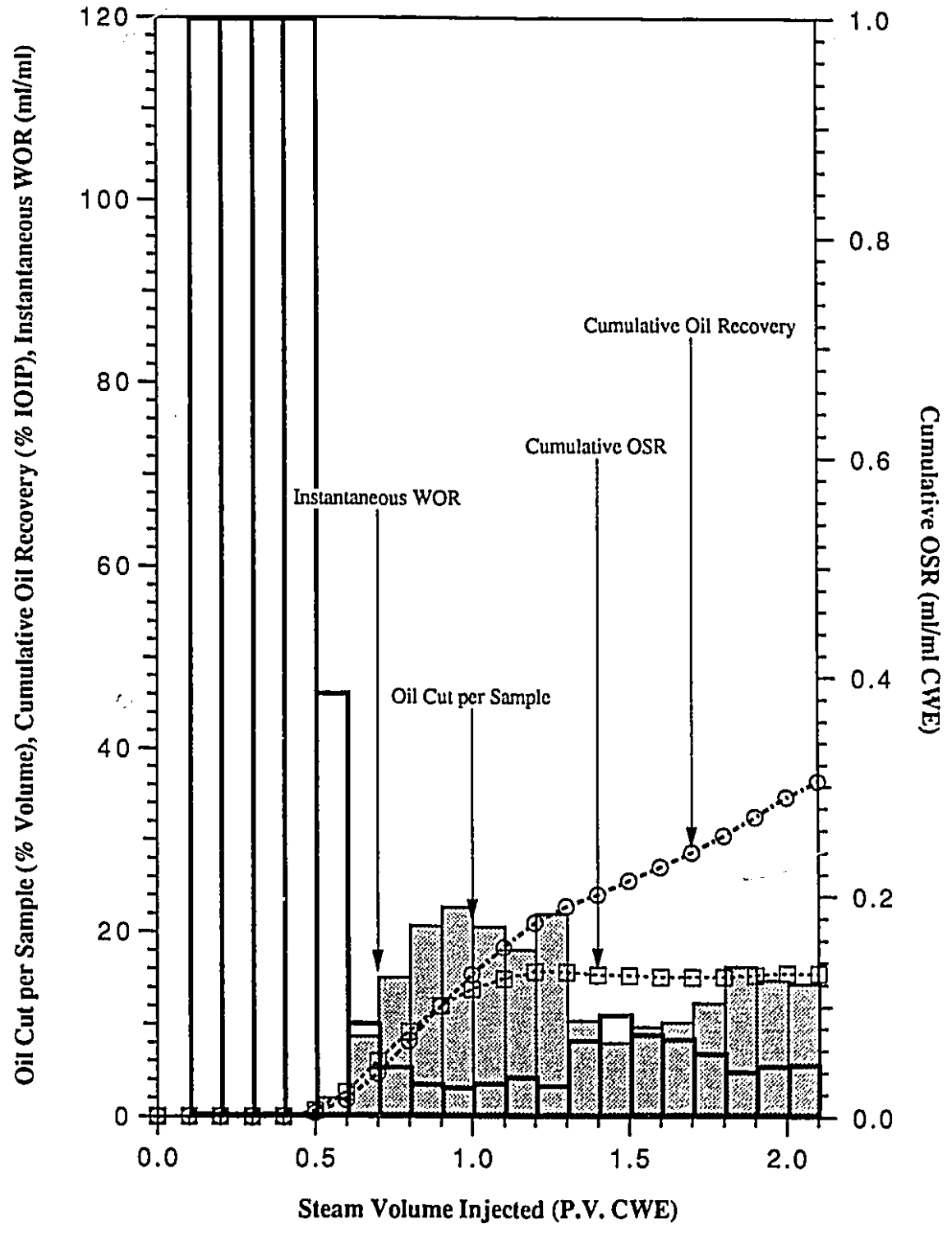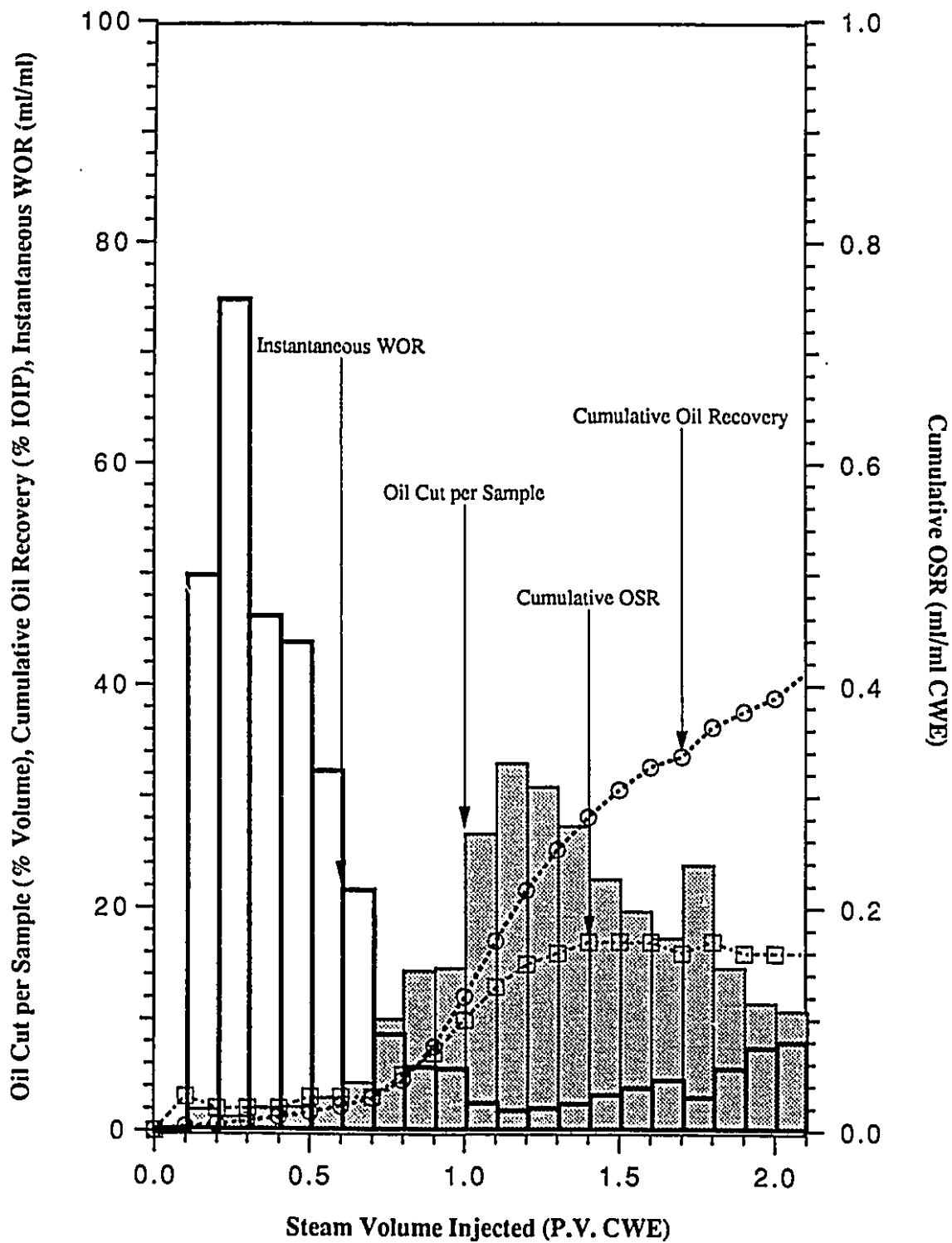
Figure 6.28: Production History of Run 13,
Steamflood with pattern inversions using pairs of horizontal injectors
and producers (wells elevated above the oil-water contact) in a
horizontal reservoir having 20% net-pay bottom water.

a) 0.50 PV (CWE) Inj.

b) 1.00 PV (CWE) Inj.

c) 1.50 PV (CWE) Inj.

d) 1.80 PV (CWE) Inj.

Legend: ——— Upper Model Temperature, °C

– – – Lower Model Temperature, °C

Port 3   Port 4

Port 1   Port 2
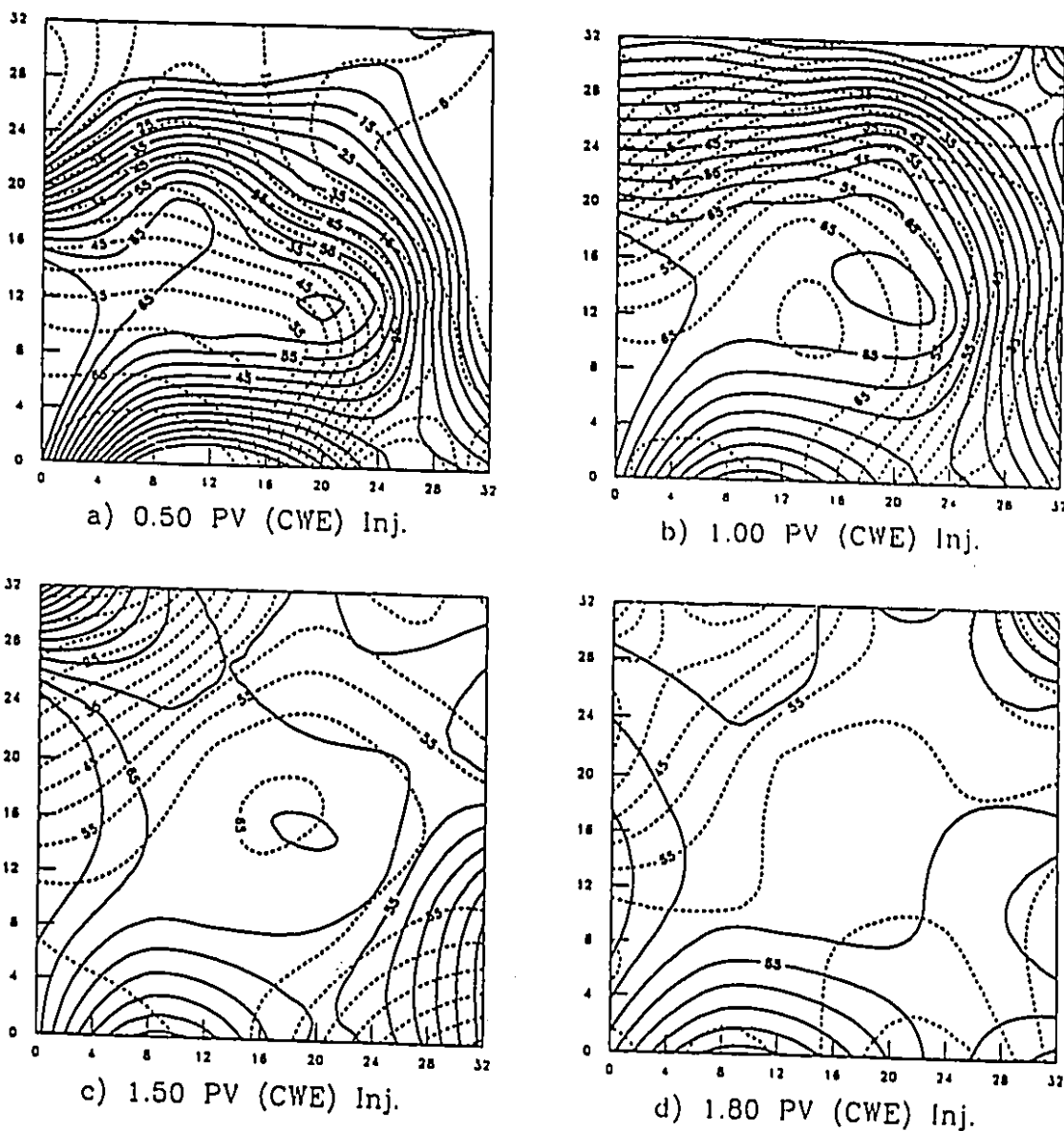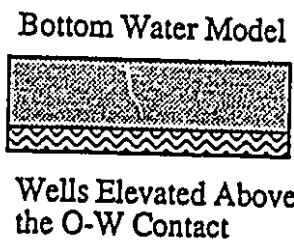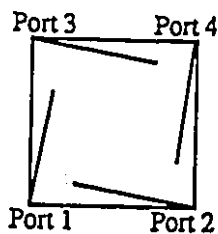
Bottom Water Model Legend:

Inj. for 1.6 PV using ports 1 and 4

0.1 PV	2 and 4
0.1 PV	1 and 3
0.1 PV	2 and 3
0.1 PV	1 and 3
0.1 PV	1 and 4

Wells Elevated Above
the O-W Contact

Figure 6.29:   Plan view of the temperature distribution inside the model along
with injection and production strategy for Run 13.

Based on the temperature contours, Figures 6.26 (a) and 6.29 (a) show that the elevation of the horizontal injectors and producers reduced the amount of heat entering the bottom water layer. The overall recovery, after 2.1 PV of steam injected, for Runs 13 and 11 was 41.18% and 36.6%, respectively. Yet, the recovery between these two experiments was essentially the same after 1.1 PV of steam was injected. The higher cumulative recovery, obtained from Run 13, was attributed to the elevation of both the horizontal injectors and the producers, that is increased stand-off, along with the delay in inverting the pattern. Figure 6.29 (a) shows that initially the majority of the energy injected went into the bottom water zone. Only a small portion of the injected heat was carried by steam override to the upper oil formation. As heat was continuously injected into the reservoir, the growth of the steam zone increased significantly after 1.0 PV of steam had been injected, as seen from Figure 6.29 (b). While in Run 11, the temperature contour plots, Figures 6.26 (a) and (b), showed the steam–condensate interface, indicated by T = 60°C, remained at approximately the same location during the injection of 0.5 to 1.0 PV of steam. As mentioned earlier, it is believed that pattern inversion was not appropriate for Run 11. In this experiment, the delay in pattern inversion allowed the build-up and propagation of the oil bank toward the producer.

The production data for Run 11 shows that the increase in cumulative oil recovery was small. Before pattern inversions, the increment was only about 1.7%. The production data for Run 13, where pattern inversions were not made until 1.6 PV of steam had been injected, shows the incremental recovery is increasing steadily. Figure 6.27 shows that the cumulative oil recovery in Run 13 exceeded the recovery obtained from Run 11 after 1.2 PV of steam had been injected. Hence, by delaying the use of pattern inversions, the overall recovery for Run 13 turned out to be 4.6% higher than for Run 11.

In the later stages of Run 13, quick pattern inversions – defined as rapid changes in injection and/or production strategies, typically 0.1 to 0.2 PV per pattern – were attempted after 1.6 PV of steam was injected. The idea in utilizing quick pattern inversions was to re-saturate the flow channels, that were previously established, with movable oil from outside of the original sweep pattern. This was accomplished by using a different pattern in the subsequent inversion for 0.1 or 0.2 PV injected, then changing back to the original pattern. An illustration of quick pattern inversion is as follows: if the existing injection and production patterns are at Ports 2 and 3, then the next pattern could either be injection at Port 1 and production at Port 4, or injection at Port 2 and production at Port 4. After injecting another 0.1 or 0.2 PV of steam using either one of the two patterns, the original

pattern is again used to take advantage of the fluids (oil and condensate) that re-saturate the flow channels.

Quick pattern inversions were seen to have some effect on the incremental recovery of Run 13. This can be observed from the production history plot, as the total production was 1695 ml, of which 250 ml was oil, after 1.8 PV of steam had been injected. Comparing this value with the average value from other experiments, after the same injection periods, showed the difference was approximately 25% higher.

Runs 11 and 13 led to the conclusion that pattern inversions in a horizontal reservoir with a thick bottom water layer should be avoided. The use of pattern inversions was found to be best suited for a homogeneous formation where an oil bank is present in the flow path between the injector and producer, or for steeply dipping reservoirs.

In Run 13, the increase in the elevation of both horizontal injection and production wells, that is, increasing the stand-off, and delaying pattern inversions did lead to the formation of a larger steam zone. However, another factor caused the growth of the steam zone – the Neoprene sealant sheet. The good insulating properties of the material reduced heat loss to the overburden. As a result, more heat was stored at the top of the reservoir, and the growth of the steam zone was promoted. Therefore, it is concluded that the results of this experiment would be rather optimistic when scaled-up to field conditions.

In previous studies made by Chang et al.[23], it was found that for reservoirs with a bottom water layer that was about 10% of the net pay, steam injection into the bottom water was beneficial as an increase in oil production was obtained. In this strategy, steam was first injected into the bottom water layer to heat the formation from below. Heat conduction from the heated zone caused the oil near the oil-water contact zone to become mobile. Subsequent steam injection into the oil zone resulted in better displacement and sweep efficiency. The above procedure works well when the heat loss to the underburden was small. If the heat capacity (M_{ob}) of the surrounding rocks is large, energy may be wasted because of the heat loss to the underburden.

From the three bottom water experiments – Runs 9, 11 and 13, it was concluded that steamflooding a steeply dipping heavy oil reservoir with 20 % net pay bottom water is a viable option, provided that the heat loss to the underburden is not large. With the use of horizontal injectors and producers, attempts were made to first heat the bottom water layer.

As the injection time increased, the temperature of the bottom water layer also increased. This led to the conduction of heat into the heavy oil formation. With the viscosity of the oil lowered, the mobility of the condensate carried the mobile oil along to the producing horizontal well. After a longer period of injection, the formation of a steam zone was observed as more heat accumulated in the reservoir. At this stage, oil production was a result of downward steam zone expansion from the top of the formation.

6.10   The Effect of Gas Injection on Cumulative Recovery

The effect of injecting gas into a reservoir, during a steamflood to increase recovery was studied. In the first experiment, a steamflood was temporarily interrupted for injecting slugs of gas into the model. After a period of time, the injection of gas stopped, and the steamflood resumed. In the second experiment, simultaneous injection of gas with steam was made for a short period of time during a steamflood.

In previous work, Matthias[56] also attempted to study the effect of gas injection on steamflooding. In this work, the injection rate for the nitrogen gas was 2060 cc/min. From this study, Matthias[56] found that due to the high permeability of the glass bead pack, the injected gas was quickly observed at the production well. Therefore, he concluded that it was not feasible to inject gas into a thin reservoir having high permeability.

6.10.1 The Injection of Gas (Slugs) During a Steamflood

In Run 14, the effect of gas injection (slugs) on oil recovery by a steamflood was studied. The porosity of the glass bead pack was 29.0%, the initial oil saturation was 89.6% and the steam injection rate was 205 ml/min. This run started with the injection of steam at Port 2, and production at Port 3 for 1.0 PV. The steamflood was then temporarily interrupted for gas injection. Next, using the same injection and production strategy, a slug of nitrogen gas (N_2) was injected for the next 0.5 PV. Subsequently, the steamflood was resumed with the same pattern, for the next 0.3 PV. Then, injection of steam using Port 1 and production at Port 3 for 0.4 PV, and injection at Port 2 and production at Port 4 followed for another 0.1 PV. The final pattern inversion utilized injection at Port 1 and production at Port 4 for 0.2 PV. The rate of flow for nitrogen gas was 544 ml/min.

The injection rate for the nitrogen gas, unlike the injection rate of steam, was unscaled. A bubble meter was used for measuring the injection rate. With the gas line connected to the

bottom of a glass cylinder, a soap bubble was formed by slightly squeezing the bulb. As the bubble was formed, the gas displaced the bubble towards the top of the glass cylinder, and the rate was measured by tracking and timing the distance traveled by the bubble. Due to the unstable flow rate of gas, ten measurements were made and the average value was used. The collection and measurement of the nitrogen gas at the producer proved to be a difficult task. As a result, the amount of gas remaining in the model, and the amount of gas produced were not known.

In this experiment, Run 14, the flow rate of gas was approximately 2.5 times the injection rate of wet steam; therefore, the period of time for gas to traverse 0.5 PV was short compared to that for wet steam. In this run, it took approximately 11 minutes and 10 seconds for gas to traverse 0.5 PV. During the injection of the gas slugs, production samples were taken at 0.25 PV (considering gas flow). In other words, the two samples were collected at 5 minutes and 35 seconds apart. The total volume of gas injected was 5065 cu ft, and the gas injection pressure varied between 2.6 psi (18 kPa) and 2.9 psi (20 kPa), gauge.

Figure 6.30 shows the production history, and Figure 6.31 shows the temperature profiles for Run 14. The cumulative oil recovery was 62.6% IOIP, after 1.9 PV of steam and 0.5 PV of nitrogen gas had been injected. Many similarities in the trend of the oil cut, the cumulative recovery and the cumulative OSR for this run and Run 12 (base case experiment) can be observed. However, the oil cut, the cumulative OSR and the cumulative recovery were higher in this experiment.

A comparison of the two experiments showed that injection of gas did not lead to higher oil recovery. If the oil cut and instantaneous oil production in the two experiments, for periods of time after gas injection, were to be compared, a different conclusion would be reached. The oil produced for periods after gas injection – for Run 12 – was found to be 265 ml more than for Run 14. Yet the overall recovery in Run 14 was higher. This clearly contradicted the conclusion made on the basis of the ultimate oil recovery. The gain in the overall recovery, for Run 14, was reflected from the injection period between 0.1 PV and 1.0 PV. In supporting the above view, a simple material balance for both experiments was done to calculate the steam zone volume. In Run 12, after 0.8 PV of steam had been injected, the volume occupied by steam was found to be 0.001441 m^3, and the ratio of cumulative injection to cumulative production, CI/CP, was 0.876. In Run 14, after a
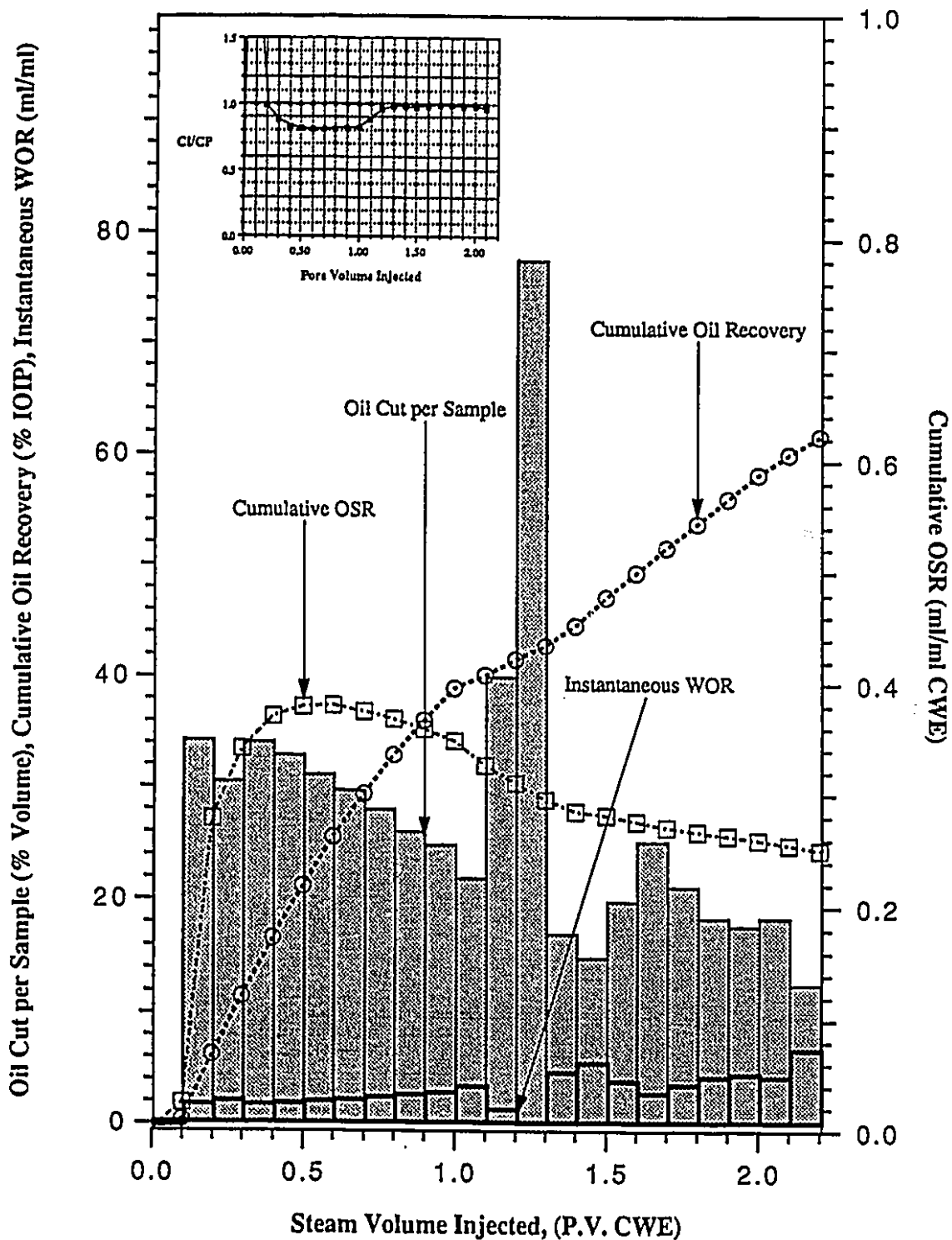
Figure 6.30: Production History of Run 14,
Steamflood and nitrogen gas injection (slugs) with pattern
inversions using pairs of horizontal injectors and producers in
a homogeneous, horizontal reservoir.

a) 0.50 PV (CWE) Inj.

b) 1.00 PV (CWE) Inj.

c) 1.20 PV (CWE) Inj.

d) 1.50 PV (CWE) Inj.

Legend: ———— Upper Model Temperature, °C

— — — Lower Model Temperature, °C

Port 3   Port 4

Port 1   Port 2
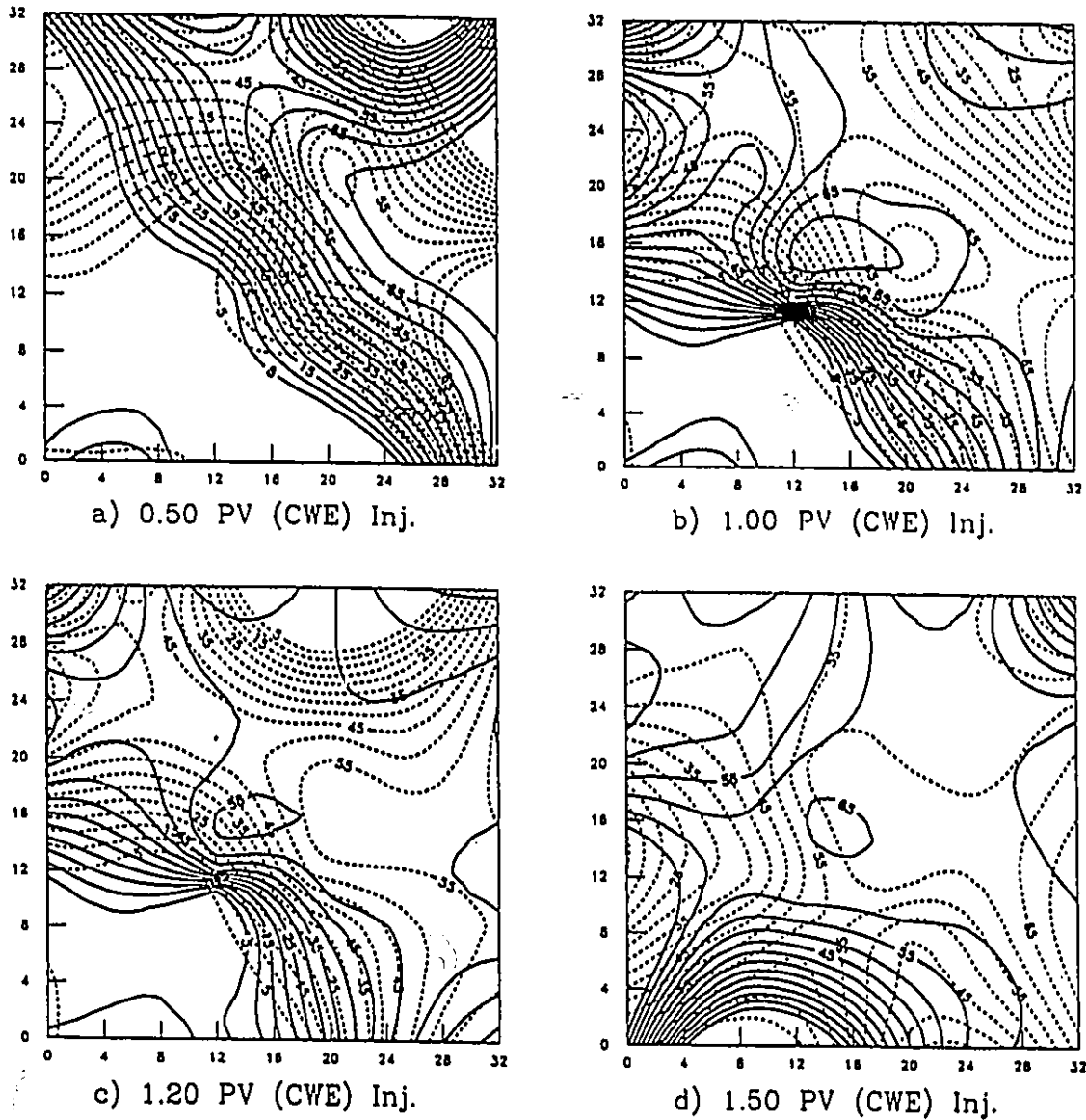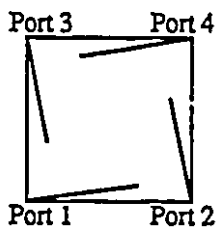
Homogeneous Model Legend:

Inj. for 1.0 PV using ports 2 and 3
Gas Inj., Using the Same Pattern, for 0.5 PV
Inj. for 0.3 PV using ports 2 and 3

0.4 PV	1 and 3	
0.1 PV	2 and 4	
0.2 PV	1 and 4	

Nitrogen Gas Injection (Slugs)

Figure 6.31:   Plan view of the temperature distribution inside the model along with injection and production strategy for Run 14.

similar period of injection, the steam zone volume was 0.002262 m^3, and the ratio of CI/CP was 0.811.

The difference in the oil cut and cumulative oil recovery were probably due to the location and the height of the horizontal injection and production wells. The horizontal wells were located at an angle that had a larger exposure to the reservoir. As a result, the area exposed to the steam front was larger. Also the horizontal injection and production wells were perhaps located lower in the formation. As a result, the oil column exposed to the steam front was larger. Based on the complete set of data, it was concluded that the higher cumulative recovery, and the higher cumulative OSR in Run 14, compared to the base case experiment – Run 12 – were due to better volumetric sweep and not because of gas injection.

6.10.2 Co-injection of Gas and Steam

In Run 16, the performance of the reservoir subjected to simultaneous injection of gas and steam for a short period of time during a steamflood was studied. The horizontal well configurations and well pattern were similar to those used in Run 14. The porosity of the glass bead pack was 30.3% and the initial oil saturation was 91.0%. The injection rate of steam was 213 ml/min., while the flow of gas was approximately 498 ml/min. Steam was first injected for 1.0 PV, with injection at Port 2 and production at Port 3. Simultaneous injection of gas and steam was followed for the next 0.4 PV, using the same pattern. Gas injection was then stopped, and the steamflood was allowed to proceed, using the same pattern, for the another 0.2 PV. After 1.6 PV of steam had been injected, quick pattern inversions were made to study how resaturation contributed to incremental oil recovery. Figures 6.32 and 6.33 show the production history and temperature contours for this experiment, respectively.

The simultaneous injection of gas and steam into the model was problematic because steam entered the gas injection line. The reason for steam entering the gas injection line was the existence of a pressure gradient between the steam injection point and the gas line. To overcome this problem, the pressure of the gas being injected into the model had to be set to 10 psi (69 kPa) gauge. In measuring the rate of gas injection, a gas meter was used. This instrument allowed good control for both measuring and controlling the gas flow rate.
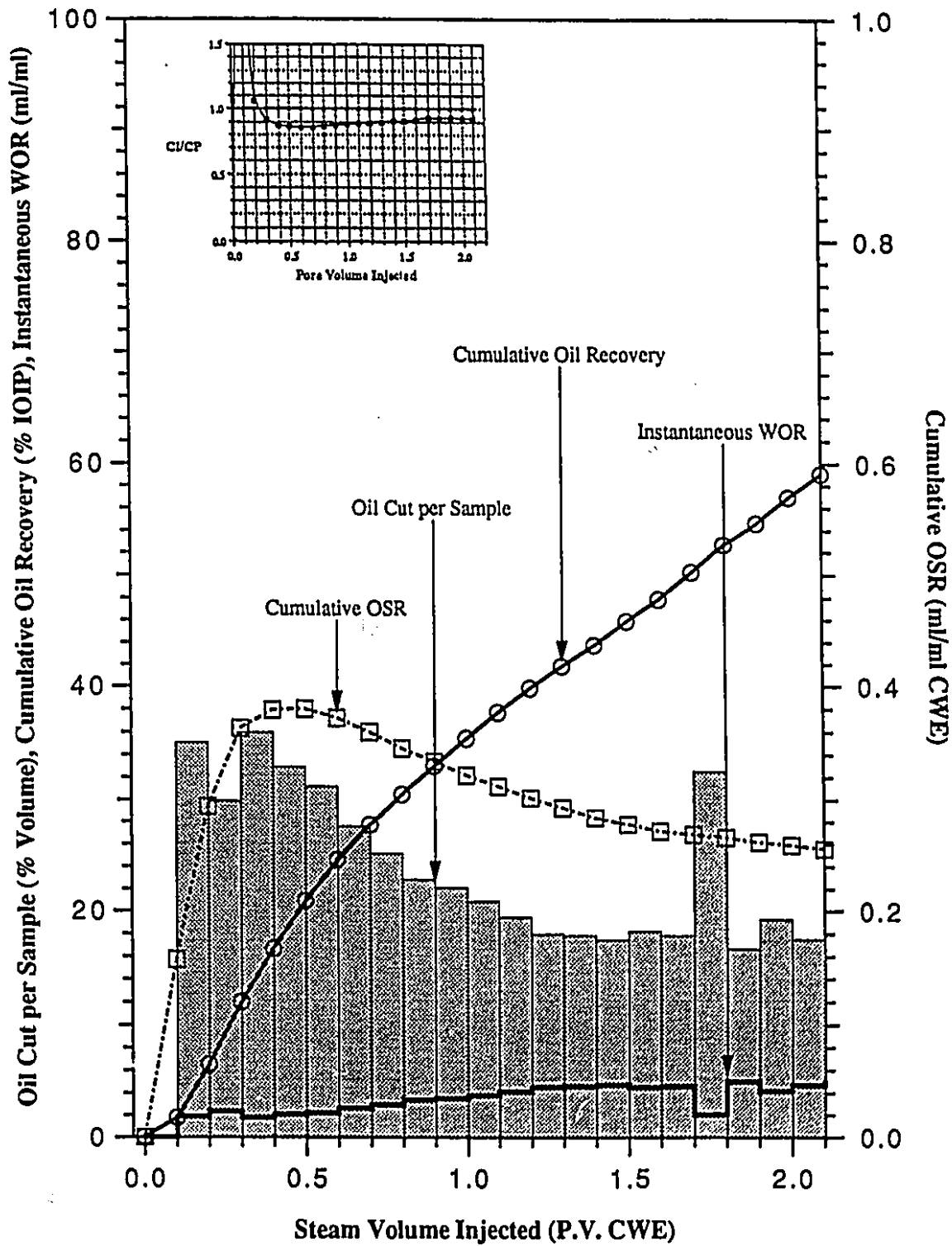
Figure 6.32: Production History of Run 16,
        Steamflood and nitrogen gas co-injection with pattern inversions using
        horizontal injectors and producers in a homogeneous, horizontal reservoir.

a) 0.50 PV (CWE) Inj.

b) 1.00 PV (CWE) Inj.

c) During Gas Injection

d) 1.50 PV (CWE) Inj.

Legend:
———— Upper Model Temperature, °C
— — — Lower Model Temperature, °C

Port 3   Port 4

Port 1   Port 2
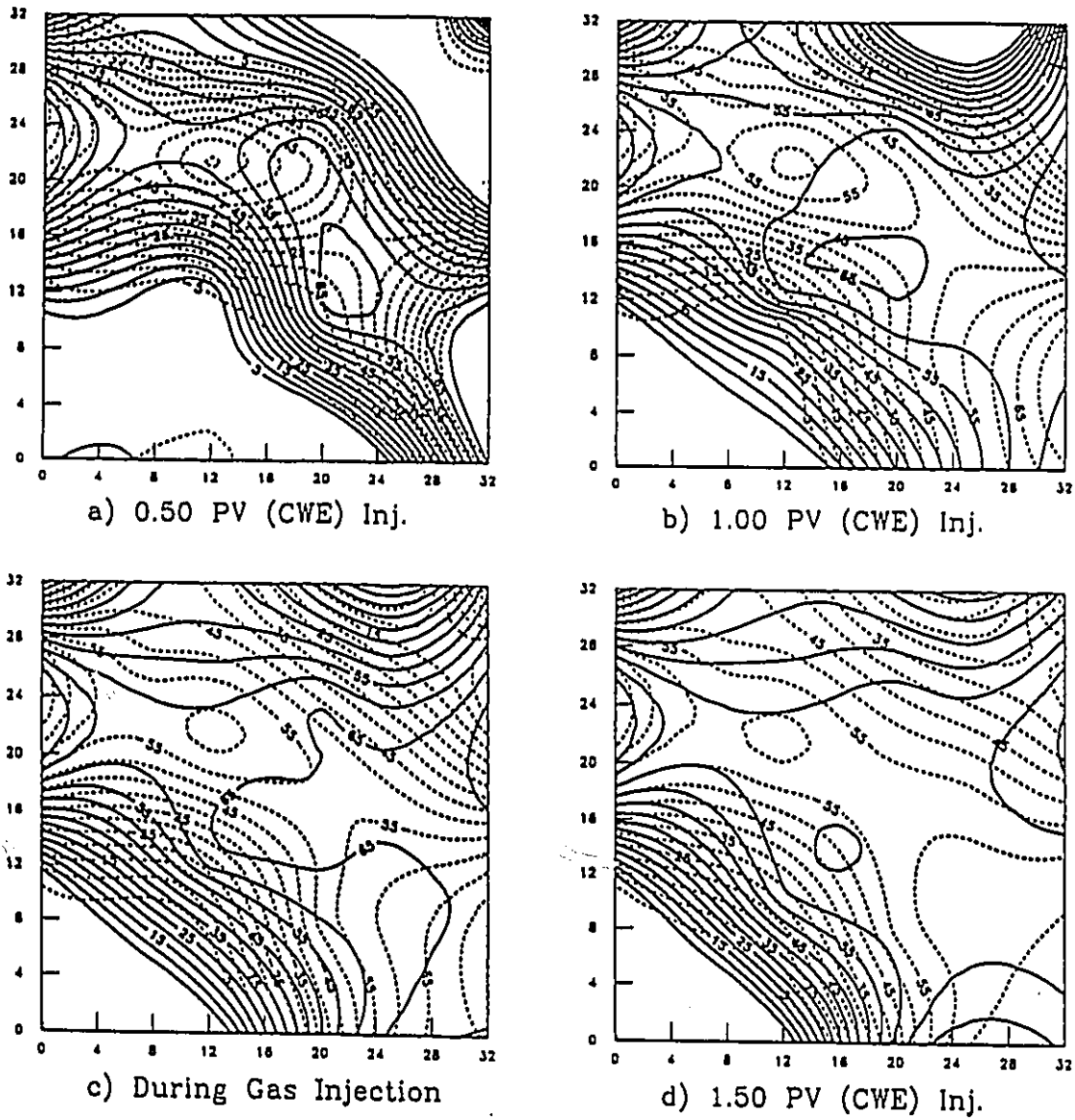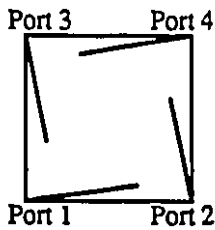
Homogeneous Model

Co-Injection of Nitrogen
Gas and Steam

Legend:
Inj. for 1.0 PV using ports 2 and 3
Co-Inj., Using the Same Pattern, for 0.4 PV
Inj. for 0.2 PV using ports 2 and 3

0.1 PV	2 and 4
0.1 PV	1 and 3
0.1 PV	1 and 4
0.1 PV	2 and 3

Figure 6.33:   Plan view of the temperature distribution inside the model along
with injection and production strategy for Run 16.

Based on the production data, the oil recovery in this run was 2.8% higher than the base case run, after 1.0 PV of steam had been injected, that is, prior to the simultaneous injection of steam and gas into the reservoir. This difference showed up in the ultimate oil recovery after 2.1 PV of steam had been injected, where the gain was 2.5%. The temperature contours, illustrated on Figure 6.33, showed similarities to those from Run 12. However, the path of the fluid was more direct between the injector and producer, the steam zone area was larger and the width of the condensate zone was also larger in Run 16. Based on the production data, the volume occupied by the steam – after 1.0 PV of steam had been injected – was 0.001602 m^3, and the CI/CP was 0.864. Again, the difference in the steam zone volume and hence oil recovery between this run and the base case experiment, Run 12, was attributed to improved sweep efficiency.

It is concluded that the injection of gas into a thin and homogeneous reservoir, having high permeability, did not increase oil recovery. The main reason is the high mobility of the gas, and its preference to traverse the most conductive (or least resistive) path between the injector and the producer. Also, the effect of gas in lowering heat loss to the overburden was not seen in this experiment. The presence of the Neoprene sealant sheet was observed to play a more effective role in preventing heat loss to the overburden than gas.

6.11 Optimistic Scale up

In the present experimental set-up, a Neoprene sheet is used to prevent fluid leakage. As previously mentioned, one of the properties inherent in the Neoprene sheet is its insulating ability. As a result, reservoir heating and heat production predominates. With this set-up, experiments conducted with the absence of the Neoprene sheet led to fluids (oil, water and steam) leakage. Therefore, experimental data for experiments where the modeled reservoir was in direct contact with the overburden and underburden (cap and base rock) were not available. Hence, the task of determining the optimistic prediction of previous experimental results is made more difficult.

To predict the oil recovery of a steamflood for a homogeneous reservoir, correlations established by Gomaa[61] were used. The procedures for estimating (predicting) the recovery – as a percentage of the initial oil in place – are illustrated in Appendix D. The correlation provided on Figure 14 of Gomaa[61]'s paper showed the maximum initial mobile oil saturation (S_{om}) – defined as the difference between the initial oil saturation prior to the steamflood and the residual oil saturation after the steamflood – was 60%. In this study,

S_{om} was approximately 78%. Therefore, the recovery for a homogenous oil reservoir was extrapolated to approximately 15% of the original oil in place (OOIP), after 0.8 PV of steam had been injected. From Run 12 (base case experiment), the recovery was found to be 25.1%, after an identical period of injection had been made.

In the base case run, horizontal injection and production wells were used for steamflooding a homogeneous reservoir. But, the correlations provided by Gomaa[61] were for vertical injection and production wells. Hence a correlation for recovery between vertical injection and production wells with horizontal injection and production wells is needed. From Chang[55], the cumulative recovery of a steamflood using a vertical injector and producer was approximately 28.5%, after 0.8 PV of steam had been injected. The recovery using a horizontal injector and producer was approximately 31%, after a similar injection period. The difference in the recovery between the two cases was 2.5%. In view of Chang[55]'s experimental results, it was concluded that the recovery for the base case run without the Neoprene sheet is approximately 17.5%, after 0.8 PV of steam had been injected. In other words, the presence of the Neoprene sheet resulted in an optimistic prediction of approximately 7.6%, after 0.8 PV of steam was injected.

In order to validate the prediction made above, a model to represent the temperature distribution through the cap rock was proposed to obtain the cumulative heat loss. The development of the model is shown in Appendix D. From Equation (D12), the heat loss was dependent on the areal steam coverage (A). By assuming that the areal steam coverage, after 0.8 PV of steam had been injected, was approximately 75%, the heat loss was found to be 1284.11 kJ. Upon knowing the heat loss to the overburden (cap rock), the net heat injected per unit volume (Q_{inj}^{*}) – defined as the difference between the heat injected and heat loss for a unit volume – was calculated. The value of Q_{inj}^{*} for the model was 98.056 MJ/m^3. Next, by assuming that the net heat injected per unit volume was directly proportional to the volumetric scale ratio, the value of Q_{inj}^{*} for the prototype was determined to be 114.7 MM Btu/ac-ft. Having found Q_{inj}^{*} attempts were made to predict the recovery. Unfortunately, the cross parameter present with the correlation charts did not match with the prototype. Hence, the recovery cannot be approximated directly. However, it was noted that Q_{inj}^{*}, obtained from the analytical model, was close to the value 133.5 MM Btu/ac-ft, which was predicted using Gomaa[61]'s correlation procedures. This validated the prediction made above. To obtain a better prediction of the recovery of a steamflood and to accurately determine the optimistic recovery of experimental results, a thermal simulator is needed.

Chapter 7

CONCLUSIONS

A number of experimental and theoretical studies were carried out in this research. Experimental objectives of this study were carried out using both a scaled physical model and an unscaled visual model. Steamflooding experiments, on the scaled physical model, were performed for a homogeneous reservoir, and for a reservoir with a 20% net pay bottom water layer. The use of the unscaled visual model allowed insight into the oil recovery mechanism. Theoretical objectives included the calculations to obtain the fluid saturations and steam zone volume in the reservoir, and the heat balance for a steamflood.

Based on the experiments conducted and the analysis made, the following conclusions are reached:

1) With the high permeability of the glass bead pack, steam was found to segregate quickly and migrate to the top of the formation. As a result, the dominant displacement mechanism in this type of reservoir was the downward expansion of steam at the top of the formation.

2) Pattern inversions were found beneficial for homogenous reservoirs, as larger volumes of oil were exposed to the steam front. However, pattern inversion is not recommended for a marginal horizontal reservoir with a thick (> 20% net pay) bottom water layer.

3) The location of the horizontal wells – in a thin homogeneous heavy oil reservoir – affected the cumulative oil recovery significantly. On the other hand, reservoir dip had little effect on recovery.

4) For experiments having similar well configurations and locations, regardless of the different sequences of pattern inversions, the recovery was found to be similar when one cyclic pattern inversion was made. This conclusion is valid if the reservoir is homogeneous and the flood time for each pattern is sufficiently long. However, the use of the right sequence enabled the recovery of oil more quickly, and with a lesser amount of steam injected.

5) The expression given by Neuman[34] to estimate the steam zone volume accurately predicted experimental results.

6) The presence of the Neoprene sealant sheet and fiberglass tray reduced the heat loss to the cap and base rock. The heat loss accounted for approximately 12% of the heat injected, after 0.8 PV of steam was injected.

7) The Neoprene sheet created conditions favourable for the formation and growth of the steam zone and hence optimistic recovery. Using Gomaa[61]'s correlation and experimental results obtained by Chang[55], the presence of the Neoprene sheet resulted in an optimistic prediction of approximately 7.6%, after 0.8 PV of steam was injected.

Chapter 8

RECOMMENDATIONS for FURTHER STUDIES

On the basis of the results obtained in this study, the following recommendations are proposed to extend the scope of the research. The recommendations include experimental modifications and theoretical studies as follows:

A. Experimental

1) Steam is currently injected – at constant rate – into the modeled reservoir. Changing the present set up to a constant pressure injection system would be more representative of field operations.

2) Variation in the steam quality should be allowed and incorporated into the injection system.

3) The Neoprene sealant sheet, and the fiberglass tray greatly reduced the heat loss to the cap and base rock. To properly represent the prototype, the modeled reservoir should be in direct contact with both the cap and base rock.

4) There should be several pressure transducers inside the model to monitor the reservoir pressure closely. There should also be more than two layers of thermocouples to allow the tracking of the steam front.

5) A thicker model should be used for active bottom water experiments.

6) The elevation in the height of the horizontal wells should be allowed to vary and should be controlled with greater precision.

7) A scaled visual model should also be designed to study the steam zone volume generated around a horizontal injection well.

B. Theoretical

1) The effect of heat loss to adjacent formation on oil recovery.

2) The steam zone volumes and the heat loss should be calculated in the absence of the fiberglass tray and the Neoprene sheet.

3) Models should be developed to study the following: a) the conditions under which counterflow of oil-water and steam will occur in the case of a light oil, a heavy oil, and a tar sand, and b) the conditions when steam override occurs for steam injection from vertical or horizontal wells.

4) Practical correlations for predicting vertical conformance should be developed.

References

1. Perrine, R.L.: "Well Productivity Increase from Drainholes as Measured by Model Studies", Petroleum Transactions, **AIME** Vol. 204, 1955, pp. 30-34.

2. Giger, F.M., Reiss, L.H. and Jourdan, A.P.: "The Reservoir Engineering Aspects of Horizontal Drilling", SPE 13024, presented at the 59th Annual Technical Conference and Exhibition of the Society of Petroleum Engineers, Houston, Texas, September 16-19, 1984.

3. Joshi, S.D.: "Augmentation of Well Productivity Using Slant and Horizontal Wells", SPE 15375, presented at the 61st Annual Technical Conference and Exhibition of the Society of Petroleum Engineers, New Orleans, LA, October 5-8, 1986.

4. Karcher, B.J., Giger, F.M. and Combe, J.: "Some Practical Formulas to Predict Horizontal Well Behaviour", SPE 15430, presented at the 61st Annual Technical Conference and Exhibition of the SPE, New Orleans, Louisiana, October 5-8, 1986.

5. Giger, F.: "Low-Permeability Reservoir Development Using Horizontal Wells", SPE/DOE 16406, presented at the SPE/DOE Low Permeability Reservoirs Symposium, Denver, Colorado, May 18-19, 1987.

6. Ozkan, E. and Raghavan, R.: "Performance of Horizontal Wells Subject to Bottom Water Drive", SPE 18545, presented at the SPE Symposium on Energy, Finance, and Taxation Policies, Washington, DC., September 19-20, 1988.

7. Babu, D.K. and Odeh, A.S.: "Productivity of a Horizontal Well", SPE Reservoir Engineering, November 1989, pp. 417-421.

8. Joshi, S.D.: "Production Forecasting Methods for Horizontal Wells", SPE 17580, presented at the SPE International Meeting on Petroleum Engineering, Tianjin, China, November 1-4, 1988.

9. Chaperon, I.: "Theoretical Study of Coning Toward Horizontal and Vertical Wells in Anisotropic Formations: Subcritical and Critical Rates", SPE 15377, presented at the 61st Annual Technical Conference and Exhibition of the Society of Petroleum Engineers, New Orleans, LA, October 5-8, 1986.

10. Muskat, M.: "The Flow of Homogeneous Fluids Through Porous Media", 1st Edition, 2nd Printing, J.W. Edwards Inc. (1946).

11. Papatzacos, P., Herring, T.R., Martinsen, R. and Skjaeveland, S.M.: "Cone Breakthrough Time for Horizontal Wells", SPE 19822, presented at the 64th Annual Technical Conference and Exhibition of the Society of Petroleum Engineers, San Antonio, Texas, October 8-11, 1989.

12. Sheikholeslami, B.A., Schlottman, B.W., Seidel, F.A. and Button, D.M.: "Drilling and Production Aspects of Horizontal Wells in the Austin Chalk", JPT, July 1991, pp. 773-779.

13. Bosio, J.C. and Reiss, L.H.: "Site Selection Remains Key to Success in Horizontal Well Operations", Oil & Gas Journal, March 21, 1988, pp. 71-76.

14. Damgaard, A.P., Bangert, D.S., Murray, D.J., Rubbo, R.P. and Stout, G.W.: "A Unique Method for Perforating, Fracturing and Completing Horizontal Wells", SPE Production Engineering, February 1992, pp. 61-69.

15. Butler, R.M., McNab G.S. and Lo, H.Y.: " Theoretical Studies on the Gravity Drainage of Heavy Oil During In-Situ Steam Heating", Canadian Journal of Chemical Engineering, Vol. 59, August 1981, pp 455-460.

16. Butler, R.M. and Stephens, D.J.: "The gravity Drainage of Steam Heated Heavy Oil to Parallel Horizontal Wells", JCPT, April-June 1981, pp 90-96.

17. Butler, R.M., Stephens, D.J. and Weiss, M.: "The Vertical Growth of Steam Chambers in the In-situ Thermal Recovery of Heavy Oils", Proceedings of the 30th Canadian Chemical Engineering Conference, Edmonton, Alberta, October 19-22, 1980, Volume 4, pp. 1152-1167.

18. Griffin, P.J. and Trofimenkoff, P.N.: "Laboratoires Studies of the Steam Assisted Gravity Drainage Process", presented at the AOSTRA 5th Annual 'Advances in Petroleum Recovery & Upgrading Technology' Conference, June 14-15 1984, Calgary, Alberta.

19. Edmunds, N.R., Haston, J.A. and Best, D.A.: "Analysis and Implementation of the Steam Assisted Gravity Drainage Process at the AOSTRA UTF", paper no. 125, Proceedings of the Fourth UNITAR/UNDP Conference on Heavy Crude and Tar Sands, Edmonton, August 7-12, 1988.

20. Butler, R.M. and Petela, G.: "Theoretical Estimation of Breakthrough Time and Instantaneous Shape of Steam Front During Vertical Steamflooding", AOSTRA Journal of Research, Volume 5, Number 4, Fall 1989, pp.359-381.

21. Sugianto, S. and Butler, R.M.: "The Production of Conventional Heavy Oil Reservoirs with Bottom Water Using Steam Assisted Gravity Drainage", JCPT, March-April 1990, pp. 78-86.

22. Huygen, H.A. and Black, J.B.: "Steaming Through Horizontal Wells and Fractures-Scaled Model Tests", Proceedings of 2nd European Symposium on Enhance Oil Recovery, Paris, France, November 8-10, 1982, 507-517.

23. Chang, H.L., Farouq Ali, S.M. and George, A.E.: "Performance of Horizontal Vertical Well Combination for Steamflooding Bottom Water Formations", JCPT, May 1992, pp. 41-51.

24. Matthias, R.C.M., Doan, Q.T., Farouq Ali, S.M. and George, A.E.: "Scale up of Horizontal Wells for Steamflooding a Bottom Water Reservoir", CIM 92-59, presented at the CIM Annual Technical Conference in Calgary, June 7-10, 1992.

25. Dietrich, J.K.: "The Kern River Horizontal Well Steam Pilot", SPE Reservoir Engineering, August 1988, pp. 935-944.

26   Rial, R.M.: "3D Thermal Simulation Using a Horizontal Wellbore for Steamflooding", SPE 13076, presented at the 59th Annual Technical Conference and Exhibition of the Society of Petroleum Engineers, Houston, Texas, September 16-19, 1984.

27.   Jain, S. and Khosla, A.: "Predicting Steam Recovery of Athabasca Oil Through Horizontal Wells", CIM 85-36-28, presented at the 36th Annual Technical Meeting of the Petroleum Society of CIM, Edmonton, Alberta, June 2-5, 1985.

28.   Huang, W.S. and Hight, M.A.: "Evaluation of Steamflood Processes Using Horizontal Wells", SPE 14130, presented at the SPE 1986 International Meeting on Petroleum Engineering, Beijing, China, March 17-20, 1986.

29.   Combe, J., Burger, J., Renard, G. and Valentin, E.: "New Technologies in Thermal Recovery: Contribution of Horizontal Wells", paper 117, Proceedings of the Fourth Unitar/UNDP Conference on Heavy Crude and Tar Sands, Edmonton, August 7-12, 1988.

30.   Marx, J.W. and Langenheim, R.H.: "Reservoir Heating by Hot Fluid Injection", Petroleum Transactions, **AIME** Volume 216, 1959, pp. 312-315.

31.   Mandl, G. and Volek, C.W.: "Heat and Mass Transport in Steam Drive", SPEJ, March 1969, pp 59-79.

32.   Myhill, N.A. and Stegemeier, G.L.: "Steam Drive Correlation and Prediction", JPT, February 1979, pp. 173-182.

33.   Van Lookeren, J.: "Calculation Methods for Linear and Radial Steam Flow in Oil Reservoirs", SPE 6788, presented at the 52nd SPE Annual Technical Conference, Denver, October 9-12, 1977.

34.   Neuman, C.H.: "A Gravity Override Model of Steamflood", JPT, January 1985, pp. 163-169.

35.   Miller, M.A and Leung, W.K.: "A Simple Gravity Override Model of Steamdrive", SPE 14241, presented at the 60th Annual Technical Conference, Las Vegas, NV September 22-25, 1985.

36.   Kumar, D., Patel, H.N. and Denbina, E.S.: "The Use of Gravity Override Model of Steamflooding at Cold Lake", pre-print manuscript of the Petroleum Society of CIM 1990.

37.   Jones, J.: "Steam Drive Model for Hand-Held Programmable Calculator", JPT, September 1981, pp. 1583-1598.

38.   Farouq Ali, S.M.: "Steam Injection Theories-A Unified Approach", SPE 10746, presented at the Cailifornia Regional Meeting, San Francisco, CA, March 24-26, 1982.

39.   Chen, H.L. and Sylvester, N.D.: "Appraisal of Analytical Steamflood Models", SPE 20023, presented at the 60th California Regional Meeting of the SPE, Ventura, CA, April 4-6, 1990.

40.   Peake, W.T.: "Steamflood Material Balance Applications", SPE Reservoir
       Engineering, August 1989, pp. 357-362.

41.   Moughamian, J.M., Woo, P.T., Dakessian, B.A. and Fitzgerald, J.G.:
       "Simulation and Design of Steam Drive in a Vertical Reservoir", JPT, July 1982,
       pp. 1546-54.

42.   Hong, K.C.: "Optimum Well Location for Steamflooding Steeply Dipping
       Reservoirs", SPE 21771, presented at the California Regional Meeting of SPE,
       Long Beach, CA, March 1991.

43.   Leverett, M.C., Lewis, W.B. and True, M.E.: Petroleum Transactions, AIME
       Volume 146, 1942, pp. 175.

44.   Rapoport, L.A. and Leas, W.J.: Petroleum Transactions, AIME Volume 198,
       1953, pp. 139.

45.   Offeringa, J. and van der Poel, C.: Petroleum Transactions, AIME Volume 201,
       1954, pp. 310.

46.   Geertsma, J., Croes, G.A., and Schwarz, N.: "Theory of Dimensionally Scaled
       Models of Petroleum Reservoirs", Petroleum Transactions, AIME Vol. 207,
       1956, pp. 118-127.

47.   Rojas, G.A., and Farouq Ali, S.M.: "Scaled Model Studies of Carbon Dioxide–
       Brine Injection Strategies for Heavy Oil Recovery from Thin Formations", JCPT,
       January-February 1986, pp. 85-94.

48.   Pujol, L. and Boberg, T.C.: "Scaling Accuracy of Laboratory Steam Flooding
       Model", SPE 4191, presented at the California Regional Meeting of the Society of
       Petroleum Engineers, Bakersfield, November 8-10, 1972.

49.   Farouq Ali, S.M. and Redford, D.A.: "Physical Modelling of In-Situ Recovery
       Methods of Oil Sands", Proceedings of the Canada-Venezuala Oil Sands
       Symposium, Edmonton, Canada, CIM Special Volume No.17, pp. 319-326, 1977.

50.   Kimber, K., Farouq Ali, S.M. and Puttagunta, V.R.: "Verification of Scaling
       Approaches for Steam Injection Experiments", CIM 88-39-17, presented at the 39th
       Annual Technical Meeting of the Petroleum Society of CIM, Calgary, June 12-16,
       1988.

51.   Stegemeier, G.L., Laumbach, D.D. and Volek, C.W.: "Representing Steam
       Process with Vacuum Models", SPEJ, June 1980, pp. 151-174.

52.   Kristoff, B.J., Saskatchewan Research Council, Regina, Personal Communication
       (1991).

53.   Proctor, M.L.: "Steam Injection Experiments in a Scaled Physical Model", M.Sc.
       Thesis, University of Alberta (Fall 1985).

54.   Oracheski, D.: "Bottom Water Solvent Steam Injection Studies", M.Sc. Thesis,
       University of Alberta (Fall 1988).

55. Chang, H.L.: "Horizontal Well Strategies for Steamflooding Oil Formations With a Communicating Water Zone", M.Sc. Thesis, University of Alberta (Fall 1990).

56. Matthias, R.C.M.: "Scaled Experiments of Heavy Oil Recovery Strategies in a Low Pressure Physical Model", M.Sc. Thesis, University of Alberta (Spring 93).

57. Doan, Q.T., Farouq Ali, S.M. and George, A.E.: "Scaling Criteria and Model Experiments of Horizontal Wells", JCPT, November 1992, pp. 57-65.

58. Van Wylen, G.J. and Sonntag, R.E.: Fundamentals of Classical Thermodynamics, Third Edition, SI Version, John Wiley & Sons, 1985.

59. Wygal, R.J.: "Construction of Models that Simulate Oil Reservoirs", SPEJ, December 1963, pp. 281-286.

60. Prats, M.: Thermal Recovery, Monograph Volume 7, SPE Henry L. Doherty Series, Chapters 6 and 7, Society of Petroleum Engineers of AIME (1982).

61. Gomaa, E.E.: "Correlation for Predicting Oil Recovery by Steamflood", JPT, February 1980, pp. 325-332.

62. Hong, K.C.: Steamflood Reservoir Management – Thermal Enhanced Oil Recovery, PennWell Books, Chapter 9, 1994.

63. Farouq Ali, S.M.: Heavy Oil Recovery, Chapter 5, 1989

64. Tortike, W.S. and Farouq Ali, S.M.: "Saturated Steam Property Functional Correlations for Fully Implicit Thermal Reservoir Simulation", SPE Reservoir Engineering, November 1989, pp. 471-4774.

65. Necati Ozisik, M.: Heat Conduction, John Wiley & Sons, 1980.

Appendix A

SATURATION CALCULATIONS

Two Zones Material Balance Equations: Steam and Oil Zones

The following assumptions are made in the derivation of the material balance equations (MBEs) for the oil and the steam zones.

1) There is no water influx into the reservoir (model).

2) The pore space in the reservoir remains constant; i.e. the porosity is constant.

3) The reservoir is incompressible; that is, $c_t = 0$.

4) There is no initial gas saturation.

5) The injected steam remains in the reservoir; that is, steam does not travel toward the producer.

Consider Figure A1 below as the starting point.
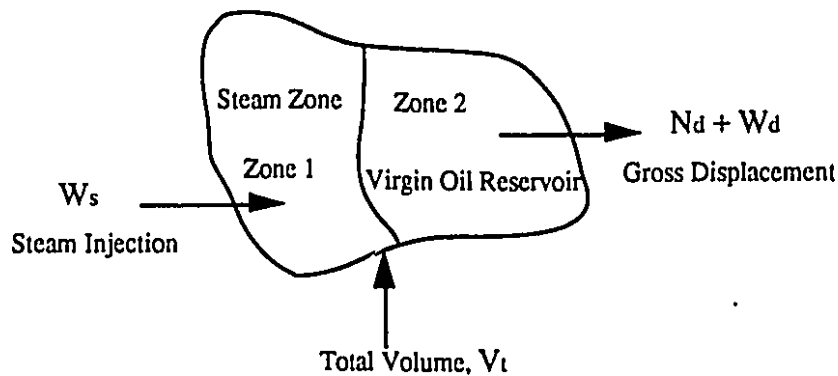
Figure A1: Simplified Two Zone Material Balance Reservoir Model

From the diagram, the incremental oil displaced, ΔN_d, between any two time periods during which the steam zone changes by ΔV_1, is given by

$$\Delta N_d = \phi \left[\left(\frac{S_o}{B_o}\right)_2 - \left(\frac{S_o}{B_o}\right)_1 \right] \Delta V_1 \qquad \ldots \ldots \text{(A1)}$$

and the corresponding incremental volume of water displaced, ΔW_d, is

$$\Delta W_d = \phi \ [\ (\tfrac{S_w}{B_w})2 - (\tfrac{S_w}{B_w} + \tfrac{S_s}{B_s})1 \ ] \ \Delta V_1 + \Delta W_s \qquad\qquad \ldots\ldots \quad (A2)$$

Where	$B_{o,w}$	= Formation volume factor for oil and water
	B_s	= Formation volume factor for steam
	$S_{o,w,s}$	= The saturations of oil, water, and steam
	ΔV_1	= Steam zone volume
	ΔW_s	= Incremental steam injected

Adding Equations (A1) and (A2) gives:

$$\Delta N_d + \Delta W_d = \Delta W_s + \phi \ [\ (\tfrac{S_o}{B_o})2 + (\tfrac{S_w}{B_w})2 - (\tfrac{S_o}{B_o})1 - (\tfrac{S_w}{B_w} + \tfrac{S_s}{B_s})1 \ ] \ \Delta V_1$$

$$\ldots\ldots \quad (A3)$$

Three Zones Material Balance Equations: Steam - Hot Water - Oil Zones

Material balance equations for the three zones (steam-condensate-and oil) reservoir are developed in the same fashion as that for two zones.
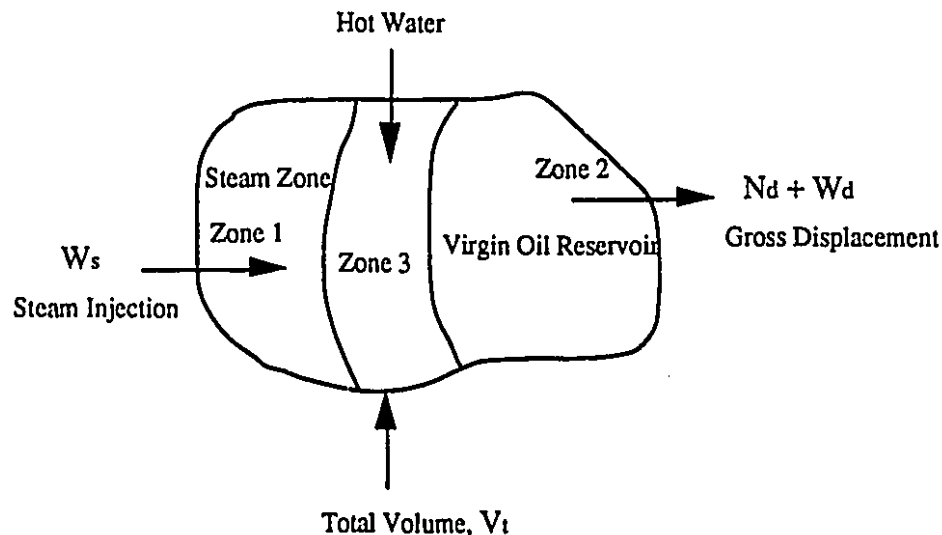
Figure A2: Simplified Three Zone Material Balance Reservoir Model.

As seen from Figure A2, the incremental volume of oil displaced, ΔN_d, is given by

$$\Delta N_d = \phi \left[\left(\frac{S_o}{B_o}\right)_2 - \left(\frac{S_o}{B_o}\right)_1 \right] \Delta V_1 + \phi \left[\left(\frac{S_o}{B_o}\right)_2 - \left(\frac{S_o}{B_o}\right)_3 \right] \Delta V_3 \quad \ldots\ldots \quad (A4)$$

and the corresponding incremental volume of water displaced, ΔW_d, is

$$\Delta W_d = \phi \left[\left(\frac{S_w}{B_w}\right)_2 - \left(\frac{S_w}{B_w} + \frac{S_s}{B_s}\right)_1 \right] \Delta V_1 + \phi \left[\left(\frac{S_w}{B_w}\right)_2 - \left(\frac{S_w}{B_w}\right)_3 \right] \Delta V_3 + \Delta W_s$$

$$\ldots\ldots \quad (A5)$$

Adding Equations (A4) and (A5) gives:

$$\Delta N_d + \Delta W_d \quad = \Delta W_s + \phi \left[\left(\frac{S_o}{B_o} + \frac{S_w}{B_w}\right)_2 - \left(\frac{S_o}{B_o} + \frac{S_w}{B_w} + \frac{S_s}{B_s}\right)_1 \right] \Delta V_1$$

$$+ \phi \left[\left(\frac{S_o}{B_o} + \frac{S_w}{B_w}\right)_2 - \left(\frac{S_o}{B_o} + \frac{S_w}{B_w}\right)_2 \right] \Delta V_3 \quad \ldots\ldots \quad (A6)$$

The above equations were used to determine oil and water saturations in different zones, as shown in the following for the base case experiment (Experiment 12). Examining the CI/CP inset graph of Figure 6.4 it was seen that oil production between 0.0 and 0.2 PV of steam injected into the reservoir was due mostly to a hot water flood, as the steam zone was not yet formed. Given the existence of two zones in the reservoir, the two-zone material balance equations were used. Equation (A2) was modified to reflect the absence of steam in Zone 1, as shown in the following,

$$\Delta W_d = \phi \left[\left(\frac{S_w}{B_w}\right)_2 - \left(\frac{S_w}{B_w}\right)_1 \right] \Delta V_1 + \Delta W_s \quad \ldots\ldots \quad (A7)$$

To determine the oil saturation profile in Zones 1 and 2, the material balance for the oil phase, Equation (A1) was modified slightly by introducing the following assumption: $B_{o2} = B_{o1} = 1$, giving

$$\Delta N_d = \phi \left[S_{o2} - S_{o1} \right] \Delta V_1 \quad \ldots\ldots \quad (A8)$$

In order to obtain a unique solution for these two unknowns, S_{o1} and S_{o2}, in Equation (A8), the following constraint is invoked,

$$S_o = S_{o1} + S_{o2} \quad \ldots\ldots \quad (A9)$$

where S_o represents the overall oil saturation remaining in the model at any time t. It was determined by the following formula,

$$S_o = \frac{\text{Initial hydrocarbon volume - Volume of oil produced}}{\text{Pore volume}}$$

$$\ldots\ldots \quad (A10)$$

Equations (A8) and (A9) were used in conjunction with Kramer's Rule to determine S_{o1} and S_{o2}. The water saturation in each zone was then obtained by invoking the overall saturation constraint in each zone. For example, for Zone 1: $S_{o1} + S_{w1} + S_{wir} = 1$.

Referring to the CI/CP inset graph of Figure 6.4, it appears that a steam zone formed after 0.2 PV of steam had been injected into the model. As such, the three-zone material balance model becomes applicable. Equation (A4) which described the material balance for the oil phase was modified slightly by introducing the assumption : $B_{o1} = B_{o2} = B_{o3} = 1$, giving

$$\Delta N_d = \phi \, (\, S_{o2} - S_{o1} \,) \, \Delta V_1 + \phi \, (\, S_{o2} - S_{o3} \,) \, \Delta V_3 \qquad \ldots\ldots \quad (A11)$$

Thus there are three unknowns: S_{o2}, S_{o1}, and S_{o3} in the above equation. Oil saturation in the steam zone was next assumed to be equal to steamflood residual oil saturation, that is, $S_{o1} = S_{orst}$. The residual oil saturation in the steam zone was assumed to be 0.12 for this study. This value was chosen as it was within the range of values typical of unconsolidated sandstone, California reservoirs[62]. This assumption reduced the number of unknowns in Equation (A11) from three to two. Finally, Equation (A12) which describes the constraint of the overall oil saturation in all three zones of the reservoir was introduced. It enabled the two saturations (S_{o2} and S_{o3}) to be determined.

$$S_{orst} + S_{o2} + S_{o3} = S_o \qquad \ldots\ldots \quad (A12)$$

The steam zone volume in Equation (A11), ΔV_3, was determined using the Surfer$^{\text{TM}}$ program which generated isotherms from thermocouple readings, and integrated the volumes enclosed between different isotherms. Based on engineering judgment, the condensate volume was assumed to be the volume enclosed between the 40°C and the 65°C temperature contours. Table A1 shows the steam zone volume, the condensate volume, steam saturation, water saturation and the oil saturations in Zones 1, 2 and 3 at different times. Figure A1 shows the saturations of oil in Zones 1, 2 and 3 for various periods of steam injection. Figure A2 illustrates the overall oil, water and steam

Table A1: The Oil Saturations in the Steam, Condensate, and Oil Zones Along with the Saturations of Steam and Water at Various Injection Periods.

Pore Volume Injected (PV)	Saturation of Oil Remaining in the Reservoir S_o	Average Steam Zone Volume (m³)	Average Condensate Volume (m³)	Saturation of Steam	Saturation of Oil in Zone 1	Saturation of Oil in Zone 2	Saturation of Oil in Zone 3	Saturation of Water
0.1	0.8824	0.00000	0.00211	0.0000	0.0000	0.6474	0.2350	0.1176
0.2	0.8381	0.00000	0.00552	0.0000	0.0000	0.5873	0.2508	0.1619
0.3	0.8009	0.00030	0.00649	0.0238	0.2279	0.4530	0.1200	0.1753
0.4	0.7644	0.00062	0.00778	0.0488	0.2355	0.4090	0.1200	0.1867
0.5	0.7295	0.00093	0.01110	0.0727	0.2489	0.3606	0.1200	0.1977
0.6	0.7021	0.00111	0.01335	0.0872	0.2565	0.3256	0.1200	0.2107
0.7	0.6770	0.00128	0.01524	0.1001	0.2517	0.3053	0.1200	0.2229
0.8	0.6527	0.00144	0.01537	0.1130	0.2412	0.2915	0.1200	0.2343
0.9	0.6331	0.00117	0.02229	0.0914	0.2421	0.2711	0.1200	0.2755
1.0	0.6139	0.00119	0.02229	0.0933	0.2326	0.2613	0.1200	0.2928
1.1	0.5947	0.00131	0.02338	0.1031	0.22238	0.2509	0.1200	0.3022
1.2	0.5747	0.00144	0.02426	0.1132	0.2137	0.2410	0.1200	0.3121
1.3	0.5696	0.00027	0.02404	0.0211	0.2210	0.2286	0.1200	0.4093
1.4	0.5453	0.00097	0.02672	0.0763	0.1956	0.2297	0.1200	0.3784
1.5	0.5281	0.00173	0.02912	0.1354	0.1944	0.2137	0.1200	0.3365
1.6	0.5085	0.00198	0.03292	0.1554	0.1843	0.2042	0.1200	0.3362
1.7	0.4838	0.00202	0.03408	0.1585	0.1689	0.1949	0.1200	0.3578
1.8	0.4591	0.00197	0.03423	0.1541	0.1562	0.1829	0.1200	0.3868
1.9	0.4355	0.00204	0.03478	0.1600	0.1451	0.1705	0.1200	0.4045
2.0	0.4136	0.00214	0.03538	0.1682	0.1349	0.1586	0.1200	0.4182
2.1	0.3928	0.00228	0.03582	0.1787	0.1251	0.1477	0.1200	0.4285

Porosity 0.304
Residual Oil Saturation 0.120

Initial Oil Saturation 0.9032
Irreducible Water Saturation 0.0968
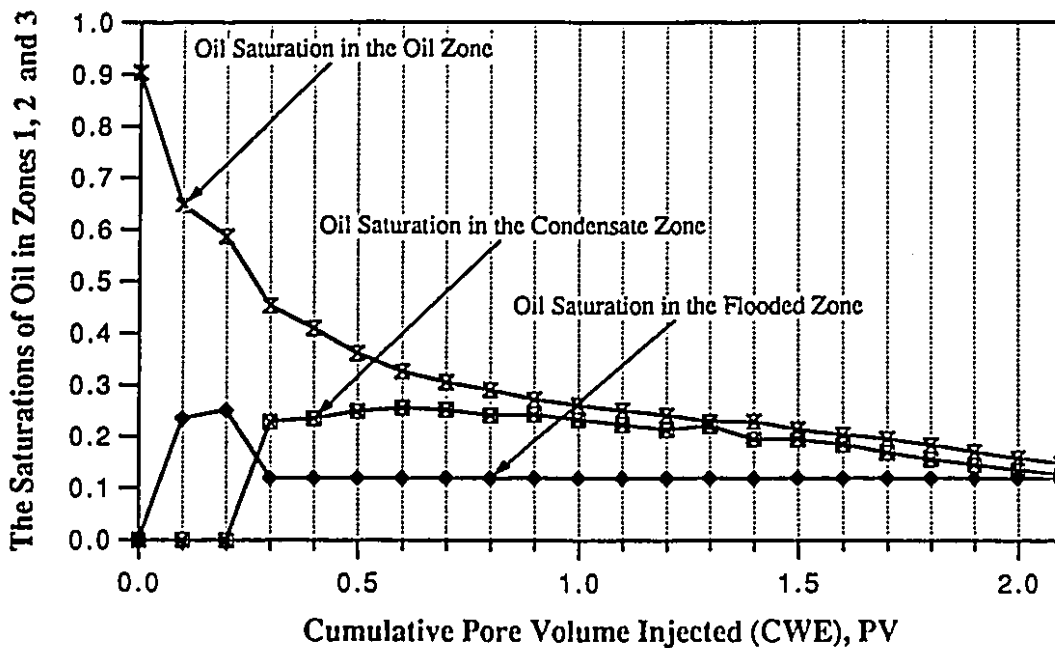
Figure A3:   The Saturations of oil in the oil, condensate and steam flooded
              zones at various cumulative injection periods, for the base case run.
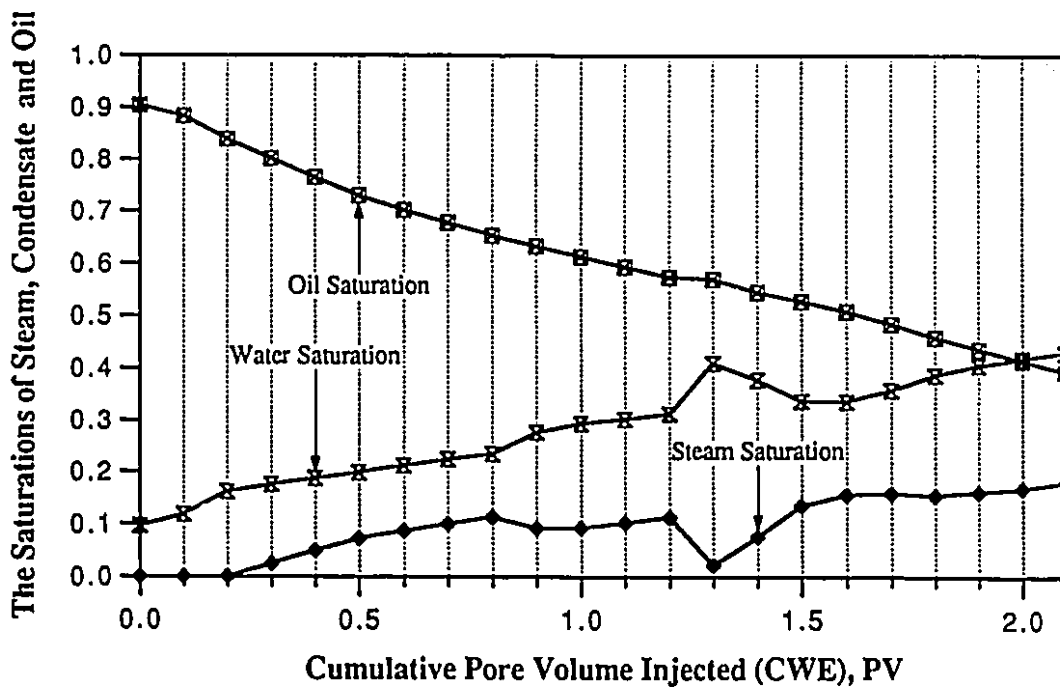
Figure A4:   The saturations of steam, condensate and oil in the reservoir
              at various cumulative injection periods, for the base case run.

saturations at various periods of steam injection. Experimentally, the overall steam saturation was determined by the difference between the cumulative injected and cumulative produced volumes. As seen in Figure A1, it was important to recognize the fact that subsequent to pattern inversions, the steam zones did not collapse, as shown at 0.9 PV and 1.3 PV. The steam zone was still present in the reservoir. However, due to the change in the pattern, the area exposed to the steamflood increased, and cold oil was produced.

In developing a two zone (hot water and oil) and a three zone (steam, condensate and oil) model reservoir, to allow the construction of the oil saturations in each zone, two important assumptions were made. In the first assumption, the amount of oil displaced (ΔN_d) in the reservoir – as given by Equations (A8) and (A11) – is assumed to be produced (ΔN_p). The second assumption implied the saturations in the reservoir at a given time – as given by Equations (A9) and (A12) – are independent of the changes in the individual volumes.

It is important to understand that the oil saturation profiles of the three zones (steam, condensate and oil) in the reservoir cannot be constructed based solely on the MBEs for the oil and water phase. An equation describing the variation in the saturations with distance (that is, moving saturation boundaries) is also required.

Appendix B

STEAM ZONE VOLUME CALCULATION

Frontal Displacement Model – Mandl and Volek Equations

Mandl and Volek[31] recognized the effect of the convective heat transport of hot water in the mobilization and displacement of oil during a steamflood. They concluded that this effect was substantial when the flood time was greater than the critical time, t_c, which was defined to be the time when the predominant mode of heat transfer – from the steam and condensate zones to the oil zones – changed from conduction to convection. As such, the convective heat transfer from the condensate zone to the oil zone ahead was negligible when time was less than the critical time, t_c. On the other hand, when the critical time was exceeded, convective heat transfer became dominant. The following procedure was suggested by Mandl and Volek[31] to determine the critical time:

1) Calculate the variable B, using the following equation,

$$B = \frac{f_{si} L_v}{c_w (T_s - T_R)} \qquad \ldots\ldots \quad (B1)$$

2) Calculate the variable F_{2c} as follows,

$$F_{2c} = \frac{1}{1 + B} \qquad \ldots\ldots \quad (B2)$$

3) Determine $\sqrt{t_{DC}}$ from Table 5.1 or Figure 5.3[63]

   where t_{DC} is the dimensionless critical time.

4) Calculate t_c in hours using Equation (B3),

$$t_c = \frac{M_s^2 h_t^2 t_{DC}}{4 k_{hob} M_{ob}} \qquad \ldots\ldots \quad (B3)$$

Knowledge of the critical time enabled the appropriate steam zone volume to be calculated, as illustrated by the following:

$$V_s = \frac{\dot{Q_i} M_s h_t^2}{4 k_{hob} M_{ob}(T_S - T_R)} \bullet F_1 \qquad (t < t_c) \qquad \dots\dots \quad (B4)$$

and

$$V_s = \frac{\dot{Q_i} M_s h_t^2}{4 k_{hob} M_{ob}(T_S - T_R)} \bullet F_3 \qquad (t \geq t_c) \qquad \dots\dots \quad (B5)$$

where F_1, t_D and F_3 are defined as,

$$F_1 = e^{t_D} erfc\sqrt{t_D} + 2\sqrt{\frac{t_D}{\pi}} - 1 \qquad\qquad t_D = \frac{4 k_{hob} M_{ob}}{M_s^2} \cdot \frac{t}{h_t^2}$$

and

$$F_3 = e^{t_D} erfc\sqrt{t_D} + 2\sqrt{\frac{t_D}{\pi}} - 1 -$$

$$\sqrt{\frac{t_D - t_{Dc}}{\pi}} \left\{ \left[1 + \frac{f_{st} L_v}{c_w(T_s - T_R)} \right]^{-1} + \left(\frac{t_D - t_{Dc} - 3}{3} \right) e^{t_D} erfc\sqrt{t_D} - \frac{t_D - t_{Dc}}{3\sqrt{\pi t_D}} \right\}$$

For the base case run (Experiment 12), the critical time, t_c, was found to be 6325.07 seconds, using the above procedure. The time to inject 0.8 PV of steam was 2915 seconds. As this time was less than the critical time, the steam zone expression given by Equation (B4) was used. Table B1 contains the steam zone volumes predicted by Mandl-Volek[31]'s model, together with the steam zone volumes calculated using Neuman[34]'s model (as illustrated below).

Gravity Override Model - Neuman's Equations

Neuman[34] considered the effect of steam override on steamflood recovery performance. In Neuman's model, three important assumptions were made. First, steam was assumed to rise quickly to the top of a permeable reservoir; that is, this time was considered to be negligible compared with the time required to heat the total reservoir area. Second, the horizontal pressure gradient in the steam zone was assumed to be much less than the vertical pressure gradient. Lastly, the saturations of oil and water were assumed to remain constant throughout the steam zone. Equations were derived to determine the velocity of the steam/liquid interface, steam zone thickness, the areal growth of the steam zone, the

Table B1: The Steam Zone Volumes Obtained from Neuman's Equations, Mandl and Volek's Equation and Experimental After 0.8 PV of Steam was Injected.

S_w (dimensionless)	S_o (dimensionless)	S_{st} (dimensionless)	M_s (kJ/m³K)	f_{pi} (dimensionless)	V_s from Neuman (m³)	V_s from experiment (m³)	V_s from Mandl & Volek (m³)
0.1176	0.8824	0.0000	2203.7700	0.0991	0.000000	0.000000	0.000000
0.1619	0.8381	0.0000	2240.6440	0.1698	0.000000	0.000000	0.000000
0.1753	0.8009	0.0238	2239.6325	0.1947	0.000695	0.000304	0.013014
0.1867	0.7644	0.0488	2239.4464	0.2226	0.000889	0.000623	0.017016
0.1977	0.7295	0.0727	2236.7654	0.2418	0.001083	0.000928	0.021221
0.2107	0.7021	0.0872	2239.2998	0.2540	0.001276	0.001112	0.025249
0.2229	0.6770	0.1001	2241.6628	0.2610	0.001474	0.001277	0.029473
0.2343	0.6527	0.1130	2242.4255	0.2690	0.001669	0.001441	0.033049

133

amount of oil displaced from the heated reservoir beneath the steam zone and the reduced steam injection rate to maintain a constant area covered by steam. In this study, the equations for predicting the thickness of the steam zone (h), the area covered by steam (A_s) and the steam zone volume (V_s) were considered. The thickness of the steam zone was given by [34]

$$h = \frac{4k_h C_w \Delta T_s}{M_s L_v} \sqrt{\frac{(t-\tau)}{\pi \alpha}} \qquad \text{.....} \quad (B6)$$

where

k_h	= the thermal conductivity, (kJ/mKs)
C_w	= the specific heat capacity of water, (kJ/kgK)
ΔT_s	= the difference between reservoir temperature and steam temperature, (^{o}K)
α	= the thermal diffusivity, (m^2/s)
L_v	= the heat of vaporization of water, (kJ/kg)

From Equation (B6), the heat capacity of the formation (M_s) is

$$M_s = (1-\phi)\rho_{ma}C_{ma} + \phi \rho_w S_{wrs} C_w + \phi \rho_o S_{ors} C_o \qquad \text{.....} \quad (B7)$$

where

$\rho_{ma}C_{ma}$ is the volumetric heat capacity of the matrix, (kJ/m^{3}K)

The area covered by steam at different times was calculated, using Equation (B8)[34]

$$A = \left[\frac{f_d(1-f_p)i\rho_w L_v}{k_h \Delta T_s}\right]\sqrt{\frac{\alpha t}{\pi}} \qquad \text{.....} \quad (B8)$$

where

f_d	= the steam quality downhole, (fraction)
f_p	= the fraction of injected heat that is produced, (fraction)
i	= the injection rate (C.W.E.), (m^3/s)

The steam zone volume, V_s, is given by the following equation[34]

$$V_s = \frac{f_d(1-f_p)i\rho_w C_w t}{M_s} \qquad \text{..... (B9)}$$

Table B1 contains calculated values for the steam zone volume, and vertical sweep, as determined from Neuman's model. Figure B1 shows the steam zone volume obtained from Neuman's model along with the steam zone obtained from the experimental data. The two sets of steam zone volume values were compared for up to 0.8 PV of steam injected into the model, before the first pattern inversion was implemented.

It was observed from Figure B1 that the steam zone predicted by Neuman's model[34] matched the experimental results closely. The following explanation discusses the close match between experimental and theoretical results. Careful examination of Equation (B9) revealed that the steam zone volume was not directly dependent on the volumetric heat capacity of the overburden, M_{ob}. Rather, it was dependent on the parameter, f_p, the fraction of injected heat produced. The following definition is provided for this parameter,

$$f_p = \frac{Q_{prod.}}{Q_{inj.}} = 1 - Q_{loss} - Q_{form.} \qquad \text{..... (B10)}$$

As can be seen from this equation, the heat loss and heat accumulated appearing on the right hand side of the above equation became insignificant, as changes in these two factors were reflected upon the amount of heat produced appearing on the left hand side. Since the heat loss depended on the properties of the overburden and underburden, this dependence was also absorbed into the term Q_{prod}. As a consequence, the accuracy of the of the steam zone expression was dependent on a precise knowledge of the heat injected and the heat produced. In field operations, the amount of heat injected and produced were easily obtained, with accuracy, from injection and production data.

The steam zone volumes predicted by the Mandl-Volek's model, on the other hand, were approximately 25 times the experimental values. Examining Equations (B4) and (B5), it is seen that Mandl-Volek[31]'s steam zone volume is dependent on the thermal conductivity, k_{hob}, of the cap rock and base rock. As a result of the experimental set up, the overburden was composed of two different layers: the Neoprene sheet in direct contact with the reservoir, and the granite cap rock. In using Equation (B4), the thermal conductivity of the Neoprene sealant sheet was the value k_{hob} as the effective thermal conductivity of the overburden were not known. This value, when compared with the actual overburden,
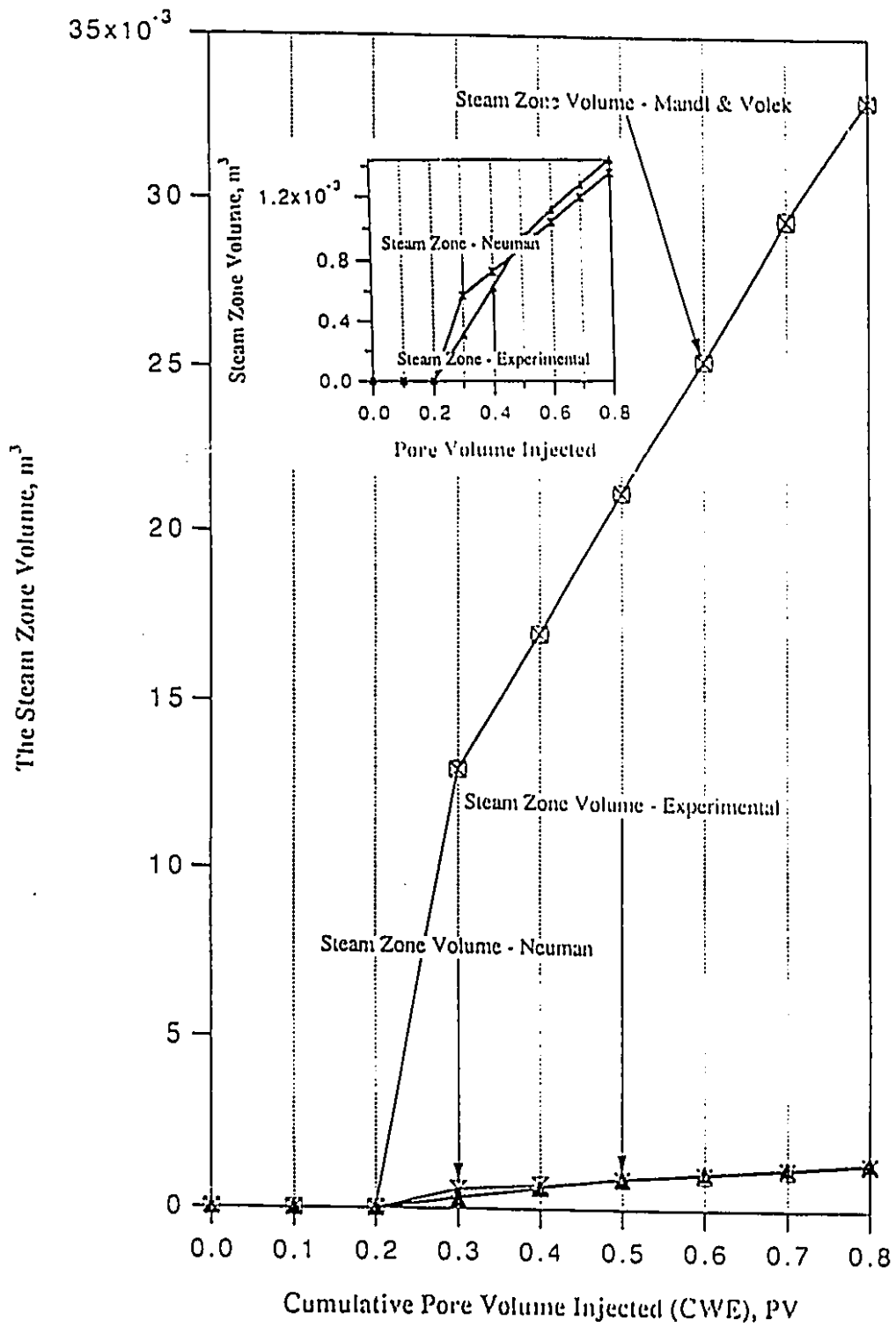
Figure B1:   The steam zone volume obtained from Neuman's steam override model, Mandl and Volek's frontal drive model, and experimental results.

differed by two order of magnitudes. As a result, the steam zone volume predicted by Mandl and Volek greatly exceeded the values obtained experimentally

Appendix C

HEAT LOSS CALCULATION

An understanding of the utilization of the injected energy – including the heat loss from the reservoir to the cap and base rock, as well as the heat accumulated in the reservoir – is important for the success of steamflooding and other thermal recovery processes. This appendix examines the distribution of the injected heat for the steamflooding process involved in the experiments. Specifically, the following discussion examines the cumulative heat balance calculation for a steamflood experiment. Applying the heat conservation principle, the overall heat balance at any time t is given by

$$Q_{inj} = Q_{prod} + Q_{loss} + Q_{formation} \qquad \dots (C1)$$

where Q_{inj} = energy injected into the formation, kJ

Q_{prod} = energy removed from reservoir due to fluids production, kJ

Q_{loss} = heat loss to overburden and underburden, kJ

$Q_{formation}$ = heat accumulated in the model; including glass beads, oleic phase, aqueous (condensate) phase, and vapor (steam) phase, kJ

Heat Injected, Q_{inj}, and Heat Produced, Q_{prod}

The heat injected into the reservoir, Q_{inj}, and the heat contained in the produced fluids, Q_{prod}, were easily obtained from the injection and production data. The experiments carried out in this study involved a constant injection rate. As such, the heat injected at the end of any time t was given by the following equation,

$$Q_{inj.} = i_{st}\left(h_{inj} - h_{res} + f_{st}L_v\right) * t \qquad \dots (C2)$$

in the above equation,

i_{st} = the mass flow rate of steam (kg/s),

h_{inj} = the enthalpy of saturated water (kJ/kg),

h_{res} = the enthalpy of water at the initial reservoir temperature (kJ/kg),

f_{st} = the quality of steam (dimensionless),

L_v = the latent heat of vaporization (kJ/kg),

t = the injection time (sec),

The procedure for determining the heat produced was similar to that given by Matthias[56]. Experimentally, data from the thermocouple at the producer revealed that the temperature of the produced fluids, which were collected every 0.1 PV of steam injected, varied slightly during each sampling period. Consequently, an arithmetic average was taken of the temperatures recorded during each sampling period. This average temperature was then taken as the representative temperature of the fluids (oil and water) produced. The cumulative heat contained in the fluids produced was, therefore, given by

$$Q_{prod} = \sum_{i=1}^{n} \left\{ \left(V_{w,i} \times C_{w,i} \times \rho_{w,i} + V_{o,i} \times C_{oi} \times \rho_{o,i} \right) \times \Delta T \right\} \qquad \ldots\ldots\ (C3)$$

where

i	= any production sample of oil and condensate.
n	= total number of samples.
ΔT	= the temperature difference between the initial reservoir temperature and the average temperature of production sample i.
C_w	= the specific heat of water, kJ/kgK.
	= $4.3245 - 3.696e^{-3}T + 2.482e^{-5}T^2$
C_o	= the specific heat of oil, kJ/kgK.
	= $1.7915 + 0.00361T$ kJ/kgK
$\rho_{w,o}$	= The density of the water and oil, kg/m^3.
ρ_w	= $\dfrac{1}{[0.001 + 1.436e^{-6}(-4.8872 + 0.134186T + 0.00212868T^2)]}$
ρ_o	= 879.9 kg/m^3.

The specific heat and density for the oil used in this study (Faxam 100 mineral oil) were provided by the manufacturer, Imperial Oil Resources Limited. While, the specific heat and density of water are obtained from correlations provided by Tortike and Farouq Ali[64]. Table C1 shows the calculated values for both the heat injected (Q_{inj}) and the heat produced (Q_{prod}) for the base-case experiment (Experiment 12).

Heat Accumulation in the Formation, $Q_{formation}$

The energy accumulated in the formation at any time was more difficult to determine than either the heat injected (Q_{inj}) or the heat produced (Q_{pro}). In this study the approach used to calculate this parameter, $Q_{formation}$, was to sum the energy contained in the matrix, and reservoir fluids. Given the non-uniform temperature distribution, the reservoir was

Table C1: The Amount of Heat Injected and Produced After 0.8 PV of Steam was Injected, Experiment 12.

Temperature °C	C_w kJ/kgK	ρ_w kg/m³	C_o kJ/kgK	ρ_o kg/m³	Water Volume mL	Oil Volume mL	ΔT °C	time of injection sec.	Heat Produced kJ	Cum. Heat Injected kJ
29.7	4.2366	998.6006	1.89871	879.9	555	265	27.7	364.4	77.3042	714.2870
33.6	4.2283	997.1010	1.91279	"	1140	565	31.6	728.8	181.9295	1396.0283
35	4.2255	996.5412	1.9178	"	1130	475	33.0	1093.2	183.4774	2077.7447
42.3	4.2125	993.4410	1.94420	"	1130	465	40.3	1457.7	222.6357	2727.0528
45.2	4.2081	992.1257	1.95467	"	1135	445	43.2	1822.1	237.7729	3408.7693
46.1	4.2068	991.7079	1.95792	"	1110	350	44.1	2186.6	230.8136	4072.6952
46.2	4.2067	991.6612	1.95828	"	1120	320	44.2	2551	230.8844	4772.3892
43.7	4.2103	992.8119	1.94925	"	1130	310	41.7	2915.4	219.1431	5367.2781

Steam Quality   0.1   Rate of Steam Injection 3.4115×10^{-3} kg/sec

partitioned into different zones each of which was bordered by two temperature "boundaries" (isotherms). As stated previously, the Surfer™ program was used to determine and draw isotherms from the temperature data recorded by different thermocouples, as well as to integrate the areas/volumes bounded by two isotherms. As such, the heat accumulated inside the reservoir at any time t was given by

$$Q_{formation} = \sum_{k=1}^{m} V_{R,k} \times \left\{ \phi S_{o,k} \rho_{o,k} C_{o,k} + \phi S_{w,k} \rho_{w,k} C_{w,k} + \phi S_{st,k} \rho_{st,k} C_{st,k} + (1 - \phi) \rho_{matrix,k} C_{matrix,k} \right\}$$

..... (C4)

Where	m	= the number of temperature contours
k	= an incremental representation for any temperature contour,
$V_{R,k}$	= the volume corresponding to an temperature contours, (m^3)
ϕ	= the porosity of the glass beads reservoir, (dimensionless)
$S_{o,w,s,k}$	= the saturations for oil, water and steam for a given temperature contour k, (dimensionless)
$\rho_{o,w,s,k}$	= the density of the oil, water and steam for a given temperature contour k, (kg/m^3)
$C_{o,w,s,k}$	= the heat capacity of the oil, water and steam for a given temperature contour k, (kJ/kgK)
$\rho_{matrix,k}$	= the density of the matrix, (kg/m^3),
$C_{matrix,k}$	= the heat capacity of the matrix, (kJ/kgK).

Table C2 provides the calculated values for heat accumulated inside the reservoir for the base-case experiment (Experiment 12). These values were obtained from the volume enclosed by isotherms, along with calculated values for oil, water and steam saturations.

Given the values calculated for Q_{inj}, Q_{prod} (Table C1) and $Q_{formation}$ (Table C2), it was seen that at the end of 0.8 PV of steam injected into the reservoir, the heat loss which was yet to be determined, was approximately 595.6 kJ (from Equation (C1)) or 11% of the total heat injected into the formation. In the following, the heat loss from the reservoir to the cap and base rock was examined in more detail.

Table C2: The Total Amount of Heat Accumulated in the Model After 0.8 PV of Steam (CWE) Was Injected, Experiment 12.

Temp. Contour (°C)	Upper Volume (m³)	Lower Volume (m³)	S_o normalized	V_o (m³)	S_w normalize	V_w (m³)	S_{st} normalized	V_{st} (m³)	Heat in Oil (kJ)	Heat in Water (kJ)	Heat in Matrix (kJ)	Heat in Steam (kJ)
0	0.018603	0.016710	0.4466	0.004790	0.5534	0.005935	0	0.000000	0.0000	0.0000	0.0000	0
5	0.000877	0.001016	0.4466	0.000257	0.5534	0.000318	0	0.000000	2.0447	6.8942	14.0556	0
10	0.000727	0.001021	0.4466	0.000237	0.5534	0.000294	0	0.000000	3.8129	12.6650	25.9522	0
15	0.000706	0.001213	0.4466	0.000260	0.5534	0.000322	0	0.000000	6.3395	20.7488	42.7275	0
20	0.000728	0.001160	0.4466	0.000256	0.5534	0.000317	0	0.000000	8.3994	27.0936	56.0626	0
25	0.000770	0.001163	0.4466	0.000262	0.5534	0.000325	0	0.000000	10.8517	34.5059	71.7356	0
30	0.000838	0.001251	0.4466	0.000283	0.5534	0.000351	0	0.000000	14.2068	44.5421	93.0224	0
35	0.000909	0.001499	0.4466	0.000327	0.5534	0.000405	0	0.000000	19.2869	59.6365	125.0967	0
40	0.001009	0.001789	0.4466	0.000380	0.5534	0.000470	0	0.000000	25.8580	78.8717	166.1542	0
45	0.001169	0.002103	0.3695	0.000367	0.6305	0.000627	0	0.000000	28.4067	117.7263	218.5805	0
50	0.001549	0.001345	0.3695	0.000325	0.6305	0.000554	0	0.000000	28.1772	115.2461	214.8298	0
55	0.001846	0.000979	0.3695	0.000317	0.6305	0.000541	0	0.000000	30.5293	123.2598	230.6513	0
60	0.002492	0.000774	0.3695	0.000366	0.6305	0.000625	0	0.000000	38.8478	154.8635	290.8604	0
65	0.002683	0.000477	0.1839	0.000176	0	0.000000	0.8161	0.000783	20.4518	0.0000	304.9271	1.3595
70	0.001084	0.000315	0.1839	0.000078	0	0.000000	0.8161	0.000347	9.8363	0.0000	145.3593	1.9259
75	0.000977	0.000238	0.1839	0.000068	0	0.000000	0.8161	0.000301	9.2405	0.0000	135.3595	2.7075

Porosity	0.3037	
Density of the Matrix	2425.0 (kg/m³)	
Energy in the Oil Phase	256.290 (kJ)	
Energy in the Water Phase	796.054 (kJ)	
Heat loss	589.6051 (kJ)	

Specific Heat Capacity	0.8792 (kJ/kgK)
Volumetric Heat Capacity	2132.06 (kJ/m³K)
Energy in the Vapour Phase	5.993 (kJ)
Energy in the Matrix	2135.375 (kJ)

Heat Loss to the Overburden (Q_{loss})

As described previously, the glass bead reservoir in the experiments in this study was not in direct contact with the granite cap rock (and base rock). Between these media was a sheet of Neoprene in the case of the cap rock, and the fiberglass model tray in the case of the base rock. As such, the cap rock (and the base rock) was actually made up of two regions, each having different properties. This composite structure of the cap rock (and base rock), as shown in Figure C1, created difficulties in the determination of the heat loss.
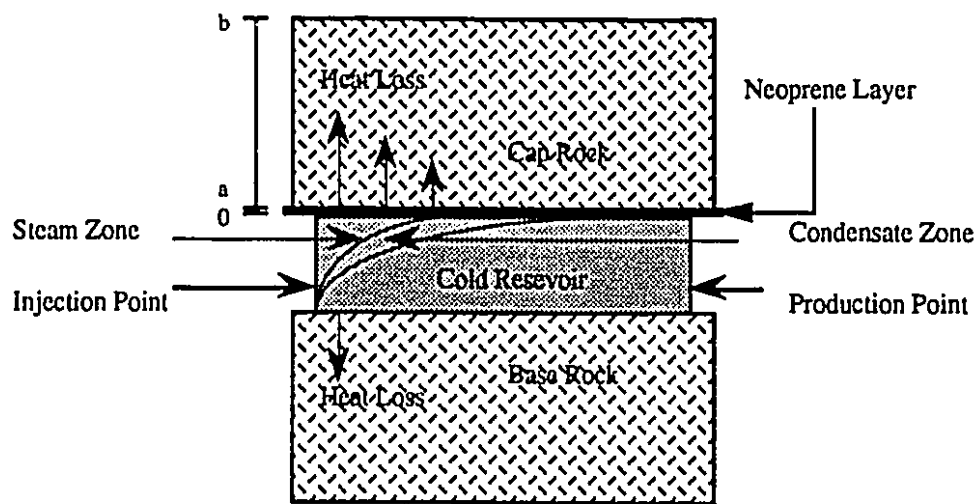
Figure C1: Illustrates a schematic diagram of the composite heat transfer problem

The drawing above shows the presence of steam overriding the top of the formation, the condensate zone ahead of the steam front, and the virgin oil reservoir. Also shown is the instantaneous heat loss to the cap rock and base rock, as indicated by the arrows perpendicular to and pointing away from the modeled reservoir. The different heights of these arrows signify the relative magnitudes of heat loss at different distances along the model length.

The differential equations describing the heat transfer process between two composite medium; that is, the Neoprene sheet and the cap rock, are given below.

$$\frac{\partial^2 T_1}{\partial x^2} = \frac{1}{\alpha_1}\frac{\partial T_1(x,t)}{\partial t} \qquad \text{in } 0 < x < a, t > 0 \qquad \ldots \ldots \quad (C5)$$

$$\frac{\partial^2 T_2}{\partial x^2} = \frac{1}{\alpha_2}\frac{\partial T_2(x,t)}{\partial t} \qquad \text{in } a < x < b, t > 0 \qquad \dots \dots \quad (C6)$$

The above equations are subject to the following boundary conditions:

$$T_1(x,t) = f_1 \qquad\qquad \text{at } x = 0, t > 0 \qquad \dots\dots \quad (C7\text{-a})$$

$$T_1(x,t) = T_2(x,t) \qquad\quad \text{at } x = a, t > 0 \qquad \dots\dots \quad (C7\text{-b})$$

$$k_1 \frac{\partial T_1(x,t)}{\partial x} = k_2 \frac{\partial T_2(x,t)}{\partial x} \qquad \text{at } x = a, t > 0 \qquad \dots\dots \quad (C7\text{-c})$$

$$k_2^{\bullet} \frac{\partial T_2(x,t)}{\partial x} + h_3 T_2 = h_3 f_2 \qquad \text{at } x = b, t > 0 \qquad \dots\dots \quad (C7\text{-d})$$

The initial conditions are:

$$T_1(x,t) = F_1(x) \qquad\qquad \text{for } t = 0, 0 < x < a \qquad \dots\dots \quad (C8\text{-a})$$

$$T_2(x,t) = F_2(x) \qquad\qquad \text{for } t = 0, a < x < b \qquad \dots\dots \quad (C8\text{-b})$$

Both the Neoprene sheet and granite cap rock are assumed to be homogeneous, and the properties including ρ, C_p, k and α are uniform and constant for each of these two materials. In addition, the Neoprene sheet and the granite cap rock are assumed to be in perfect thermal contact.

The general solutions for the system of differential equations, for any boundary and initial conditions were obtained using the procedure suggested by Ozisik[65], as follows

$$T_i(x,t) = \theta_i(x,t) + \phi_i(x) * f_1 + \psi_i(x) * f_2 \qquad\qquad \dots\dots \quad (C9)$$

As seen in Equation C9, the heat transfer for the composite overburden system is broken up into three smaller problems. The functions $\theta_i(x,t)$, i = 1, 2, represent the solution of the transient problem. The second and the third functions, $\phi_i(x)$ and $\psi_i(x)$, i = 1, 2, respectively, represent two solutions to two steady state problems. These problems are explained in more detail in the following.

In the first problem, the solutions of the functions $\phi_i(x)$, where i=1,2 satisfy the steady state composite heat conduction problem given by

$$\frac{d^2\phi_1(x)}{dx^2} = 0 \qquad \text{in } 0 < x < a \quad \ldots\ldots \quad \text{(C10)}$$

and

$$\frac{d^2\phi_2(x)}{dx^2} = 0 \qquad \text{in } a < x < b \quad \ldots\ldots \quad \text{(C11)}$$

The above equations are subject to the following boundary conditions:

$$\phi_1(x) = 1 \qquad \text{at } x = 0 \qquad \ldots\ldots \quad \text{(C12-a)}$$

$$\phi_1(x) = \phi_2(x) \qquad \text{at } x = a \qquad \ldots\ldots \quad \text{(C12-b)}$$

$$k_1\frac{d\phi_1(x)}{dx} = k_2\frac{d\phi_2(x)}{dx} \qquad \text{the interface} \quad \ldots\ldots \quad \text{(C12-c)}$$

$$k_2^{\bullet}\frac{d\phi_2}{dx} + h_3\phi_2 = 0 \qquad \text{at } x = b \qquad \ldots\ldots \quad \text{(C12-d)}$$

The solutions representing the functions $\phi_i(x)$, where i=1,2 are

$$\phi_1(x) = \frac{k_2}{k_1}\left[-\frac{h_3}{k_2^{\bullet} + h_3 b - a h_3\left(1 - \frac{k_2}{k_1}\right)}\right]x + 1 \qquad \text{in } 0 < x < a \quad \ldots\ldots \quad \text{(C13)}$$

and

$$\phi_2(x) = \{-\frac{k_1 h_3}{k_2^{\bullet}k_1 + h_3 b k_1 - a h_3(k_1 - k_2)}\}\times[x - a(\frac{k_1 - k_2}{k_1})] + 1 \quad \text{in } a < x < b \quad \ldots\ldots \quad \text{(C14)}$$

The solutions were evaluated at the boundary conditions to verify their validity.

In the second problem, the solutions of the functions $\psi_i(x)$, where i=1,2, satisfy the steady state composite heat conduction problem that is similar to the first problem but with different boundary conditions.

$$\frac{d^2\psi_1(x)}{dx^2} = 0 \qquad \text{in } 0 < x < a \qquad \ldots\ldots \quad \text{(C15)}$$

and

$$\frac{d^2\psi_2(x)}{dx^2} = 0 \qquad \text{in } a < x < b \qquad \ldots\ldots \quad \text{(C16)}$$

Equations C15 and C16 are subject to the following boundary conditions

$$\psi_1(x) = 0 \qquad \text{at } x = 0 \qquad \ldots\ldots \text{(C17-a)}$$

$$\psi_1(x) = \psi_2(x) \qquad \text{at } x = a \qquad \ldots\ldots \text{(C17-b)}$$

$$k_1 \frac{d\psi_1(x)}{dx} = k_2 \frac{d\psi_2(x)}{dx} \qquad \text{the interface} \qquad \ldots\ldots \text{(C17-c)}$$

$$k_2^* \frac{d\psi_2}{dx} + h_3\psi_2 = h_3 \qquad \text{at } x = b \qquad \ldots\ldots \text{(C17-d)}$$

The steady state solutions of the functions $\psi_i(x)$, where i=1, 2 are

$$\psi_1(x) = k_2\left[\frac{h_3}{k_2^*k_1 + h_3bk_1 + ah_3(k_2 - k_1)}\right]x \qquad \text{in } 0 < x < a \qquad \ldots\ldots \text{(C18)}$$

and

$$\psi_2(x) = \left\{\frac{h_3k_1}{k_2^*k_1 + h_3k_1b + ah_3(k_2 - k_1)}\right\} \times \left[x + a\left(\frac{k_2 - k_1}{k_1}\right)\right] \qquad \text{in } a < x < b \qquad \ldots\ldots \text{(C19)}$$

Again, the correctness of the solutions was verified by evaluating the solutions at the boundary conditions.

The two solutions for the functions $\theta_i(x,t)$, where i = 1, 2, represent the transient solution of the composite heat conduction equations.

$$\frac{\partial^2\theta_1(x,t)}{\partial x^2} = \frac{1}{\alpha_1}\frac{\partial\theta(x,t)}{\partial t} \qquad \text{in } 0 < x < a, t > 0 \qquad \ldots\ldots \text{(C20)}$$

and

$$\frac{\partial^2\theta_2(x,t)}{\partial x^2} = \frac{1}{\alpha_2}\frac{\partial\theta(x,t)}{\partial t} \qquad \text{in } a < x < b, t > 0 \qquad \ldots\ldots \text{(C21)}$$

The equations above are subject to the following boundary conditions:

$$\theta_1(x,t) = 0 \qquad \text{at } x = 0, t > 0 \qquad \ldots\ldots \text{(C22-a)}$$

$$\theta_1(x,t) = \theta_2(x,t) \qquad \text{at the interface} \qquad \ldots\ldots \text{(C22-b)}$$

$$k_1\frac{d\theta_1}{dx} = k_2\frac{d\theta_2}{dx} \qquad x = a, t > 0 \qquad \ldots\ldots \text{(C22-c)}$$

$$k_2^*\frac{d\theta_2}{dx} + h_3\theta_2 = 0 \qquad \text{at } x = b, t > 0 \qquad \ldots\ldots \text{(C22-d)}$$

and the initial conditions are

$$\theta_1(x,t) = F_1(x) - f_1\theta_1(x) - f_2\psi_1(x) \equiv F_1^*(x) \quad t > 0, \text{ in } 0 \le x \le a \quad \dots \quad (C23)$$

$$\theta_2(x,t) = F_2(x) - f_1\theta_2(x) - f_2\psi_2(x) \equiv F_2^*(x) \quad t > 0, \text{ in } a \le x \le b \quad \dots \quad (C24)$$

Following Ozisik[65], the solutions were obtained by the method of separation of variables. The general form of the temperature distribution in the Neoprene sheet; medium i = 1, and the cap rock; medium i = 2, is given by,

$$\theta_i(x,t) = \sum_{n=1}^{\infty} \frac{1}{N_n} e^{-\beta_n^2 t} Y_{in}(x) \left[\frac{k_1}{\alpha_1} \int_{x=0}^{a} F_1^*(x') Y_{1n}(x') dx' + \frac{k_2}{\alpha_2} \int_{a}^{b} F_2^*(x') Y_{2n}(x') dx' \right]$$

$$i = 1, 2 \quad \dots \quad (C25)$$

Where

$$N_n = \frac{k_1}{\alpha_1} \int_{o}^{a} Y_{1n}^2(x') dx' + \frac{k_2}{\alpha_2} \int_{a}^{b} Y_{2n}^2(x') dx' \quad \dots \quad (C26)$$

$$Y_{1n}(x) = \sin\left(\frac{\beta_n}{\sqrt{\alpha_1}} x\right) \quad \dots \quad (C27)$$

$$Y_{2n}(x) = A_{2n} \sin\left(\frac{\beta_n}{\sqrt{\alpha_2}} x\right) + B_{2n} \cos\left(\frac{\beta_n}{\sqrt{\alpha_2}} x\right) \quad \dots \quad (C28)$$

The coefficients A_{2n} and B_{2n} are given by the two expressions below

$$A_{2n} = \frac{1}{\Delta} \left[-\sin\gamma \sin\left(\frac{a}{b}\eta\right) - K\cos\gamma \cos\left(\frac{a}{b}\eta\right) \right] \quad \dots \quad (C29)$$

and

$$B_{2n} = \frac{1}{\Delta} \left[K\cos\gamma \sin\left(\frac{a}{b}\eta\right) - \sin\gamma \cos\left(\frac{a}{b}\eta\right) \right] \quad \dots \quad (C30)$$

where

$$\Delta = -\sin^2\left(\frac{a}{b}\eta\right) - \cos^2\left(\frac{a}{b}\eta\right) = -1$$

In Equations (C39) and (C30), the variables γ, η, H, and K are given by

$$\gamma \equiv \frac{a\beta_n}{\sqrt{\alpha_1}} \qquad \eta \equiv \frac{b\beta_n}{\sqrt{\alpha_2}} \qquad H \equiv \frac{bh_2}{k_2} \qquad K \equiv \frac{k_1}{k_2}\sqrt{\frac{\alpha_2}{\alpha_1}} \qquad \ldots \ldots \quad \text{(C31)}$$

The functions $F_1^*(x)$ and $F_2^*(x)$ are the initial conditions for this transient problem, and their expressions are given by Equations (C34) and (C24). As seen, in order to determine these two functions, the steady state solutions $\psi(x)$ and $\phi(x)$ are required.

The determination of the coefficients A_{2n} and B_{2n} depends on the eigenvalues β_n. These eigenvalues were determined from the solution of the transcendental equation:

$$\left[\frac{\sqrt{\alpha_2}H}{b\beta_n}\sin\left(\frac{b\beta_n}{\sqrt{\alpha_2}}\right) + \cos\left(\frac{b\beta_n}{\sqrt{\alpha_2}}\right)\right]\left[-\cos\left(\frac{b\beta_n}{\sqrt{\alpha_2}}\right)K\cos\left(\frac{a\beta_n}{\sqrt{\alpha_1}}\right) - \sin\left(\frac{a\beta_n}{\sqrt{\alpha_1}}\right)\sin\left(\frac{a\beta_n}{\sqrt{\alpha_2}}\right)\right]$$
$$+\left[\sin\left(\frac{b\beta_n}{\sqrt{\alpha_2}}\right) - \frac{H\sqrt{\alpha_2}}{b\beta_n}\cos\left(\frac{b\beta_n}{\sqrt{\alpha_2}}\right)\right]\left[\sin\left(\frac{a\beta_n}{\sqrt{\alpha_1}}\right)\cos\left(\frac{a\beta_n}{\sqrt{\alpha_2}}\right) - \sin\left(\frac{a\beta_n}{\sqrt{\alpha_2}}\right)K\cos\left(\frac{a\beta_n}{\sqrt{\alpha_1}}\right)\right] = 0$$

$$\ldots \ldots \quad \text{(C32)}$$

For each of these eigenvalues, there is a corresponding set of coefficients. The determination of these roots symbolically was not possible. Several programs, Mathematica™ and MatLab™, were tried to determine the eigenvalues. However, neither one can accomplish this task. Finally, Excel™ was used to solve, by trial-and-error, solutions to Equation (C32). The first seven eigenvalues were obtained and are shown in Table. C3.

Equipped with the general solutions to the problem, the temperature distribution in the system was constructed for the base case experiment. The time used corresponded to 0.8 PV. The pertinent data required for the calculations are given in Table C3. Equations (C33) and (C34), listed below, describe the temperature distribution in the system.

149

Table C3: Calculated Values of Various Terms Appearing in the Analytical Solution of the Composite Heat Transfer Problem

Eigenvalues n	Residuals	N_n	$\int_o^a F_1^*(x)\cdot\sin\left(\dfrac{\beta_n}{\sqrt{\alpha_1}}x\right)dx$	$\int_a^b F_2^*(x)\left[A_{2n}\sin\left(\dfrac{\beta_n}{\sqrt{\alpha_2}}\right)x+B_{2n}\cos\left(\dfrac{\beta_n}{\sqrt{\alpha_2}}\right)x\right]dx$	$coeff_{T_{1*}}$	$\dfrac{\Delta T}{\Delta x}$
0.024807	3.91e-05	7.174731	0.322935	-0.35537	0.685835	-36.3285
0.041345	1.10e-05	18.93195	0.912416	-0.098751	-0.028982	-2.4920
0.057885	2.34e-05	35.80765	1.791154	0.016351	0.000458	0.0529
0.074425	9.38e-06	56.9334	2.945437	-0.074444	4.39e-07	6.17e-05
0.090966	2.34e-05	81.22143	4.357229	0.027526	2.76e-10	4.40e-08
0.107509	8.40e-06	107.4206	6.004447	-0.061218	1.55e-14	2.66e-12
0.124054	1.07e-05	134.1803	7.861231	0.030028	2.85e-19	5.04e-17

Thermal Conductivities:

Neoprene sheet:	3×10^{-5} kJ/mKs
Granite Block (cap rock):	3×10^{-3} kJ/mKs

Thicknesses:

Neoprene:	0.003175 m
Granite Block (cap rock):	0.225375 m

Conductivity in air: 2.49×10^{-5} kJ/mKs

Heat Loss (Analytical model): 643.434 kJ

Heat Loss (Measured Temperature) - Neoprene 664.268 kJ
- Cap Rock 602.499 kJ

Thermal Diffusivity:

Neoprene sheet:	2.13×10^{-7} m^2/sec
Granite Block (cap rock):	1.42×10^{-6} m^2/sec

Convection Constant: 2.5×10^{-2} kJ/m^{2}Ksec

$$T_1(x,t) = \sum_{n=1}^{7} coeff_{T_{1n}} * \sin\left(\frac{\beta_n}{\sqrt{\alpha_2}}x\right) + \left[\frac{-k_2 h_3}{k_2^* k_1 + h_3 k_1 b - h_3 a(k_1 - k_2)}\right](60x) + 70$$

..... (C33)

and

$$T_2(x,t) = \sum_{n=1}^{7} coeff_{T_{2n}} * \left[A_{2n} \sin\left(\frac{\beta_n}{\sqrt{\alpha_2}}x\right) + B_{2n}\cos\left(\frac{\beta_n}{\sqrt{\alpha_2}}x\right)\right]$$

$$+ \left[\frac{k_1 h_3}{k_2^* k_1 + h_3 k_1 b - h_3 a(k_1 - k_2)}\right] * 60\left(-x + a - a\frac{k_2}{k_1}\right) + 70 \qquad ..... (C34)$$

where

$$coeff_{T_{1n}} = coeff_{T_{2n}} = \frac{1}{N_n}e^{-\beta_n^2 t} \bullet \left[\frac{k_1}{\alpha_1}\int_{x'=0}^{a} F_1^*(x')Y_{1n}(x')dx' + \frac{k_2}{\alpha_2}\int_{x'=a}^{b} F_2^*(x')Y_{2n}(x')dx'\right]$$

The function – $T_1(x,t)$ – represents the temperature distribution in the Neoprene sheet, which was in the region $0 < x < a$. The function – $T_2(x,t)$ – represents the temperature distribution in the cap rock, which is valid in the regions $a < x < b$. The values $coeff_{T_{1n}}$ were obtained from combining Equations (C26 - C32). These are shown in Table C3. The temperature distribution at three different times: t = 100, 600 and 2915 seconds - was evaluated. The purpose of these calculations was to examine the stability of the solutions. The temperature distribution in the Neoprene sheet along with the cap rock at various penetration distances, and at various snapshots in time is shown in Table C4. A graph showing the temperature distribution at various penetrating distances and times inside both the Neoprene sheet and the cap rock is shown in Figure C2. At times t = 100 and 600 seconds, the instability of the temperature distribution in the cap rock is observed. This implied that the solutions are valid at longer times.

After 0.8 PV of steam was injected into the reservoir, the analytical model predicted the temperature at the interface between the Neoprene sheet and the granite cap rock (x = a) to be 36.3°C. Previously, Matthias[56] conducted experiments to measure the temperature at the interface (x = a) for the entire steamflood. Matthias[56] found the temperature was 33.5°C, after 0.8 pore volume of steam (CWE) had been injected for the base case run. This illustrates the precise treatment of the composite heat transfer problem for the present experimental set-up.

Penetration Distance (m)	Temperature Distribution		
	time = 100 sec. °C	time = 600 sec. °C	time = 2915 sec. °C
0.0000	70.000	70.000	70.000
0.0005	65.866	64.653	64.691
0.0010	61.718	59.306	59.382
0.0015	57.542	53.958	54.072
0.0020	53.327	48.609	48.763
0.0025	49.059	43.260	43.454
0.0030	44.725	37.909	38.145
0.003175	43.191	36.037	36.287
0.0050	34.317	34.317	34.317
0.0100	40.899	33.067	33.761
0.0500	21.935	28.393	29.411
0.0750	28.097	26.501	26.756
0.1000	26.057	25.044	24.107
0.1250	25.409	22.880	21.431
0.1500	20.422	19.604	18.702
0.1750	15.316	15.800	15.915
0.2000	9.583	12.458	13.077
0.225375	8.506	9.993	10.160

Table C4:   Illustrates the temperature distribution at various snapshot in times (t = 100, 600 and 2915 seconds).
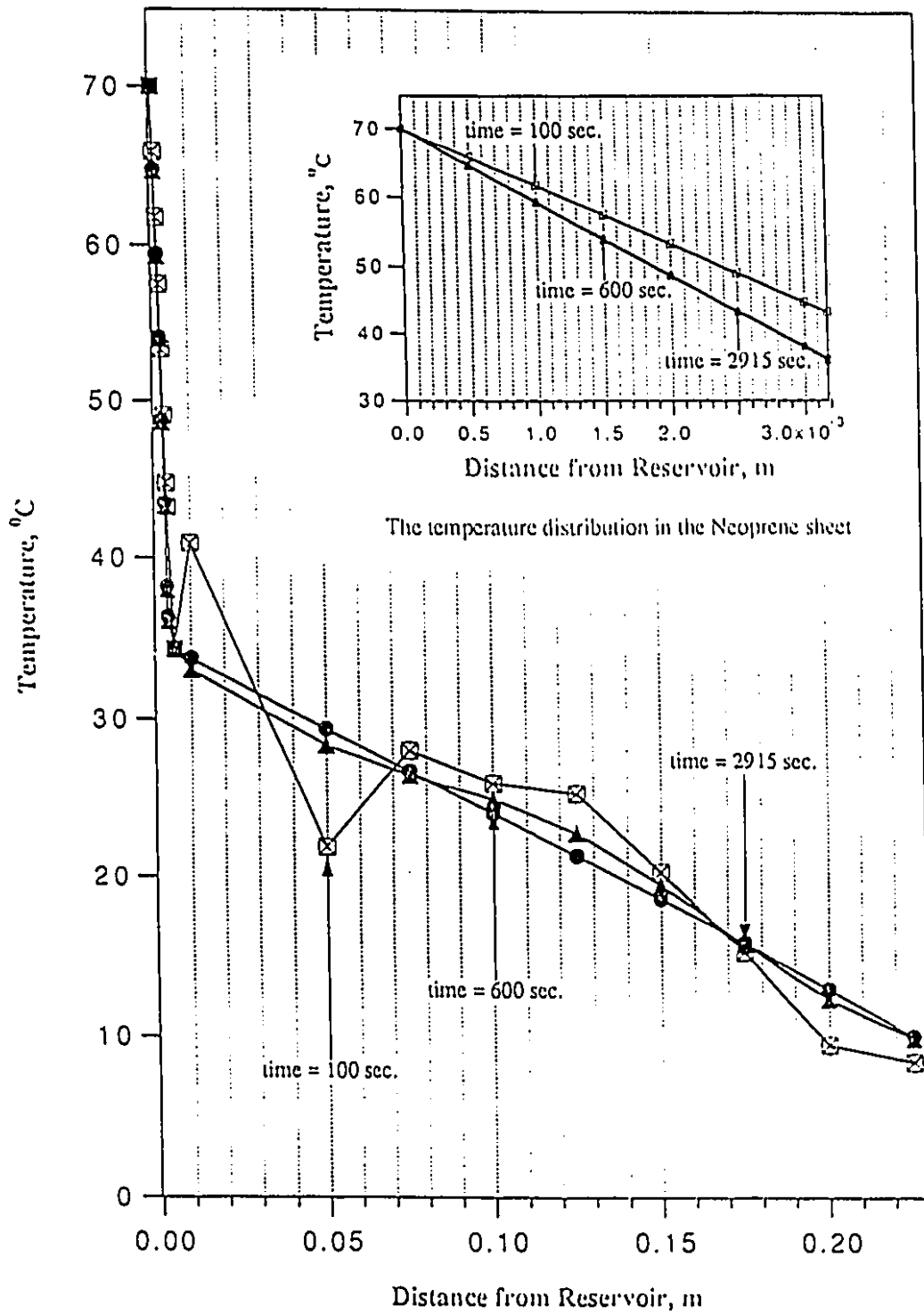
Figure C2: The temperature distribution in the Neoprene sheet and cap rock after 100, 600, 2915 (0.8 PV) seconds.

Given the temperature distribution, the rate of heat loss to the overburden was found from the equation:

$$\dot{Q} = -kA\frac{dT}{dx}$$ ..... (C35)

The rates of heat loss through the Neoprene sheet and the cap rock are

$$\dot{Q}_1 = k_1 A \frac{dT_1}{dx} \qquad\qquad \dot{Q}_2 = k_2 A \frac{dT_2}{dx}$$

where the temperature gradient (heat flux) $\frac{dT_1}{dx}$ and $\frac{dT_2}{dx}$ is given by:

$$\frac{dT_1}{dx} = \sum_{n=1}^{7} coeff_{T_{1n}} * \frac{\beta_n}{\sqrt{\alpha_1}}\cos\left(\frac{\beta_n}{\sqrt{\alpha_1}}x\right)_0^a - \frac{60k_2h_3}{k_2^*k_1 + h_3k_1b - h_3a(k_1 - k_2)}$$

$$\frac{dT_2}{dx} = \sum_{n=1}^{7} coeff_{T_{2n}} \left[A_{2n}\frac{\beta_n}{\sqrt{\alpha_2}}\cos\left(\frac{\beta_n}{\sqrt{\alpha_2}}x\right) - B_{2n}\frac{\beta_n}{\sqrt{\alpha_2}}\sin\left(\frac{\beta_n}{\sqrt{\alpha_2}}x\right)\right]_a^b - \frac{60k_1h_3}{k_2^*k_1 + h_3k_1b - h_3a(k_1 - k_2)}$$

The rate of heat loss through the Neoprene was 0.220699 kJ/s, while the heat loss through the cap rock was 0.224094 kJ/s. The relative error between theses two values is 1.5%, which is due to perhaps round-off error.

The cumulative heat loss from the reservoir through the Neoprene sheet to the granite cap rock is

$$Q = -k_{granite}A\left[\frac{h_3f_2 - 70h_3}{K_2^* + h_3b}\, t\Big|_{t=0}^{0.8\,PV} + \sum_{n=1}^{5}\left[\frac{134}{b\lambda_n}(\cos b\lambda_n - 1) - \frac{2}{\lambda_n b}\left(\frac{h_3f_2 - 70h_3}{K_2^* + h_3b}\right)\bullet\left(\frac{1}{\lambda_n}\sin b\lambda_n - b\cos b\lambda_n\right)\right]\right] \bullet$$

$$\cos\lambda_n x\Big|_{x=0}^{b}(\lambda_n)\cdot e^{-\lambda_n^2\alpha}\Big|_{t=0}^{0.8\,PV}\left(\frac{1}{-\lambda_n^2\alpha}\right)$$

The cumulative heat loss through the Neoprene sheet, after 0.8 PV of steam was injected, was found to be 638.1 kJ. Measuring the temperature at the interface between the Neoprene sheet and the granite cap rock permitted the experimental heat loss to be calculated, and this was found to be 664.3 kJ. The error between the theoretically predicted and experimentally calculated values was 4.0 %.

Appendix D

OPTIMISTIC RECOVERY

The presence of the Neoprene sealant sheet in the system reduced the heat lost to the overburden, and allowed heat to accumulate in the model. As a result, the expansion of the steam zone is promoted, and this led to optimistic recovery. In this appendix, the procedure – established by Gomaa[61]– to predict the performance of a steamflood is illustrated first. Next, to validate this prediction, a simple analytical model is developed to predict the temperature distribution in the cap rock, and hence the heat loss. Subsequently, attempts are made to use other correlations provided by Gomaa[61] to determine the optimistic recovery obtained from experimental results. The schematic diagram representing the heat distribution during a steamflood is illustrated below.
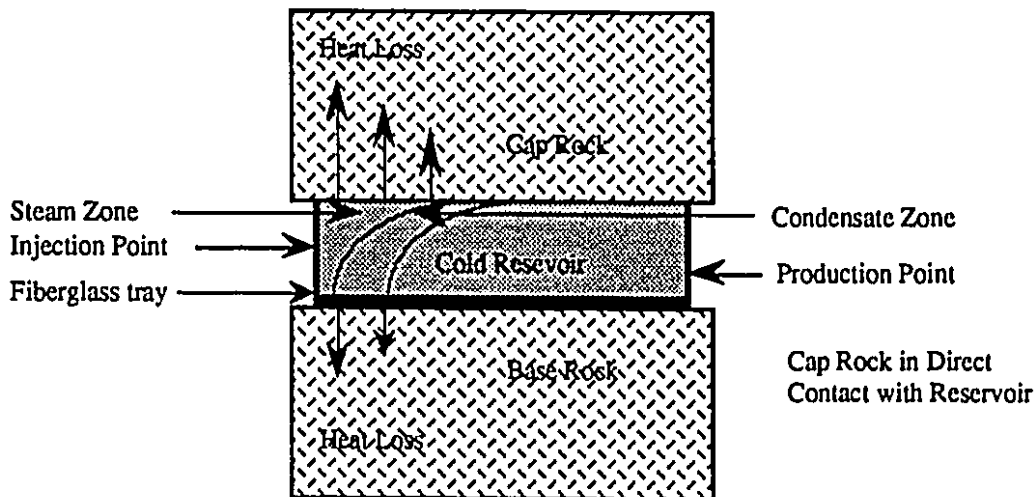
Figure D1: Illustrates a schematic diagram of the heat transfer during a steamflood

Gomaa's Correlation

Using a numerical simulator, Gomaa[61] established a set of correlation charts for predicting steamflood oil recovery and oil/steam ratio as functions of reservoir characteristics and operating conditions. The correlations emphasized the effects of steam quality, mobile oil saturation, reservoir thickness and net/gross ratio.

The procedures to predict the oil recovery for a given steamflood are summarized as follows:

1) Read the vertical heat loss (f_{hv}) as fraction of input from Figure 13[61],

> The heat injection rate was
>
> $$\dot{Q}_{inj} = i_{st}\left\{h_{inj} - h_{res} + f_{st}L_v\right\}$$
>
> Substituting
>
> | | |
> |---|---|
> | i = 37.5 m3/D (0.43403Kg/s) | h_{inj} = 1041.7 kJ/kg |
> | h_{res} = 94.901 kJ/kg | f_{st} = 0.70 |
> | L_v = 2803.1 kJ/kg | res. thickness = 35 ft |
>
> then $\dot{Q}_{inj}$ = 1262.57 kJ/s = 103.39 MMBtu/D or 0.57988 MMBtu/D/ac-ft.
>
> From Figure 13, the vertical heat loss as a percentage of input (f_{hv}) is 0.48

2) Read the heat utilization factor (Y) from Figure 12[61],

> The injected steam has a 70 % quality therefore the heat utilization factor (Y) was 0.9.

3) Calculate the net heat injected (Q_{inj}) in MMBtu/gross acre-ft using the equation

$$Q_{inj} = 0.128\sum\left[Ih(1 - f_{hv})\Delta t\right]_i$$

where

I	– is the injection rate (B/D/gross acre-ft),
h	– is the enthalpy (Btu/lbm),
Δt	– is the time increment (years),
i	– is the index of time increments.

Substituting

I = 1.3229 B/D/gross acre-ft	h = 447.85 Btu/lbm
f_{hv} = 0.48	Δt = 3.76087 years

then Q_{inj} = 148.31 MMBtu/acre-ft

4) Calculate the effective heat injected (Q_e) in MMBtu/gross acre-ft from

$$Q_e = Y \times Q_{inj}$$

Substituting
$$Y = 0.9 \qquad\qquad Q_{inj} = 148.31 \text{ MMBtu/acre-ft}$$
then $Q_e = 133.48$ MMBtu/acre-ft

5) Read the oil recovery from Figure 14[61].

From Figure 14, the cross parameter initial mobile oil saturation is defined as
$$S_{om} = S_{oi} - S_{ors}$$
where

S_{om} — is the initial mobile oil saturation,

S_{oi} — is the initial oil saturation prior to steamflood = .9032,

S_{ors} — is the residual oil saturation after steamflood = 0.120.

then $S_{om} = 0.7832$.

In Figure 14, the correlation cross parameter – initial mobile oil saturation – reached up to only 60 %. At this point, the oil recovery, as a percentage of original mobile oil was 12%. This value is expected to be higher for $S_{om} = 78.32\%$, approximately 15%.

Temperature Distribution in the Cap Rock

The temperature distribution in the cap rock was modeled by the diffusivity equation

$$\frac{\partial^2 T}{\partial x^2} = \frac{1}{\alpha_{granite}} \frac{\partial T}{\partial t} \qquad\qquad \cdots\cdots \quad (D1)$$

having the Dirichlet inner boundary condition, and a mixed outer boundary condition as

$$T(x = 0, t) = f_1 \qquad\qquad \cdots\cdots \quad (D2\text{-}a)$$
$$K_2^* \frac{\partial T}{\partial x} + h_3 T_2 = h_3 f_2 \qquad\qquad \cdots\cdots \quad (D2\text{-}b)$$

The initial condition is

$$T(x, t = 0) = f_3 \qquad\qquad \cdots\cdots \quad (D2\text{-}c)$$

Since the boundary conditions of the above problem are not homogeneous, the method of separation of variables could not be used directly to obtain the solution. The general solution is broken up into a steady state solution and a transient solution as

$$T(x,t) = V(x) + W(x,t) \qquad \dots\dots \quad \text{(D3)}$$

where $V(x)$ – the steady state solution, and

              $W(x,t)$ – the transient solution.

The steady state solution is

$$V(x) = \frac{h_3 f_2 - f_1 h_3}{K_2^* + h_3 b} x + f_1 \qquad \dots\dots \quad \text{(D4)}$$

where f_1 = the temperature at x = 0, °C

              f_2 = the temperature at x = b, °C

              f_3 = the initial temperature at t = 0, °C

              b   = the thickness of the granite block, that is, cap rock, m

              h_3 = the convection constant at x = b,

              K_2^* = the thermal conductivity of surrounding air at x = b,

In this study, the following temperatures were assumed based on engineering judgment: $f_1 = 70°C$, $f_2 = 16°C$, and $f_3 = 3°C$. Upon substituting these temperatures into Equation (D5), the steady state solution becomes

$$V(x) = \frac{h_3 f_2 - 70 h_3}{K_2^* + h_3 b} x + 70 \qquad \dots\dots \quad \text{(D5)}$$

Having found the steady state solution, the formulation of the transient solution is given by the partial differential equation

$$\frac{\partial^2 W}{\partial x^2} = \frac{1}{\alpha_{granite}} \frac{\partial W}{\partial t} \qquad \dots\dots \quad \text{(D6)}$$

Reformulating the boundary conditions at the inner and outer boundary results in

$$W(x = 0,t) = 0 \qquad\qquad (x = 0) \qquad \dots\dots \quad \text{(D7-a)}$$

$$K_2^* \frac{\partial W}{\partial x} + h_3 W = 0 \qquad\qquad (x = b) \qquad \dots\dots \quad \text{(D8-b)}$$

and the initial condition is

$$W(x, t = 0) = -(f_1 - f_3) - \frac{h_3 f_2 - f_1 h_3}{K_2^* + h_3 b} x \qquad \text{..... (D8-c)}$$

Since the boundary conditions for the transient problem are homogeneous, the method of separation of variables is used to obtain the temperature distribution in the cap rock as

$$W(x, t) = \sum_{n=1}^{\infty} \left\{ \frac{134}{b\lambda_n} (\cos b\lambda_n - 1) - \frac{2}{\lambda_n b} \left(\frac{h_3 f_2 - 70 h_3}{K_2^* + h_3 b} \right) \left[\frac{1}{\lambda_n} \sin b\lambda_n - b \cos b\lambda_n \right] \right\} \cdot$$
$$\sin \lambda_n x \cdot e^{-\lambda_n^2 \alpha t} \qquad \text{..... (D9)}$$

The parameter λ_n represents the eigenvalues of the equation

$$K_2^* \lambda + h_3 \tan \lambda b = 0 \qquad \text{..... (D10)}$$

The temperature distribution $T(x, t)$ is therefore given by

$$T(x, t) = \sum_{n=1}^{\infty} \left\{ \frac{134}{b\lambda_n} (\cos b\lambda_n - 1) - \frac{2}{\lambda_n b} \left(\frac{h_3 f_2 - 70 h_3}{K_2^* + h_3 b} \right) \left[\frac{1}{\lambda_n} \sin b\lambda_n - b \cos b\lambda_n \right] \right\} \cdot$$
$$\sin \lambda_n x \cdot e^{-\lambda_n^2 \alpha t} + \frac{h_3 f_2 - f_1 h_3}{K_2^* + h_3 b} x + f_1 \qquad \text{..... (D11)}$$

Table D1 shows the eigenvalues along with the temperature at various penetration distances into the cap rock, and Figure D1 shows the temperature distribution inside the cap rock after 0.8 PV of steam had been injected. Again, at times t = 100 and 600 seconds, the instability in the solution is observed. Having found the temperature distribution inside the cap rock, the rate of heat loss was found to be

$$\dot{Q} = -k_{granite} A \frac{dT}{dx} \qquad \text{..... (D12)}$$

where

$$\frac{dT}{dx} = \sum_{n=1}^{\infty} \left\{ \frac{134}{b\lambda_n} (\cos b\lambda_n - 1) - \frac{2}{\lambda_n b} \left(\frac{h_3 f_2 - 70 h_3}{K_2^* + h_3 b} \right) \left[\frac{1}{\lambda_n} \sin b\lambda_n - b \cos b\lambda_n \right] \right\} \cdot$$
$$\cos \lambda_n x \big|_{x=0}^{b} (\lambda_n) \cdot e^{-\lambda_n^2 \alpha t} + \frac{h_3 f_2 - 70 h_3}{K_2^* + h_3 b} \qquad \text{..... (D13)}$$

Penetration Distance (m)	Temperature Distribution		
	time = 100 sec. °C	time = 600 sec. °C	time = 2915 sec. °C
0.0000	70.0000	70.0000	70.0000
0.0250	15.1396	39.4073	55.7333
0.0500	0.9339	17.9387	42.6222
0.0750	4.7170	7.4495	31.6026
0.1000	3.6138	3.8910	23.2404
0.1250	0.8899	3.1736	17.6858
0.1500	3.8475	3.7248	14.7236
0.1750	3.4910	5.6926	13.8762
0.2000	3.5136	9.7380	14.5104
0.2254	15.3875	15.7529	15.9420

Table D1: Temperature distribution in the cap rock, with the absence of the Neoprene sheet, at three different times: t = 100, 600 and 2915 (or 0.8 PV) seconds during a steamflood.
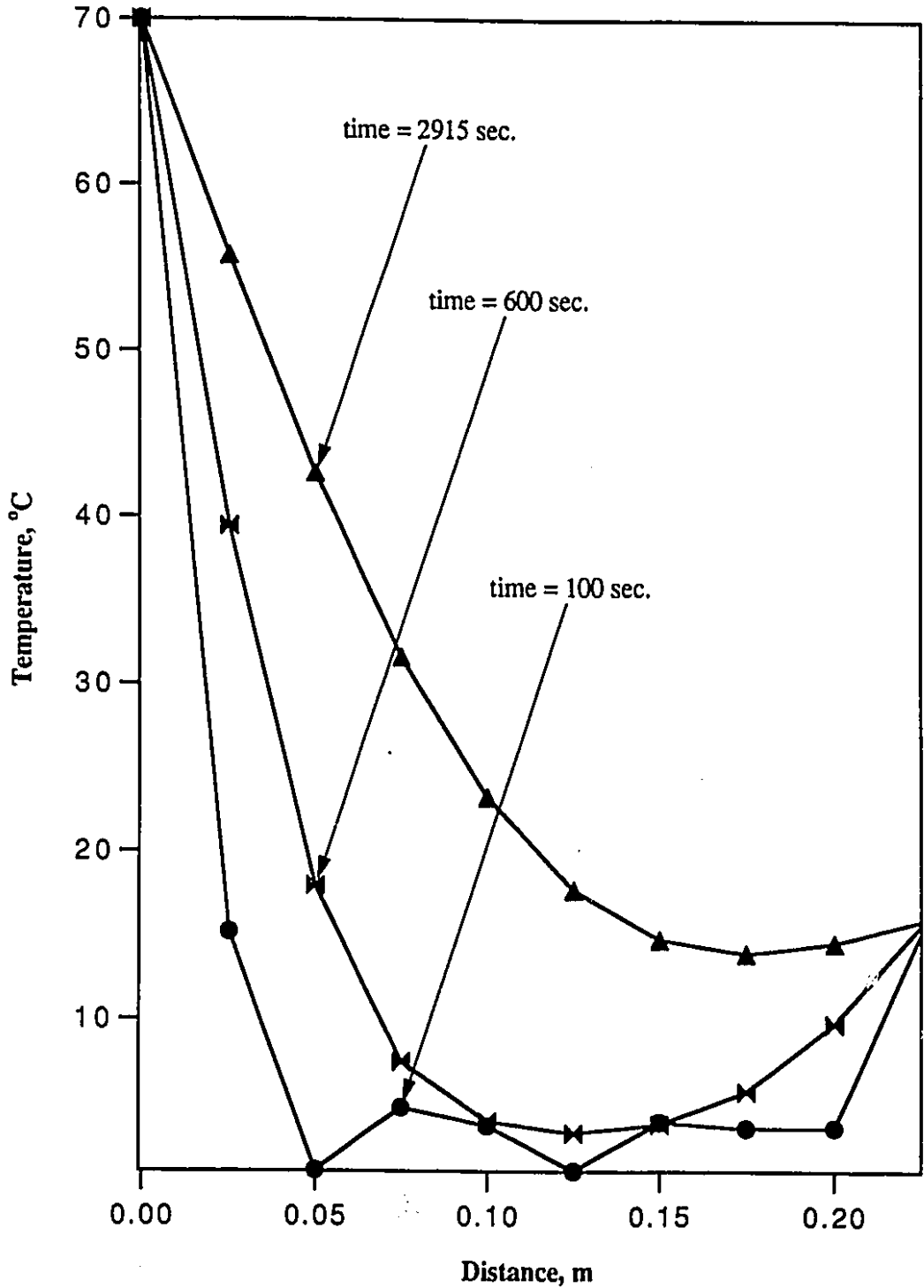
Figure D1: Temperature distribution in the cap rock, with the absence of the
Neoprene sheet, at three times: t = 100, 600 and 2915 (or 0.8 PV) seconds
during a steamflood

Therefore, the cumulative heat loss was given by

$$Q = \int_{t=0}^{t=0.8\,PV} \dot{Q}\, dt \qquad\qquad \cdots\cdots \text{(D14)}$$

or

$$Q = -k_{granite} A \left\{ \frac{h_3 f_2 - 70 h_3}{K_2^* + h_3 b}\, t \Big|_{t=0}^{0.8\,PV} + \sum_{n=1}^{5} \left[\frac{134}{b\lambda_n}(\cos b\lambda_n - 1) - \frac{2}{\lambda_n b}\left(\frac{h_3 f_2 - 70 h_3}{K_2^* + h_3 b}\right) \bullet \left(\frac{1}{\lambda_n}\sin b\lambda_n - b\cos b\lambda_n\right)\right] \right\} \bullet$$
$$\cos\lambda_n x \Big|_{x=0}^{b}(\lambda_n) \cdot e^{-\lambda_n^2 \alpha} \Big|_{t=0}^{0.8\,PV}\left(\frac{1}{-\lambda_n^2 \alpha}\right) \qquad\qquad \cdots\cdots \text{(D15)}$$

From Equation (D12), the rate of heat loss to the overburden (cap rock) was directly proportional to the areal coverage (A) of the steam zone. If the areal coverage of the steam zone was assumed to be 100 %, then the rate of heat loss was found to be 0.79718 kJ/s. Upon substituting different values into Equation (D15), the cumulative heat loss to the overburden (cap rock) - after 0.8 PV of steam had been injected - was found to be 1712.15 kJ. However, based on engineering judgment, the areal steam coverage was approximately 75%. Based on this assumption, the heat loss to the cap rock was found to be 1284.11 kJ. This value represented approximately 24% of the cumulative heat injected.